Design of smart responsive polymers and polymer nanoparticles

Dissertation

Zur Erlangung des Grades

Doktor der Naturwissenschaften

Chemie, Pharmazie, Geographie und Geowissenschaften (FB 09)

der Johannes Gutenberg-Universität Mainz

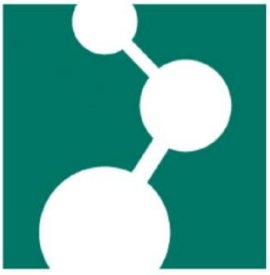

vorgelegt von

Long Yang

geboren in Shaanxi, P.R. China

Mainz, 2020

The thesis was carried out from September 2016 until October 2020 within the department of at the Max-Planck-Institute for Polymer Research, Mainz.

Dekan: Prof. Dr. Tobias Reich

Prodekan: Prof. Dr. Till Opatz

Gutachter 1: Prof. Dr.

Gutachter 2: Prof. Dr.

Date of oral examination:

Declaration

I hereby declare that I wrote the dissertation submitted without any unauthorized external assistance and used only sources acknowledged in this work. All textual passages which are appropriate verbatim or paraphrased from published and unpublished texts, as well as all information obtained from oral sources, are duly indicated and listed in accordance with bibliographical rules. In carrying out this research, I complied with the rules of standard scientific practice as formulated in the statutes of Johannes Gutenberg-University Mainz to insure standard scientific practice.

……

(Long Yang)

Content

Abstract

In the design of new materials, “smart polymers”, polymers whose properties change in response to a single or multiple triggers, have imposed themselves as a unique platform to either introduce new functions or to control existing functions. The main goal of this thesis is to harness the potential of smart-responsive polymer to enhance the performance of functional polymer and polymer nanocolloids.

For example, responsive polymers can be used as a smart “on-off” switch, which creates the potential of “on-demand”. In section 3.1, a dual temperature/light response is designed by combining in one copolymer N-isopropylacrylamide and a reversible spiropyrane-based photoacid monomer. The resulting thermoresponsive polyphotoacid is responsive to light irradiation at λ = 460 nm and can release one proton for each spiropyrane unit and is, therefore, able to acidify the solution. The opposite effect, the removal of protons and corresponding pH increase, can be observed either when keeping the polyphotoacid in the dark for several minutes or more quickly by the irradiation of UV-light. Increasing the temperature above the lower critical solution temperature (LCST) silences the photoacid behavior, and the irradiation of light at λ = 460 nm no longer leads to proton generation. Thus the activity of the thermoresponsive polyphotoacid can be finely tuned.

Similarly, functional colloidal nanoparticles can be functionalized with

stimulus-responsive polymers. In section 3.2, a library of colloidal nanoparticles is prepared *via* polymerization induced self-assembly (PISA), sonication, and core-crosslinking. The external hydrophilic canopy is designed to be thermoresponsive. The aspect ratio and rigidity of colloidal nanoparticles are tuned by varying the reaction conditions. Also, those nanocolloids can form colloidal gels at high enough volume fraction. However, the controlled aggregation of the polymer nanocolloids can also be tuned by the thermoresponsive external canopy. The mechanical properties of the resulting colloidal gels are affected by the rigidity of the colloidal building blocks, their aspect ratio but also the mechanism of aggregation.

Such anisotropic polymer nanocolloids are of high interest not only as rheology modifiers but also as drug carriers. The colloids developed in section 3.2 are then used in section 3.3 for the controlled release of a model payload. Those functional polymer colloids are a versatile delivery platform that can be used as an individual drug carrier or to build responsive drug depots.

This work clearly demonstrates that the introduction of stimulus-responsive polymers in functional materials can be used to further tune and control the properties of the materials.

Zusammenfassung

Bei der Entwicklung neuer Materialien haben sich "smarte" Polymere, d.h. Polymere, deren Eigenschaften sich als Reaktion auf einen oder mehrere Trigger ändern, als einzigartige Plattform erwiesen, um entweder neue Funktionen zu erzeugen oder bestehende Funktionen zu kontrollieren.

Die vorrangige Zielsetzung dieser Dissertation ist es, sich das Potential intelligent-reagierender Polymere zu Nutze zu machen, um die Leistung funktioneller Polymere oder Polymer-Nanokolloide zu verbessern. Bedarfsgesteuerte Polymere können zum Beispiel als intelligente "An-Aus"-Schalter genutzt werden und so eine "On-demand "-Funktion erhalten. In Abschnitt 3.1 wird ein duales, Temperatur/Licht-empfindliches Ansprechverhalten entwickelt, indem ein Copolymer aus N-Isopropylacrylamid und einem reversiblen, Spiropyran-basierten "photoaziden" Monomer erzeugt wird, welches seinen pH-Wert durch Lichtabsorption ändert. Das resultierende thermoreaktive "photoazide" Polymer reagiert auf Bestrahlung mit einer Wellenlänge von $\lambda = 460$ nm, woraufhin jede Spiropyran-Einheit ein Proton freisetzen kann und damit in der Lage ist, die Lösung anzusäuern. Der gegenteilige Effekt, die Entfernung von Protonen mit einem entsprechenden pH-Anstieg, wird entweder bei Lagerung des "photoaziden" Polymers für mehrere Minuten in

Dunkelheit oder schneller durch Bestrahlung mit UV-Licht erreicht. Bei Temperaturen oberhalb der unteren kritischen Lösungstemperatur (LCST) verschwindet das "photoazide" Verhalten und die Bestrahlung mit Licht einer Wellenlänge von $\lambda = 460$nm setzt keine Protonen mehr frei. Auf diese Weise kann das Verhalten eines thermoreaktiven "photoaziden" Polymers präzise eingestellt werden.

Ähnlich können kolloidale Nanopartikel mit einem Polymer funktionalisiert werden, welches auf einen externen Stimulus reagiert. In Abschnitt 3.2 wird eine Sammlung kolloidaler Nanopartikel durch Polymerisations-induzierte Selbstassemblierung (polymerization induced self-assembly "PISA"), Ultraschall und Kernvernetzung hergestellt. Die Systeme, auf deren Oberfläche sich hydrophile Polymerbürsten befinden, werden mit einer thermoreaktiven Funktion ausgestattet. Der Formfaktor und die Elastizität der kolloidalen Nanopartikel werden durch Variation der Reaktionsbedingungen eingestellt. Diese Nanokolloide können auch kolloidale Gele mit genügend hohem Volumenanteil ausbilden. Die Aggregation der polymeren Nanokolloide kann durch die thermo-reaktiven Polymerbürsten kontrolliert werden. Die mechanischen Eigenschaften der resultierenden kolloidalen Gele werden beeinflusst durch die Steifigkeit der kolloidalen Basiskomponenten, ihren Formfaktor aber auch vom

Aggregationsmechanismus.

Solche anisotropen polymeren Nanokolloide sind nicht nur als Modifikatoren zur Beeinflussung des Fließverhaltens, sondern auch als Arzneimitteltrager von hohem Interesse. In Abschnitt 3.3 werden die Kolloide, die in Abschnitt 3.2 entwickelt wurden, für die kontrollierte Freisetzung einer Modellladung genutzt. Diese funktionellen Polymerkolloide sind eine vielseitige Freisetzungs-Plattform und können für gezielte Pharmakotherapie genutzt werden oder um Stimulus-reaktive Medikamentendepots aufzubauen. Diese Arbeit zeigt deutlich, dass die Einführung Stimulus-reaktiver Polymere in funktionellen Materialien genutzt werden kann, um die Eigenschaften von Materialien einzustellen und zu kontrollieren.

Chapter 1. Introduction

Polymers are ubiquitous in everyday life and even play a key role in human life. For ages, polymers have been used in many fields and have help to improve the performance of a variety of materials. However, even though polymers were already in use, it took some time, before they were accurately described by Staudinger 100 years ago as composition of many elementary units (monomers) covalently bound together; such initially non-conventional idea was soon after widely accepted.[1, 2] Since then, many functional polymers have been designed, some of which, stimuli-responsive polymers, are able to respond to different physicochemical parameters by tuning the physical and/or chemical properties, [3-5] including pH, [6] temperature, [7] mechanical force, [8] and light. [9] Those smart polymers have been developed in many applications, ranging from sensors,[10] chemo-mechanical actuators, [11-13] and for many other applications. [14-16]

Interestingly, instead of using a single polymer with a single function, endowing nanoparticles with one responsive property, new multi-responsive materials are built to simultaneously benefit from multiple functions and form complex materials that can be used in new functional devices. For example, electro-responsive and magneto-responsive colloidal nanoparticles have been used for the separation of proteins [17, 18] and the recovery of catalysts. [19] Moreover,

colloidal nanoparticles with controllable size, shape, composition, structure, and crystallinity can be used to fine-tune their properties for a targeted application.

Therefore, it is essential to develop materials that incorporate different stimuli-responsive polymer in order to have the desired properties and functions. The different strategies were used to create those smart responsive materials with various functions.

Chapter 2. Literature Review

2.1 Stimuli-Responsive polymers

Stimuli-responsive polymers are involved in a broad array of research areas, including phase transition in polymer solutions or smart materials with shape memory or self-healing properties. Stimuli-responsive polymers have been used either in solution or to functionalize surface and interface or even to build more complex responsive-nanoparticles. In the last several decades, new stimuli-responsive polymers have been developed that respond to a variety of stimuli, ranging from chemical, physical to mechanical cues,[20-27] such intelligent polymers have found many applications.[28-36]

2.1.1 Temperature-responsive polymers

Temperature responsive polymers are an important class of materials, and those responsive polymers are studied due to their unique properties. Usually, in such polymers, a coil-to-globule transition occurs at a critical temperature. The conformation of the polymer chains shows flexible and expanded coil state either below or above a critical temperature, while the polymer chains experience a collapse to a globule structure either above or below that temperature (Figure 2.1).

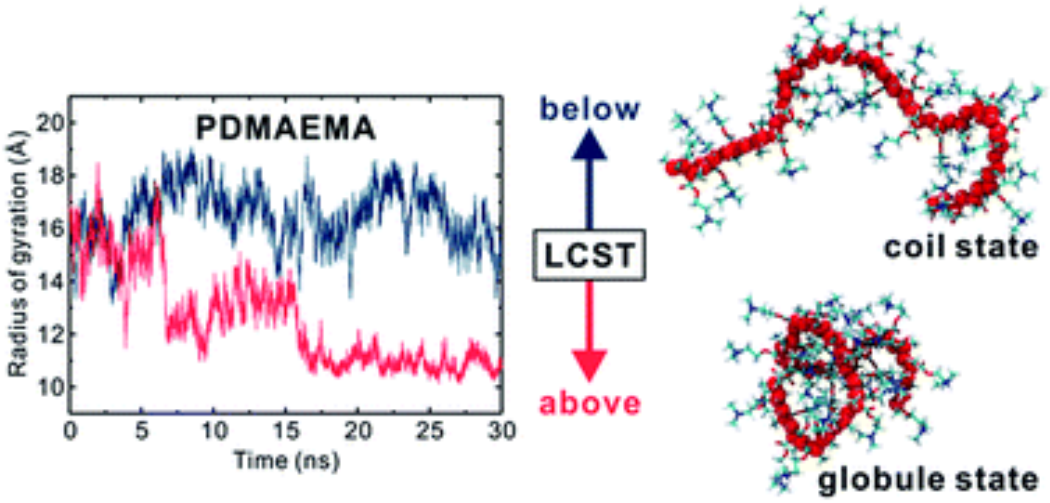

Figure 2.1. Coil-to-globule transition of poly(2-dimethylaminoethyl methacrylate) (PDMAEMA) in aqueous solution. Adapted from ref. 37 with copyright 2015 The Royal Society of Chemistry.

Temperature responsive polymers can be divided into two types; polymer having a lower critical solution temperature (LCST) and those having an upper critical solution temperature (UCST). LCST and UCST are critical temperature points below or above which the polymer chains and solvent are completely miscible, as shown in Figure 2.2. When a polymer solution is below the LCST, it is a homogeneous solution. Once the temperature rises above LCST, the polymer solution becomes cloudy. The inverse occurs for a polymer displaying a UCST; the polymer is solvated at high temperature and collapses when the temperature is decreased. The reason is that the variation of temperature induces a change in the solvent-polymer, solvent-solvent and polymer-polymer interaction. In a system

displaying a LCST, the increase in temperature lead to an increase in the entropy of the solvent in the system and this increase in entropy is more than lost enthalpy of hydrogen bonds between the water molecules and the polymer. Hence the LCST is an entropically driven effect while the enthalpy of the system governs UCST. [38]

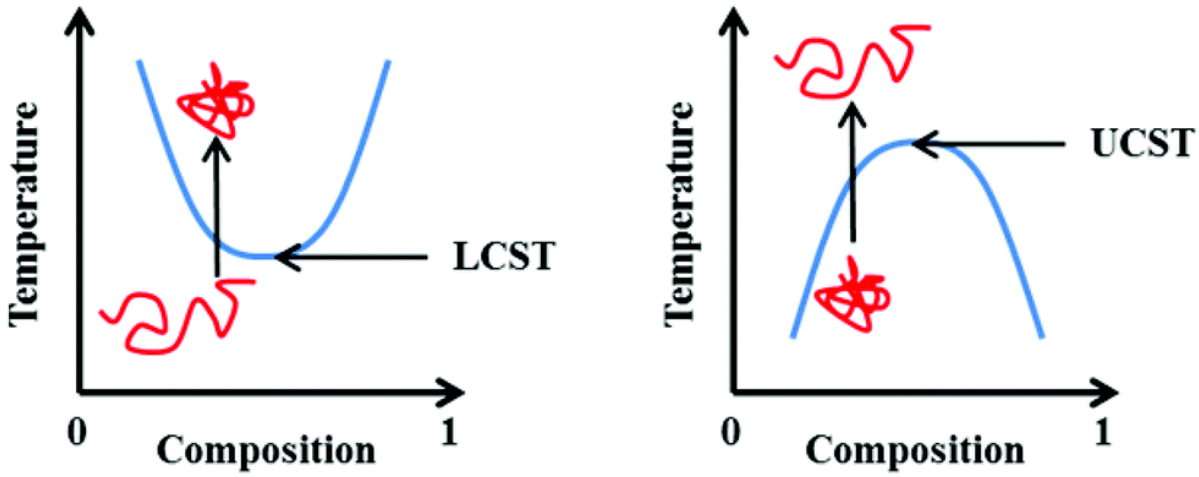

Figure 2.2. Representation of the phase transition associated with the LCST and UCST. Adapted from ref. 39 with copyright 2015 The Royal Society of Chemistry.

A well-known example of temperature-responsive polymer is poly(N-isopropylacrylamide) (PNIPAM). PNIPAM has a LCST at around 32 ℃, which is close to physiological temperature, hence this polymer is very promising for drug delivery and an array of biologically driven applications. The conformation of poly(N-isopropylacrylamide) (PNIPAM) can be reversibly changed from coil to globule by altering the temperature. Thus, when using a

PNIPAM gel loaded with a payload to be released, the release can be trigger by an external change in temperature by triggering the system to go through this cole-to-globule transition. Additionally, for individual polymer chains, the LCST of the coil-to-globule transition can be tuned by adjusting the polymer composition, the LCST shifts to higher or lower temperature by the copolymerization of NIPAM with a hydrophilic or hydrophobic monomer, respectively. Many other temperature-responsive polymers have been studied, such as, poly[*N*-[2-(diethylamino)ethylacrylamide]],[39] poly(*N*,*N*-dimethylaminoethyl-methacrylate),[39-41] poly(*N*,*N*-diethylaminoethyl methacrylate),[42] poly[oligo (ethyleneglycol) methacrylate]. [43-45] Such a range of temperature-responsive polymers offers various options for applications with different temperature response ranges.

Temperature responsive polymers can be used to prepare nanocarrier for the controlled delivery of drugs. For example, using PLGA-*block*-(PEGMEMA-*co*-PPGMA) nanocarriers, it was shown that the encapsulated drugs were released below the thermal transition temperature, simultaneously the efficiency of the cellular uptake of those nanocarriers was enhanced by small increases in temperature because of the surface of the carrier became moderately hydrophobic above the LCST leading to an effective adhesion

of the proteins of the serum which favored cellular uptake (Figure 2.3). [46]

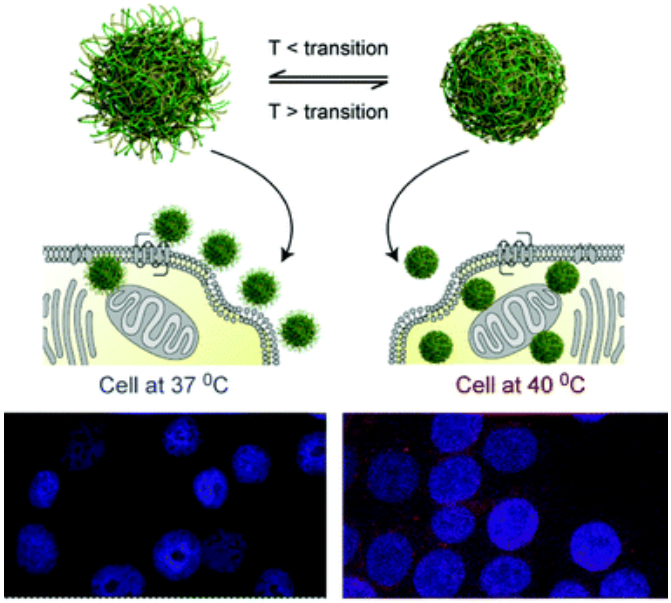

Figure 2.3. Formulation of temperature-responsive polymer and the proposed enhancement in cellular uptake due to change in surface corona upon thermal triggering. Adapted from ref. 46 with copyright 2013 The Royal Society of Chemistry.

2.1.2 pH-responsive polymers

pH-responsive polymers can respond to changes in the pH value of the solution by undergoing structural and property changes such as charge, chain conformation, solubility, and configuration. The most direct method to form pH-responsive polymers is to synthesize polymers using ionizable or acid-cleavable monomers. Ionizable polymers have weak acids or bases that can be ionized by changing the

pH value of the solution, such as poly(carboxylic acid)s,[47] poly(phosphonic acid)s,[48] poly[(2-diethylamino)ethyl methacrylate],[49] and poly[(2-diisopropylamino)ethyl methacrylate.[50] Additionally, pH-responsive polymers can be synthesized from peptides, including (L-glutamic acid) (PLGA), poly(histidine) (PHIS), and poly(aspartic acid) (PASA), which are biocompatible and degradable. [51-53]

Some of the most studied ionizable anionic polymers are polymerized using acrylic acid, methacrylic acid, boronic acid, and their derivatives.[54-57] Ionizable anionic polymers will change their solvation state and conformation when the pH value of the environment is raised above the pK_a of their monomer. For example, in Figure 2.4, pH-responsive polymers can be used as pH sensors, Seo *et al*. reported that liquid crystal 4-cyano-4′-pentyl-biphenyl (5CB) molecules were encapsulated pH-responsive polymers (PAA-*b*-PCBOA) using spin-coating, and the order of the 5CB domains was responding to the swelling of the (PAA-*b*-PCBOA) matrix itself responding to changes in the pH value of the environment. The shrinking and swelling mechanism of the PAA chains in the diblock copolymer layer changed the mechanical stress on the 5CB domains and influenced the LC order in those domains.

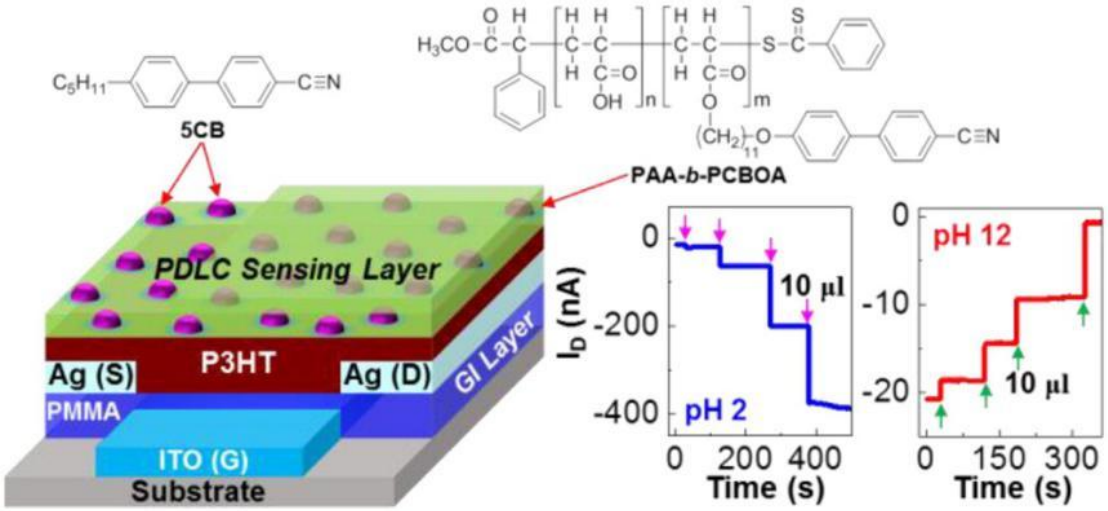

Figure 2.4. Formulation of temperature-responsive polymer and the proposed enhancement in cellular uptake due to change in surface corona with thermal response. Adapted from ref. 58 with copyright 2016 American Chemical Society.

pH-responsive polymers can be synthesized from acid-cleavable polymers and have attracted attention for applications in drug delivery. The pH gradient existing between the normal and tumor tissue can induce the cleavage of acid-cleavable polymers, resulting in the release of the cargoes.[59-61] For example, an acid-cleavable polymer PCL_{21}-*b*-P(*a*-OEGMA)$_{11}$ was used to prepare responsive polymer-carriers. In those carriers, the drug release in vitro was significantly promoted at pH 5.0 in comparison to pH 7.4 due to the acid-cleavable linkages in the polymer (Figure 2.5).

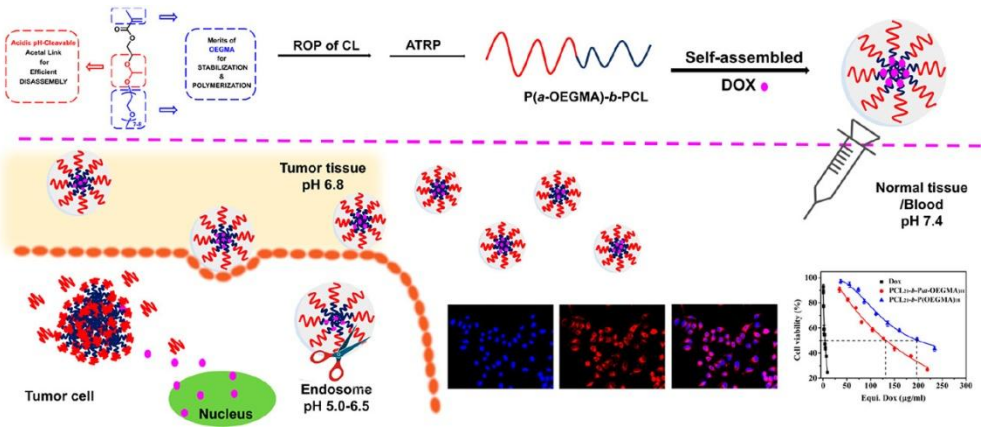

Figure 2.5. Mechanism of acid-cleavable nanocarriers and cargoes release at acid pH. Adapted from ref. 62 with copyright 2018 American Chemical Society.

2.1.3 Light-responsive polymers

Light is an interesting cue to control the properties of materials, including conformation, polarity, amphiphilicity, optical chirality, conjugation and so on. One of the main upsides of using light is that it can be switched on/off with a high spatial and temporal precision resulting in the control of the material properties with a high spatio-temporal resolution (Figure 2.6).[63] Light responsive polymers possess advantages in comparison to other stimuli-responsive polymers, the cue can be applied locally in a non-contact and remote-controlled manner, the light intensity can easily be tuned to control the time and position of the response accurately. The light-responsive polymers are commonly prepared by polymerizing light-responsive segments into copolymers. [64] The response of the polymer to light

can either result from a reversible or irreversible transformation.

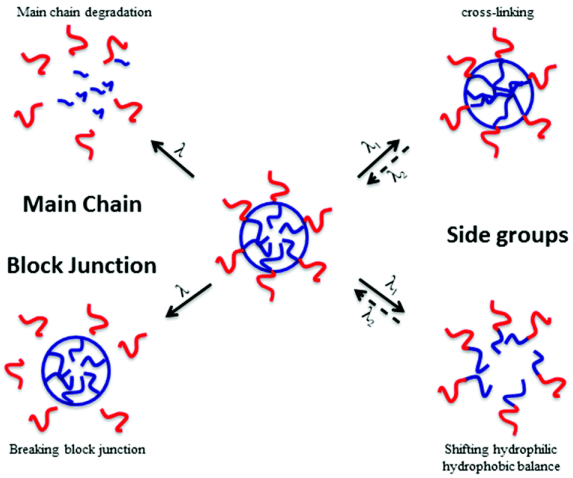

Figure 2.6. Effect of the photo-responsive moieties onto the behavior of micelles in solution under irradiation Adapted from ref. 65 with copyright 2018 American Chemical Society.

Light responsive molecules undergoing reversible photoisomerization upon irradiation include chemical compounds like azobenzene (AZO), [66-68] spiropyran (SP) [69-72] and so on. For example, Schenning and co-workers reported that light-responsive soft actuator prepared using monomer *ortho*-fluoroazobenzene and three nematic monomers (Figure 2.7). The resulting films were self-oscillating because of the *trans*→*cis* and *cis*→*trans* isomerization of the AZO groups initiated by green and blue light, respectively. The film showed an unprecedented continuous chaotic oscillating motion upon exposure to non-concentrated sunlight and was reproduced by exposure to the combined light of blue and green LEDs.

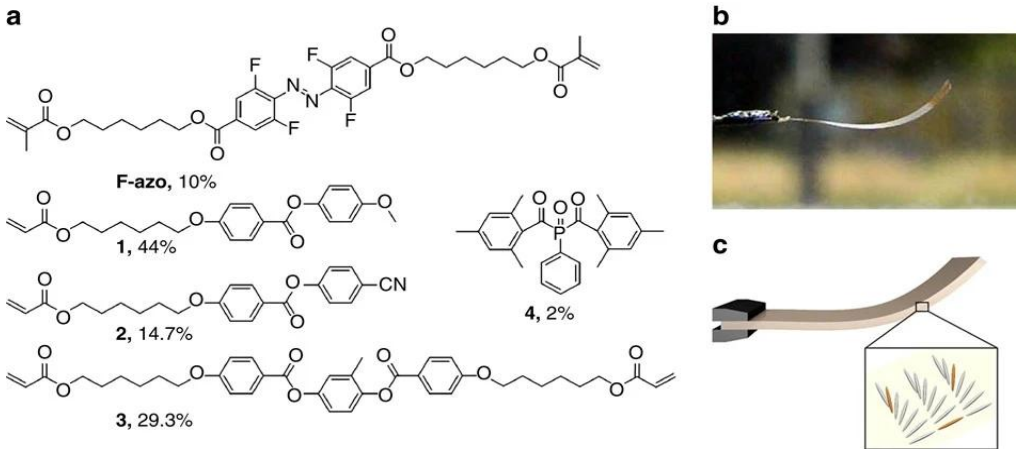

Figure 2.7. a) Chemical structures of components used to prepare the nematic liquid crystalline network. b) Photograph of splay-oriented film after removal from the cell under ambient interior light (homeotropic side on top) and c) schematic of the LC splay aligned film (grey) containing F-azo molecules (orange). Adapted from ref. 73 with copyright 2016 Nature.

An irreversible light-responsive behavior can be developed in polymers containing photo-cleavage units. One example is the o-nitrobenzyl ester (ONB) an important chromophores featuring irreversible light-responsive behavior. For example, Meier and coworkers prepared photo-triggerable nanocarriers by the self-assembly of a photocleavable amphiphilic block copolymer (PMCL-*ONB*-PAA). They encapsulated payloads, including dye and proteins, yielded a versatile carrier system for many therapeutic applications. The payloads of the nanocarriers were released upon the reorganization of the polymer chains, and the release rates of the

cargoes depended on UV intensity. Hence the release behavior of cargo occurred in a controlled manner (Figure 2.8). [74]

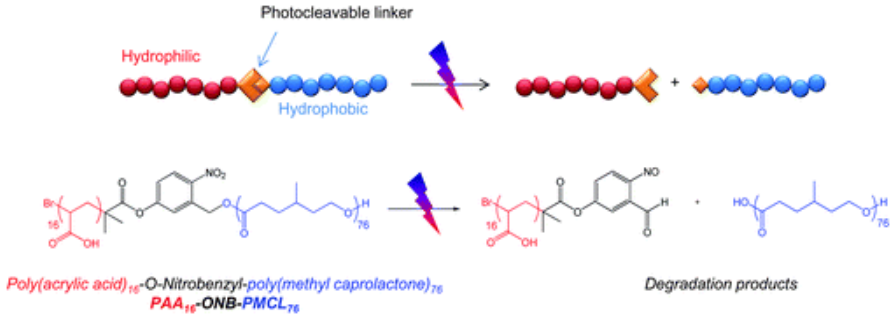

Figure 2.8. Schematic view of the amphiphilic photocleavable block copolymer, chemical structure of the poly(methyl caprolactone)-*ONB*-poly(acrylic acid) diblock copolymer, and its degradation products upon UV irradiation. Adapted from ref. 74 with copyright 2011 The Royal Society of Chemistry.

Amongst light-responsive switches, spiropyrans are extraordinarily attractive. They find application as smart-switch module in the desing of reversible photoacid, which can be used to tune the pH of aqueous solutions. Specifically, the spiropyrans-based photoacid can be used not only to transforms into a strong acid with light but also to stop or reverse it by turning off the light. Many studies have focused on the smart switches based on light-responsive materials, which can be either immobilized on the surface or incorporated in substrates, [75-77] hence tune the properties of materials. One case is water soluble alkyl-sulfonate spiropyran has a MEH structure, which is stable in both aqueous and organic media without the

addition of an external acid (Figure 2.9). The absorption of MEH decreased at 420 nm when shining the light, a new absorption peak at 300 nm appeared, which belongs to the SP, resulting in the increased acidity because of MEH-to-SP transformation. In the dark, the absorption intensity of MEH went back to the starting acidity within 5 min. The mechanism is based on the light induces trans-cis isomerization of MEH, followed by the release of protons as cis-MEH become cis-ME, then, a nucleophilic ring-closing reaction to yield SP. The process is reversible, and SP can revert back to MEH in the dark.

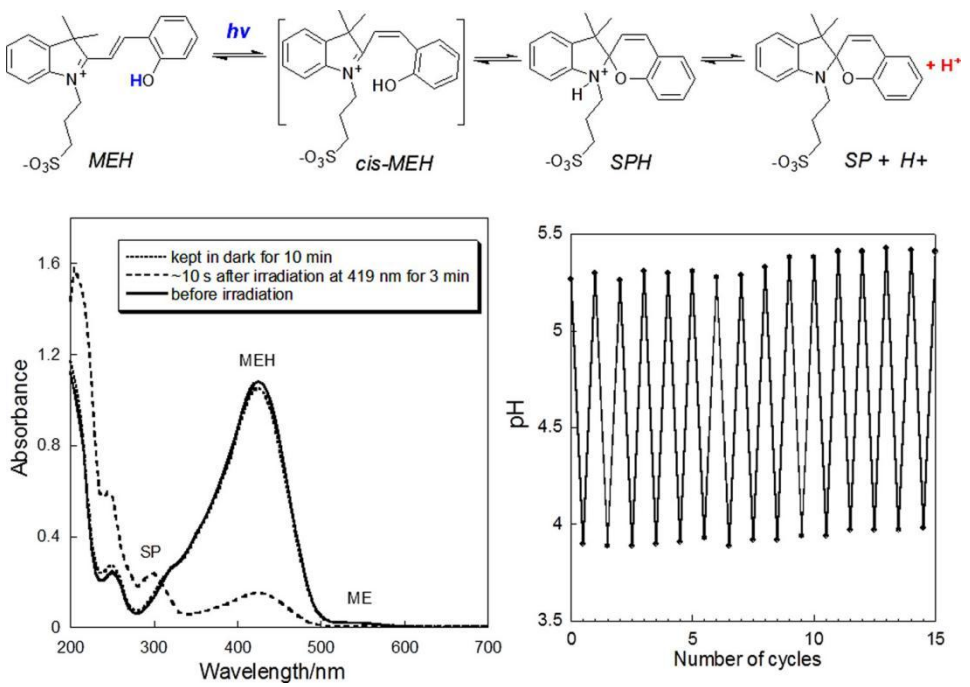

Figure 2.9. Photoreaction of photoacid, UV-vis absorption of a solution of photoacid before irradiation, 10 s after irradiation for 3 min, and kept in the dark for 10 min after irradiation (lower left), and the pH under cycles of irradiation and

darkness (lower right). Adapted from ref. 78 with copyright 2011 American Chemical Society.

Most of the works reported so far on photoacid materials have focused on solutions of small-molecules photoacid. However, embedding such smart switches in solid photoacid materials is of great interest. For example, either the photoacid molecules are copolymerized with other functional monomers, or biomolecules can be covalently linked with photoacids. Such photoacid polymers can potentially improve solubility and compatibility of photoacid molecules in different media and can avoid leakage problems. Functional materials covalently carrying photoacids do not require a solution of photoacids to alter their properties under light and are capable of producing a localized proton concentration inside and around the materials. The cellular pH dramatically influences the activity of many enzymes, which is related to many diseases; therefore, solid photoacid materials photoacids have great potential for biomedical applications, either the effects of local pH on cell growth and cell communication or photocontrolled drug delivery. For these purposes, effective methods to link photoacids to polymers and other functional materials are highly desirable. [79]

2.1.4 Redox-responsive polymer

Redox-responsive polymers have potential in drug delivery due to the existence of

different redox potential within different cells. Many studies have been constructed around the use of glutathione, which is found to have a much higher concentration in tumor tissues in comparison to the extracellular fluid, and thus creates a high intracellular redox potential.[80] Redox-responsive polymer creates the opportunity to benefit from this difference and encapsulate cargoes that could be specifically released in the tumor tissues. Functional linkages like disulfide or diselenides are sensitive to such differences in the redox-potential of the environment.

For example, Meng and coworkers prepared nanocarriers using the disulfide-linked dextran-*b*-poly(ε-caprolactone) amphiphilic block copolymer (Figure 2.10). The micelles released their cargo, doxorubicin an anti-cancer drug, within 10 h after the addition of 10 mM dithiothreitol. Confocal laser scanning microscopy images demonstrated that drug-loaded nanocarriers significantly inhibited RAW 264.7 cell reproduction.

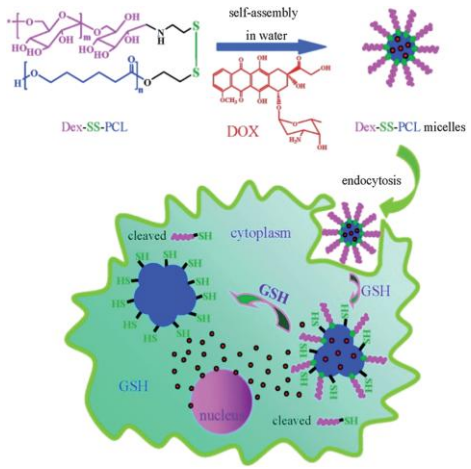

Figure 2.10. Schematic presentation of redox-responsive Dex-SS-PCL micelles and the intracellular release of DOX. Adapted from ref. 81 with copyright 2010 American Chemical Society.

In another case, reduction-responsive polymers, the diselenide-containing polyurethane triblock copolymer PEG-PUSeSe-PEG, was used to prepare nanocarriers. The Se-Se bonds were cleaved and oxidized to seleninic acid in the presence of oxidants and reduced to selenol in a reducing environment. Rhodamine B encapsulated in such polymer was released within 5 h after the addition of 0.01 M gluthathione (Figure 2.11).

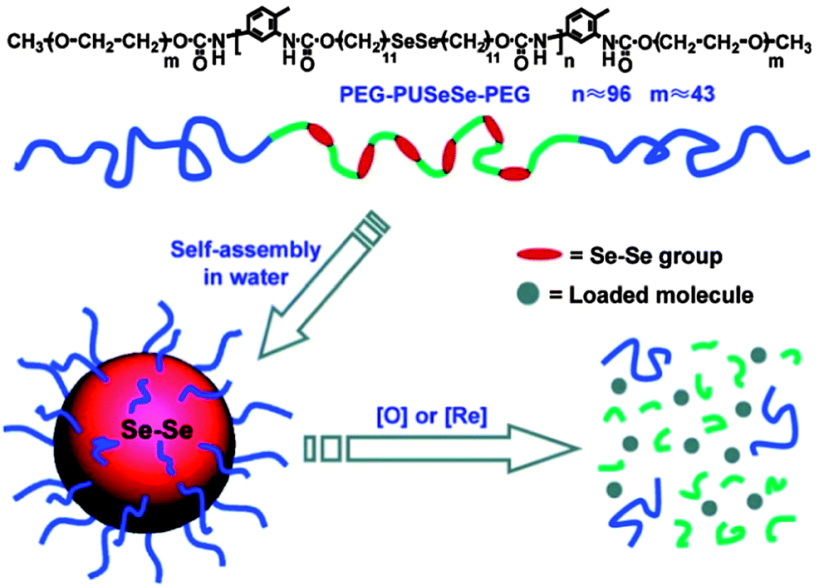

Figure 2.11. Redox-responsive diselenide-containing PEG-PUSeSe-PEG block copolymers. Adapted from ref. 82 with copyright 2010 American Chemical Society.

2.2 Synthesis of Colloidal Polymer Particles

Polymer particles have been studied for many years in materials science, either as final material in application like drug delivery or as building blocks to make more complex structures such as colloidal crystals used as sensors.[83-89] One of the reasons for the wide range of potential applications of polymer nanoparticles is that their properties can be tuned by the composition of the polymers, as well as by the shape and the size of the nanoparticles. Furthermore, the surface of the polymer particles can be modified with functional molecules during preparation or post-modification. A number of techniques exist to produce such multifunctional polymer particles, including self-assembly,[90] emulsion polymerization,[91] miniemulsion polymerization.[92]

2.2.1 Emulsion polymerization

Emulsion polymerization is one of the most common methods to prepare a wide range of polymer particles. Emulsion polymerization is a unique process where insoluble monomers are dispersed in a solution of surfactant. The monomer forms large monomer droplets in the continuous phase. Additionally, the concentration of the surfactant required in emulsion polymerization needs to be sufficiently high so that micelles can be formed in the continuous phase. The monomers are mostly stabilized in large droplets and more marginally within surfactant micelles (Figure

2.12). The mechanism of emulsion polymerization is summarized through three different intervals.[93] In the first interval, the initiator is introduced into the continuous phase where the radicals diffuse to monomer micelles, while in the continuous phase, the radical can react with monomer molecules also dissolved in the continuous phase; once the radical reach the micelles it can initiate the polymerization of the monomer-swelled micelles. The total surface area of the micelles is much larger than the total surface area of the monomer droplets; therefore, the initiator typically reacts in the micelles, not with the large reservoir droplets. In the second interval, the polymerization reaction quickly proceeds within the micelles. As the monomer conversion increase within the micelle, more monomer from the droplets will diffuse to the growing particle. In the third interval, all the free monomer reservoirs disappear and all remaining monomers are located in the particles.

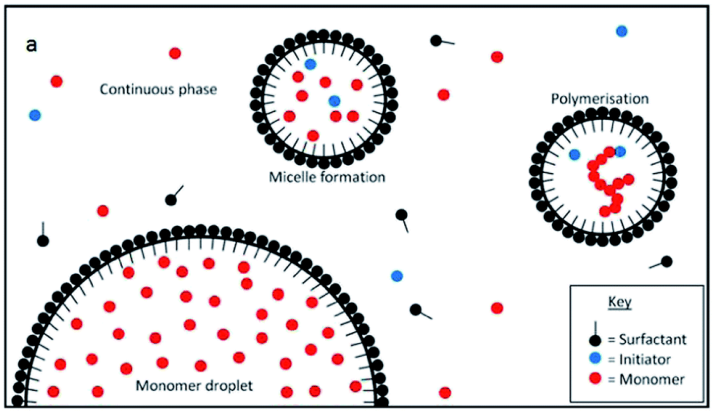

Figure 2.12. Schematic representation of emulsion polymerization.Adapted from

ref. 94 with copyright 2014 The Royal Society of Chemistry.

There are many monomers used for the emulsion polymerization including: acrylates, methacrylates, styrene, vinyl acetate, isoprene, and so on. These emulsion polymers have been developed a wide range of applications such as synthetic plastic pigments coatings, adhesives, rubbers, thermoplastics, rheological modifiers.[95- 97]

2.2.2 Polymer nanoparticles from miniemulsion polymerization

Miniemulsion polymerization is a very useful technique to produce high solid content polymer nanoparticles with a size between 50 and 500 nm. Many different monomers such as acrylates, methacrylates, fluoroacrylates, and acrylamides have been use to make nanoparticles via miniemulsion polymerization.[98-102]

In general, miniemulsions are typically formed by a mixture of a solvent forming the continuous phase containing a surfactant, and the monomer mixture forming dispersed phase under containing a costabilizer. This biphasic mixture is subjected to high power forces using ultrasound or homogenizers to break the dispersed phase in nanometer-size nanodroplets (Figure 2.13).[103] The surfactants are compounds that lower the interfacial tension between the solvent and the monomer droplets to prevent coalescence of the droplets. The costabilizer can create an osmotic pressure in the droplets to counteract the Ostwald ripening; the reason is

that costabilizer is soluble in dispersed phase, but insoluble in continuous phase, resulting in an increasing stability of emulsion by preventing the diffusion of monomer molecules from droplet to droplet.[104] This is essential because as opposed to emulsion polymerization, each droplet in a miniemulsion can be considered as an independent reactor.

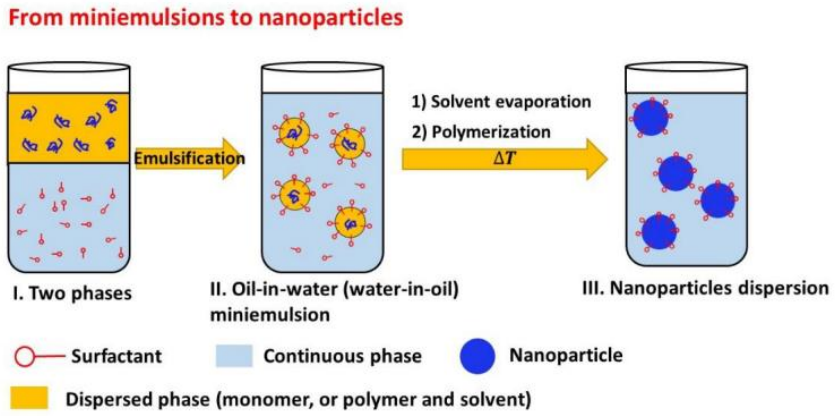

Figure 2.13. Production of polymer nanoparticles by miniemulsion process.

Adapted from ref. 105 with 2017 copyright Elsevier

Polymerization in miniemulsions droplets have been used to prepare homogeneous nanoparticles by many methods, including radical, anionic, cationic, catalytic, ring-opening metathesis acyclic diene metathesis polymerization (Figure 2.14).[106-108]

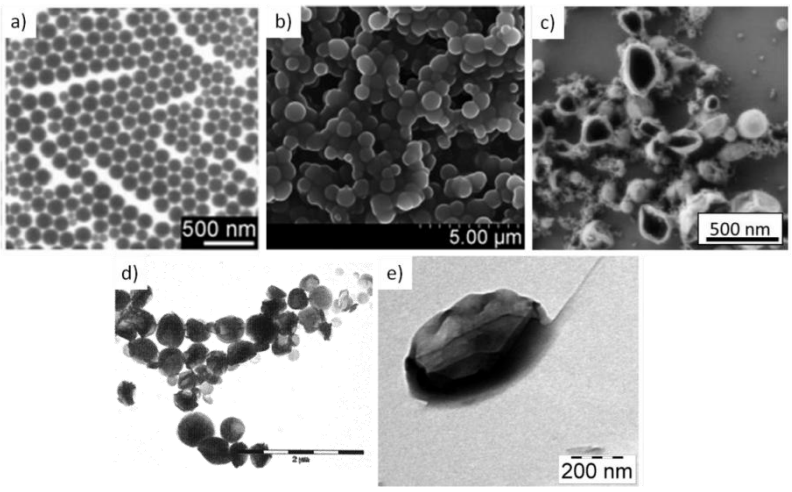

Figure 2.14. Images of a) polyisoprene nanoparticles as obtained by radical polymerization (adapted from ref. 109 with copyright 2009 John Wiley and Sons); b) poly(butyl cyanoacrylate) nanoparticles as obtained by anionic polymerization (adapted from ref. 110 with copyright 2007 American Chemical Society); c) protein nanocapsules produced by interfacial polyaddition polymerization (adapted from ref. 111 with copyright 2015 American Chemical Society); d) polyolefin nanoparticles as obtained by catalytic polymerizations (adapted from ref. 112 with copyright 2002 American Chemical Society); and e) Nanoparticles as obtained by ring-opening metathesis polymerization (adapted from ref. 113 with copyright 2007 American Chemical Society).

Miniemulsion polymerization is an excellent method to prepare nanoparticles requiring some shape-controlled, like polymer capsules. Such nanoparticles with a more complex structure are finding increasing applications in a variety of fields

like encapsulation, release and delivery of drugs. For example, protein nanocapsules can be synthesized by an interfacial polyaddition reaction occurring at the interface of protein-containing nanodroplets in water-in-oil miniemulsions (Figure 2.15). In such case, a protein like bovine serum albumin, a payload like a fluorescent dye and sodium salt is dissolved in the water phase, the sodium salt act as a Laplace pressure agent and is used to suppress the Ostwald ripening. The non-aqueous phase is composed of a water-immiscible solvent (cyclohexane) and a nonionic surfactant. Such a biphasic system is used to make a miniemulsion using ultrasonication, then a the crosslinker, such as 2,4-toluene diisocyanate (TDI), can be added dropwise to the continuous non-aqueous phase to react with the nucleophilic groups of the protein (hydroxyls and amines), resulting in the formation of water-insoluble nanocontainers with a dense and crosslinked polypeptide shell.[114]

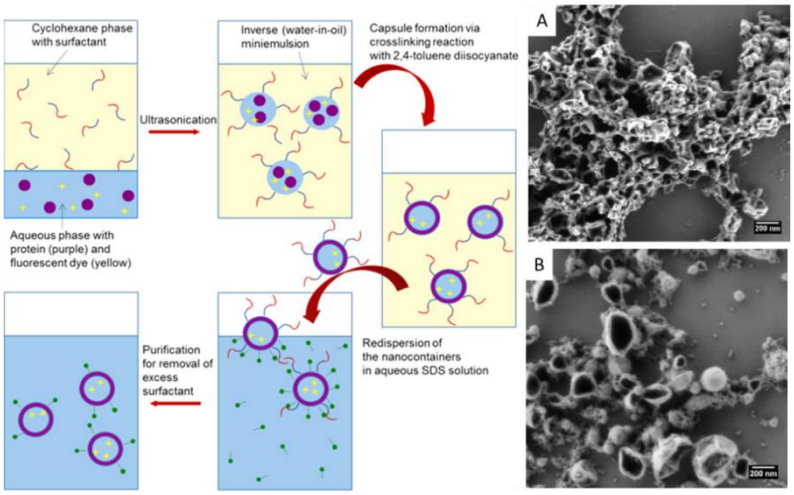

Figure 2.15. Synthetic procedure for protein nanocontainers via a miniemulsion process. Adapted from ref. 114 with copyright 2015 American Chemical Society.

Although miniemulsion-based techniques are almost a universal method to produce polymer nanoparticles, the prepared polymer nanoparticles from miniemulsion technique are usually spherical particles, it is challenging to prepare the particles with shape-anisotropy.

2.2.3 Self-assembly of block copolymers in solution

Block copolymer are polymers where two or more polymer segments of different chemical composition are linked together.[115] When the different polymer segments in the block copolymer have different solubility, block copolymers can use versatile polymer chains to create diverse polymer structures in suspension.[116, 117] When the different polymer blocks are incompatible, the block copolymer will self-assembly into a variety of objects,[118] including spheres, cylinders, bicontinuous structures, lamellae, vesicles, and many other complexes or hierarchical assemblies (Figure 2.16), the driving factors for the formation of different structures are the balance of compatibility/incompatibility of the blocks with the environment and the size of the blocks.[119-121]

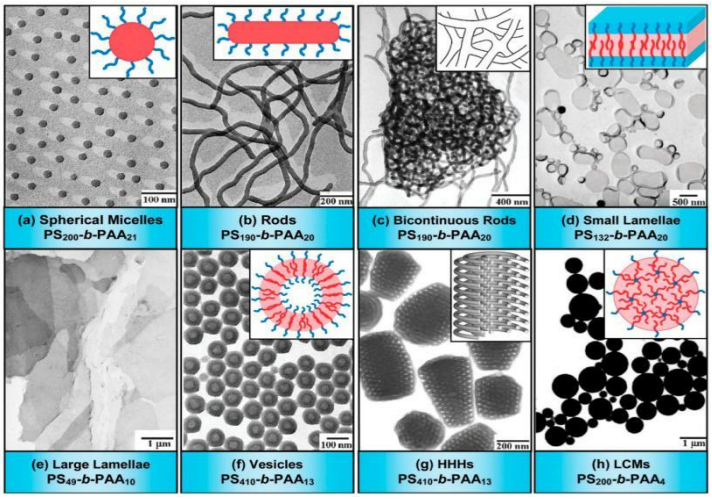

Figure 2.16. TEM images and corresponding schematic diagrams of various morphologies formed by amphiphilic PSm-b-PAAn copolymers(m and n denote the degrees of polymerization of PS and PAA, respectively): (a) spherical micelles; (b) rods; (c) bicontinuous rods; (d) small lamellae; (e) large lamellae; (f) vesicles; (g) hexagonally packed hollow hoops; (h) large compound micelles. Adapted from ref. 122 with copyright 2012 The Royal Society of Chemistry.

The most common and extensively studied block copolymers are amphiphilic block copolymers consisting of two blocks. When one block can be dissolved in a solvent, but the other block is not miscible in that solvent, the copolymer chains can reversibly self-assemble to micelles. Usually, the micelle can be prepared using the solvent exchange method. For example, the most common method consists to first dissolve the diblock copolymer in a good solvent for both blocks, such as in *N,N'*-dimethylformamide (DMF), tetrahydrofuran (THF), or dioxane, afterward,

the micelle can be obtained using dialysis against water or a selective solvent for one of the block. The resulting micelles have a more or less unswollen immiscible core surrounded by a shell of flexible swollen polymer chains at the surface of micelles.[123, 124]

The morphology of the polymer micelle is determined by the nature of the block copolymer used and the conditions of the self-assembly. The packing parameter (p) defined in equation (1):

$$p = v / a_0 l_c \qquad \text{(eq 1)}$$

where v is the volume of the hydrophobic chain, a_0 is the optimal area of the head group, l_c is the length of the hydrophobic tail. Generally, when $p \leq 1/3$, spherical micelles can be made, cylindrical micelle are obtained when $1/3 \leq p \geq 1/2$, and vesicles when $1/2 \leq p \geq 1$ (Figure 2.17).[125]

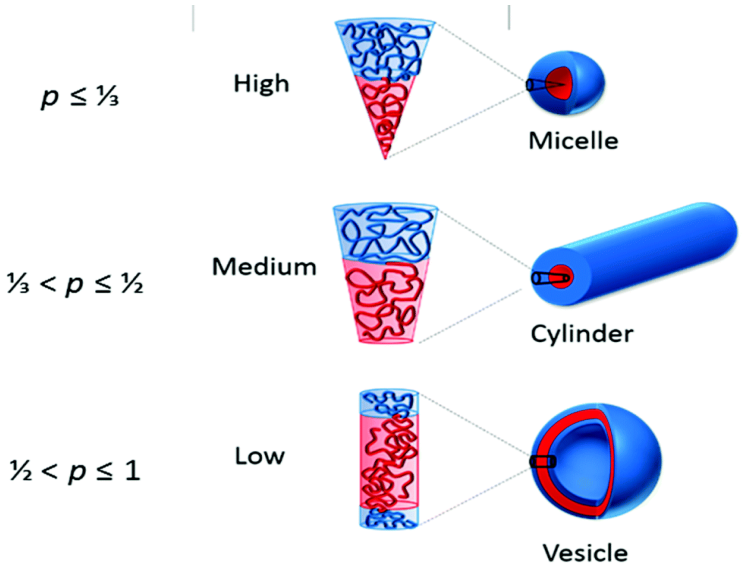

Figure 2.17. The types of formed nanostructures of amphiphilic diblock copolymers due to the inherent curvature of the polymer, as estimated by chain packing parameter. Adapted from ref. 126 with copyright 2017 The Royal Society of Chemistry.

In practice, it is extremely difficult to calculate the packing parameter (*p*). Therefore the volume occupied by both blocks is first determined by the degree of polymerization for each block, which is the more commonly considered parameters.[127] Furthermore, the volume of the hydrophobic chain changes when they have different architectures, *e.g.* polymer containing branched side chains usually occupy a larger volume than their linear counterpart at the same degree of polymerization. Moreover, altering the solvent interaction of one block will also change the volume of this chain, for example, a polymer in a good solvent will be more swollen and occupied a larger volume, and in contrast, the same chain will occupy a smaller volume in a poor solvent.

However, the traditional method of self-assembly of block copolymers always faces some obstacles, which hinder the applications. Usually, the controlled self-assembly of block copolymers is performed in very dilute solution, and this method can only with difficulty be used to prepare micelles at a large scale. Moreover, the packing parameter is challenging to calculate so that the shape of

micelles cannot be precisely controlled or predicted. Hence it can be very time-consuming to tune all the parameters involved in the self-assembly, including the degree of polymerization of each block and solvent interaction.

2.2.4 Polymerization induced self-assembly

Polymerization induced self-assembly (PISA) is an attractive and promising method that prepares micelle in a one-pot process. The basic principle of PISA is that a monomer, an initiator, and a macromolecular stabilizer acting as the site of reaction are initially soluble in the reaction medium, afterward, upon polymerization, the block copolymer chains formed by the addition of the monomers on the macromolecular stabilizer precipitate once a critical chain length is reached, leading to the formation of a particle (Figure 2.18). PISA has been studied for many years, and can be performed using controlled/living radical polymerization such as nitroxide-mediated radical polymerization (NMP), atom-transfer radical-polymerization (ATRP), reversible addition-fragmentation chain-transfer polymerization (RAFT), and iodine-transfer polymerization (ITP).[128-132] Among those methods, ATRP and RAFT polymerization are the two most versatile ways to prepare nanoparticle in a large scale.

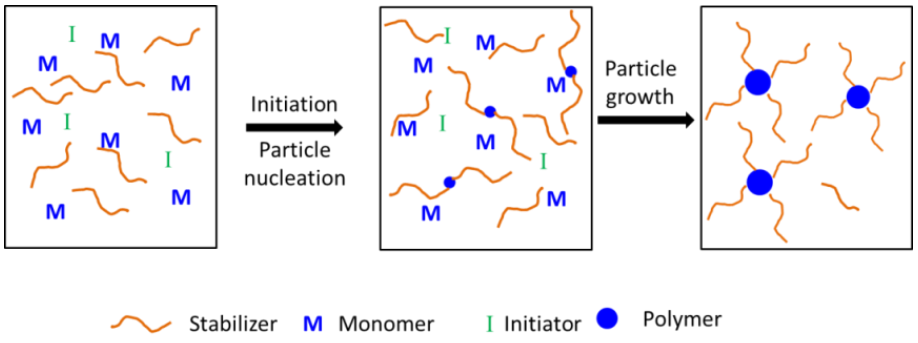

Figure 2.18. Production of polymer nanoparticles by dispersion polymerization.

PISA proceeds through a mechanism similar to the formation of polymer nanoparticles by precipitation polymerization. The main exception is that the stabilizer is tethered to the aggregate after polymerization. Using controlled polymerization mechanism like RAFT or ATRP it is possible to immobilize the site of reaction (ATRP initiator, RAFT chain transfer agent) to a macrostabilizer that would remain swollen in the reaction solvent in the course of the reaction and provide the required colloidal stability to the growing polymer chains (Figure 2.19).[133]

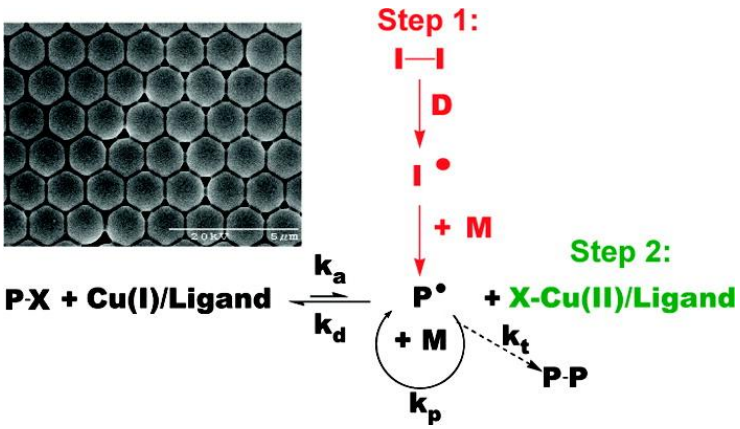

Figure 2.19. Polymer particles obtained through the ATRP polymerization of styrene in ethanol. Adapted from ref. 133 with copyright 2007 American Chemical Society.

Additionally, there are some studies used thermal-dependent monomers to prepare the colloidal nanoaparticles using PISA. For example, ATRP polymerization of N-isopropylacrylamide (NIPAM) in water using poly(ethylene glycol) methyl ether (PEG) as a macro-initiation was carried out. Since the LCST of PEG-*b*-PNIPAM was 38 ℃, the block copolymer acted as a surfactant above this temperature. When the polymerization temperature was run at 25 ℃, the block copolymer was soluble and a homogeneous solution was obtained, but phase-separation of ATRP polymerization formed micelles occurred when the polymerization temperature was raised to 50 ℃. Finally, using the same strategy, stable hydrogel nanoparticles can be formed in water by the addition of a small amount of N, N'-ethylenebisacrylamide as a crosslinker to the reaction.[134]

ATRP polymerization provides many choices for the selection of initiator and catalyst complex, but the selection the appropriate initiator, catalyst and reaction conditions need to be carefully considered because the activation rate constants of each composition are significantly different.[135, 136] Moreover, for normal ATRP, the amount of oxygen in the system is the main problem since oxygen can oxidized

the metal complex use as the catalyst to a metal with a higher oxidation state that would not undergo any polymerization.[137, 138] Additionally, monomers typically used in ATRP are molecules with substituents that can stabilize the propagating radicals, such as styrenes, (meth)acrylates, (meth)acrylamides, and acrylonitrile, hence the type of polymerizable monomer also influence their application.[139] Finally, the polymers prepared from normal ATRP polymerization always contain traces of the metal catalyst, which is not desirable for final applications, such as in the food industry or for biomedicine. Therefore, additional steps are needed to remove the metal from the final product.

Polymerization induced self-assembly using RAFT polymerization is a metal-free method which can be used in various solvents, a wide temperature range, and has a high functional group tolerance. Hence RAFT dispersion polymerization is a versatile method to prepare the polymer nanoparticles.[140] The reaction system needed to performed RAFT-PISA includes a macro-CTA, monomer, initiator and solvent. The critical step is the selection of the monomers and solvent. The monomer for the second block should be miscible in the chosen polymerization solvent so that the polymerization reaction starts in a homogeneous system, but the growing second block becomes solvophobic at some critical average degree of polymerization of the second block. Then, a transition from a homogeneous to

heterogeneous polymerization process occurs, which results in the in situ self-assembly (Figure 2.20). The morphologies of the micelle can be tuned by varying the solid content and the degree of polymerization.[124-127]

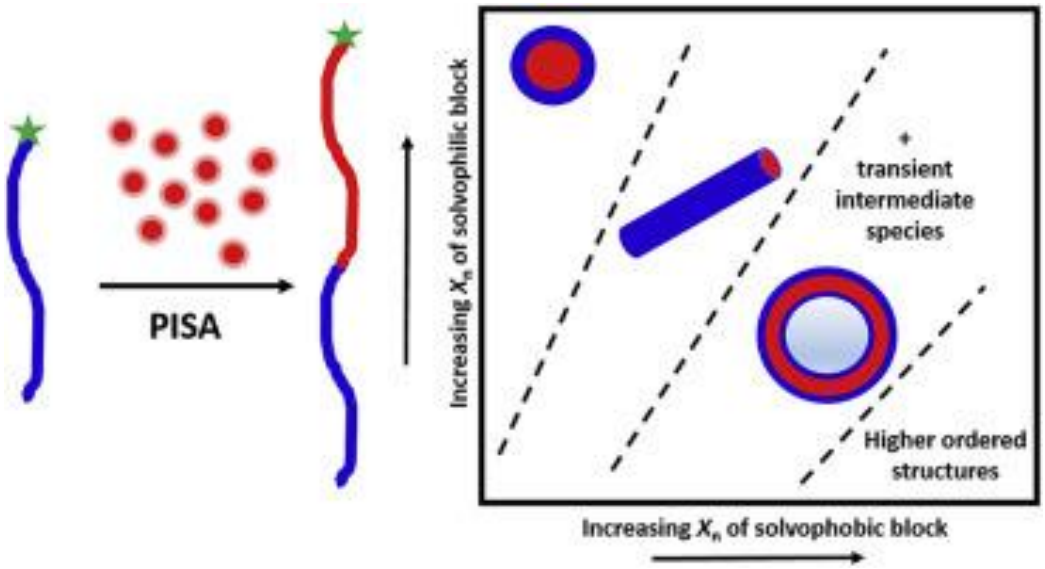

Figure 2.20. Block copolymer formation with RAFT dispersion polymerization. Adapted from ref. 140 with copyright 2016 Elsevier.

For example, RAFT alcoholic dispersion polymerization has been used to prepare nanoparticles at relatively large solid content, consisting of a variety of monomers such as poly(2-hydroxyethyl methacrylate-b-benzyl methacrylate) ($PHEMA_n$-$PBzMA_m$) and poly(2-hydroxypropyl methacrylate-b-benzyl methacrylate) ($PHPMA_n$-$PBzMA_m$).[141-145] Both the micelles composition and the reaction conditions, ranging from the solvent selection, the total solids content to

the degree of polymerization of the core-forming PBzMA chains and macro-CTA were shown to influence the resulting micellar structures obtained (Figure 2.21).

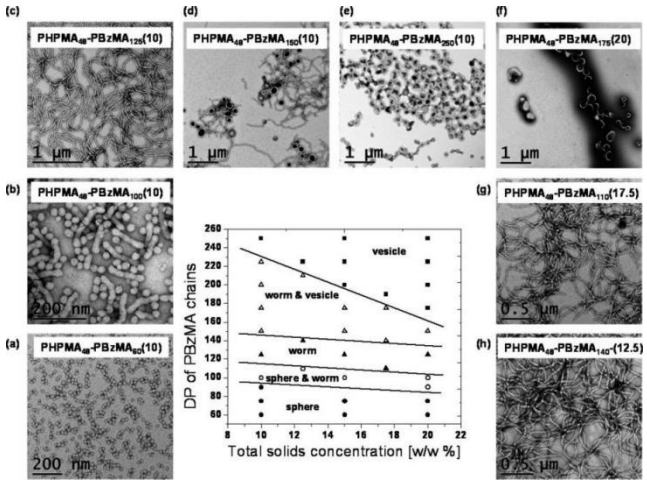

Figure 2.21. Representative phase diagram demonstrating the evolution of particle morphologies during the polymerization. Adapted from ref. 145 Copyright 2013 American Chemical Society.

In addition to the control of the original morphologies of micelles, thermo-responsive system can be prepared using RAFT-PISA. For example, thermo-responsive nanoparticles were prepared by the polymerization of a water-insoluble PNIPAm block forming the hydrophobic core of the micelles during polymerization at 70 ℃. Such micelles can be crosslinked to form responsive nanoparticles (Figure 2. 22).[146]

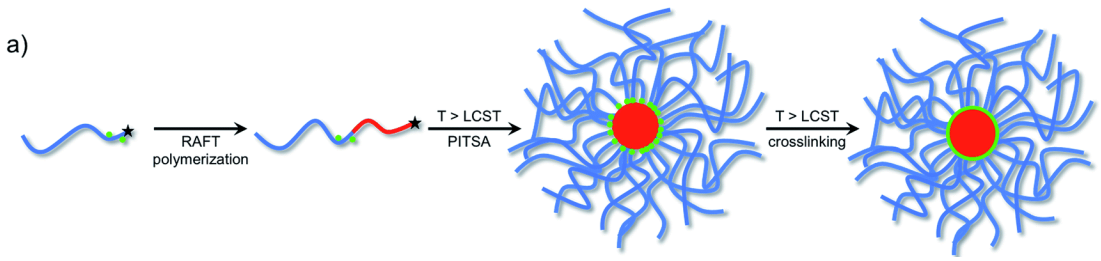

Figure 2.22. RAFT polymerization chain-extension of a hydrophilic macro chain transfer agent at 70 ℃ resulted in different self-assembled polymeric nanoparticle morphologies that were subsequently crosslinked. Adapted from ref. 146 Copyright 2015 The Royal Society of Chemistry.

In summary, the polymerization induced self-assembly (PISA) clearly offers a remarkably broad platform for the rational design of block copolymer nano-objects. Indeed, given its efficiency, versatility, and potential scalability, this approach may well ultimately prove to be the preferred synthetic route for the preparation of many vinyl-based amphiphilic diblock copolymers for commercial applications.

2.3 Application of Smart Polymer Nanoparticles

Smart polymer nanoparticles are usually formed using stimuli-responsive polymers. The smart polymer nanoparticles undergo structural changes upon exposure to external or internal stimuli, such as temperature, voltage, light, pH or mechanical loading,[147] which can tailor the nanoparticle properties and assemblies. Polymer nanoparticles have attracted considerable attention because of their broad

applications, such as rheology modifiers,[148] controlled drug-delivery and release systems,[149-151] coatings that are able to interact with and respond to their environment,[152-154] mimic the action of muscles[155] and sensor.[156-158]

2.3.1 Rheology modifier

Rheology modifiers are used to control the rheological properties of liquids and gels and influence their flow, leveling, and final appearance. Usually, the rheology is studied based on the viscosity under different shear rates. Rheology modifiers are mainly used to tune the stabilization of complex suspensions, for example, to prevent flocculation and coalescence during transport and storage while still allowing the product to flow during application.

The most common rheology modifiers are natural or synthetic polymers, which are often water-soluble polymers dispersed in a suspension. They can swell and take up space in the flow, such as carboxymethyl cellulose (CMC),[159] polyanionic cellulose (PAC),[160] polyacrylamide,[161] and polyacrylates,[162] which tune the viscosity of suspensions.

Polymer nanoparticles are the next industrial generation of rheology modifiers. The polymer nanoparticles possess an extra-large surface area to volume ratio, resulting in superior or even unexpected performances in flow.[163] Many studies have demonstrated that superior rheological properties were obtained by using very low

concentration of nanoparticles (usually <1.0 wt %). Moreover, it has been reported that the viscoplastic solid formed with nanoparticles, like colloidal gel have a more tunable structure (pore size) than viscoplastic solid made of polymer chains.[164] Additionally, the rheological modifiers based on polymer nanoparticles can be used to tune the viscosity of suspension using different properties, ranging from the rigidity of core, length of brush and aspect ratio of polymer nanoparticles.[165-168]

For example, the rheological and filtration performances of bentonite water-based drilling fluids could be tuned using microfibrillated cellulose and cellulose nanocrystals. The cellulose nanocrystals as rheology modifier showed several advantages comparing to microfibrillated cellulose, such as much smaller dimensions, more negative surface charge, higher stability in aqueous solutions, lower viscosity, and less evident shear thinning behavior, which influenced their behavior as water-based drilling fluids (Figure 2.23).

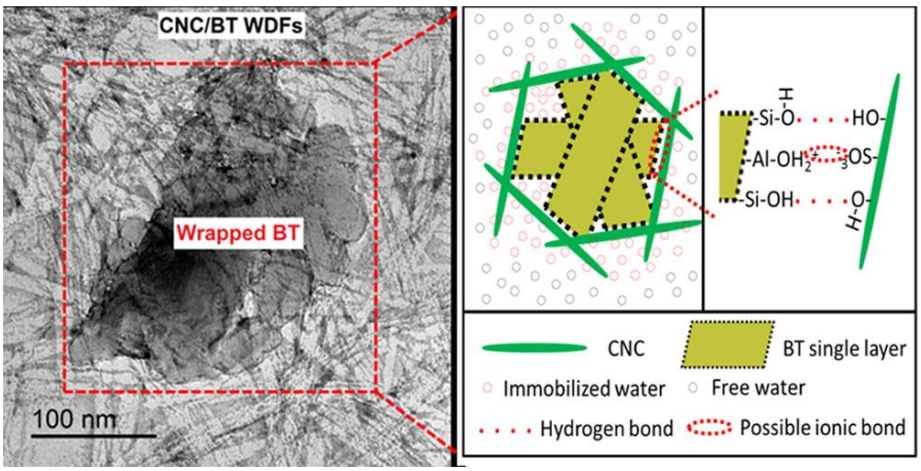

Figure 2.23. Schematic illustration of the interaction of cellulose nanocrystals and bentonite water-based drilling fluids. Adapted from ref. 168 Copyright (2015) American Chemical Society.

2.3.2 Corrosion protection

Studies report that the corrosion of material is a critical issue that has a globally massive effect on safety and on the economy. So far, organic coatings are one of the most common and used methods which control the corrosion of metallic materials. The mechanism of action of such organic coatings is to prevent the corrosion by creating a passive barrier on the surface of the metal, resulting in a decreased contact between the metal and an aggressive surrounding media. However, such passive barrier can become inefficient when damages in the coating occur, or when its properties are modified by weathering action, generating pores and microcracks. The damages, pores, and microcracks allow the contact of corrosive species with the metal surface, and the corrosion process is then initiated.[169]

In order to optimize the performance of the coating, the use of active protection coatings has been developed using responsive polymer nanoparticles in the last decade.[170, 171] In such “smart coatings”, the active agents is contained in polymer nanoparticles that are encapsulated into the coating matrix, afterwards, the release

of active agents occurs in specific sites because of the actuation of corrosion processes related to trigger mechanisms. The triggers include pH,[172] ionic strength and temperature,[173] mechanical stimuli, [174, 175] and others. Smart coatings loaded with pH-responsive nanocontainers have also been reported. For example, a double stimuli-responsive microcapsule that contains the healing agent linseed oil and the corrosion inhibitor benzotriazole has been reported. In this system, pH stimulus is to control the release of benzotriazole and prevent the electrochemical corrosion reactions. Moreover, the mechanical stimulus as a switch is used to release of linseed oil, providing self-healing ability (Figure 2.24).

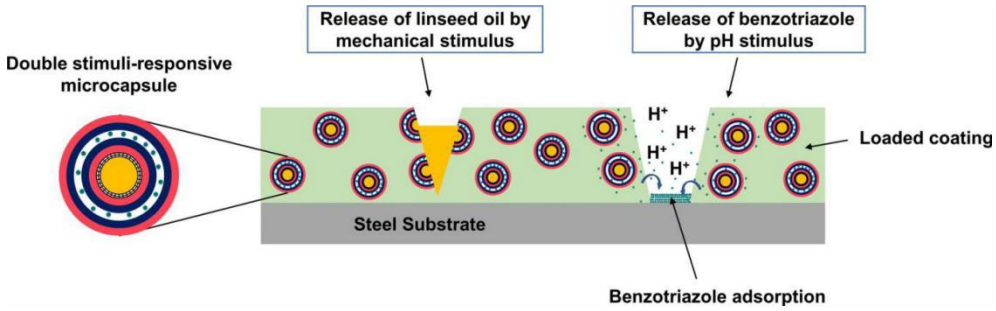

Figure 2.24. Schematic illustration of double stimuli-responsive microcapsule for coating. Adapted from ref. 176 with copyright 2018 Elsevier.

2.3.3 Drug delivery

In the last decades, polymer nanoparticles have been extensively studied as drug delivery because of their unique properties, such as easy design, preparation and functionalization, biocompatibility, broad structures variety. Drug delivery systems

based on polymer nanoparticles have been used to deliver drugs and biomacromolecules, such as peptides, proteins, plasma DNA and synthetic oligodeoxynucleotides.[177-179] Among many drug delivery systems, stimuli-responsive polymers have shown their unique properties. For example, there are many different microenvironments in the human body which can react to external stimuli by responding and adapting to changing external conditions.[180] Hence scientists have been trying to create drug delivery systems using stimuli-responsive polymer

In one example, a physiologically self-degradable microneedle patch was developed to deliver antibodies for cancer immunotherapy. The delivery device used biocompatible hyaluronic acid as microneedle patch, which were integrated with pH-sensitive dextran nanoparticles. Furthermore, antibodies and glucose oxidase (GOx) were encapsulated in the dextran nanoparticles. The design of the microneedle patches is shown in (Figure 2.25). GOx was used to convert blood glucose to gluconic acid in the presence of oxygen, which generated an acidic environment and resulted in the self-dissociation of pH-sensitive dextran nanoparticles and subsequently substantial release of the antibodies.

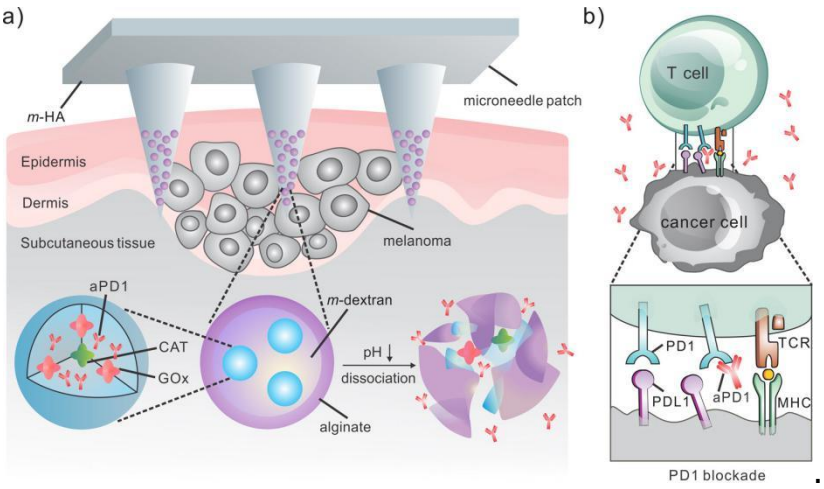

Figure 2.25. Schematic of the microneedle patch-assisted delivery of aPD1 for the skin cancer treatment. Adapted from ref. 181 with copyright 2016 American Chemical Society.

Light-responsive polymer nanoparticles have also been widely utilized in drug delivery material. For example, light-responsive polymersomes prepared using poly(ethylene oxide)-*b*-PSPA (PEO-*b*-PSPA) diblock copolymers,[182] where the SPA is a spiropyrane-based molecules and the SPA-containing segment was light-responsive . The resulting polymersomes possessed many properties, including photoswitchable and reversible bilayer permeability (Figure 2.26). Upon self-assembly into polymersomes, the SPA units underwent a reversible isomerization with light irradiation. Light was used to shift the structure from the hydrophobic spiropyran (SP) to the hydrophilic zwitterionic merocyanine (MC). The polymersome contaioning SP or MC SPA units kept their microstructures in

absence of light due to multiple cooperative noncovalent interactions, including hydrophobic, hydrogen bonding, π-π stacking, and paired electrostatic interactions. Afterward, they found that reversible phototriggered SP-to-MC polymersome transition was accompanied by changes in the membrane polarity and permeability switching from being nonimpermeable to selectively permeable toward noncharged, charged, and zwitterionic small molecule species below critical molar masses. This phenomenon was used to trigger the photoswitchable spatiotemporal release of 4′,6-diamidino-2-phenylindole within living HeLa cells.

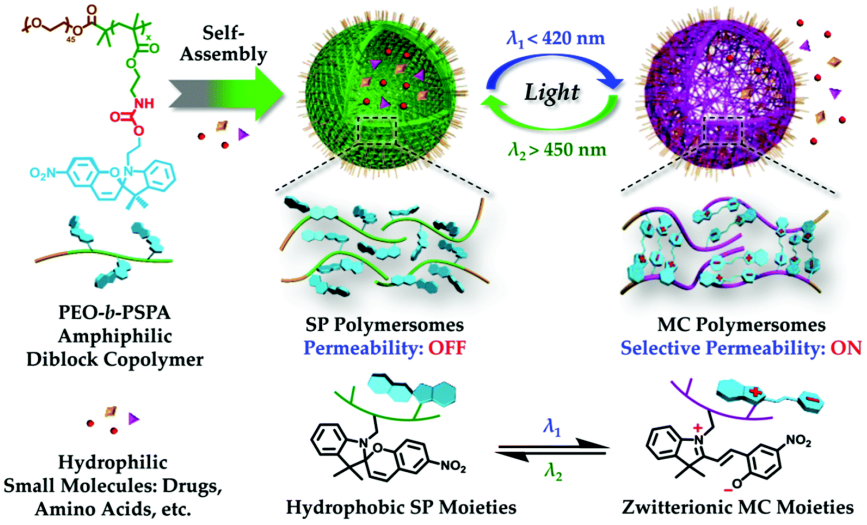

Figure 2.26. Photochromic polymersomes exhibiting photoswitchable and reversible bilayer permeability. Adapted from ref. 182 Copyright 2015, American Chemical Society.

In addition to pH and light, other stimuli can be used in the design of responsive nanoparticle. For example, redox-responsive nanocapsule can be prepared by the formation of a polytriazole shell synthesized from azide-functionalized hyaluronic acid and disulfide 1,6-hexanediol dipropiolate.[183] The addition of glutathione to a suspension of such nanoparticles was used to the encapsulated fluorescent dye after cleavage of the nanocapsules shell (Figure 2.27).

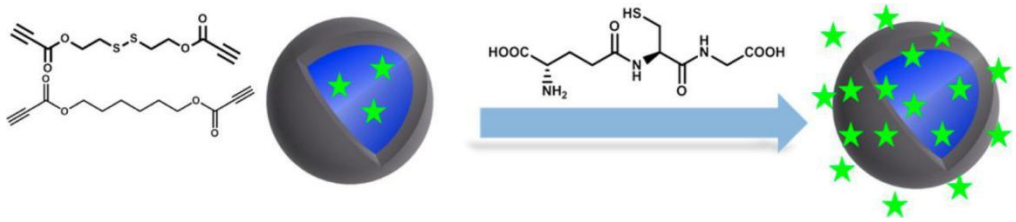

Figure 2.27. Schematic illustration of redox triggered fluorescent dye release from nanocapsule. Adapted from ref. 183 Copyright 2016, American Chemical Society.

2.3.4 Tissue engineering

Advances in tissue engineering require the development of functional materials that can be used as substitutes for damaged tissue.[184] The majority of tissue substitutes are based on the use of hydrogels, which can provide a three-dimensional porous matrix or scaffold.[185] Hydrogels have been widely used as injectable or moldable systems in which cells can adhere and proliferate in the substrate. Moreover, bioactive agents or cells can be readily incorporated into the polymer system and be delivered to the damaged tissue. Commonly the scaffolds

need to be biocompatible, controlled degradation and tunable mechanical properties, non-cytotoxic, and highly porous.

Polymer colloidal gel is a class of materials consisting of a percolating network of attractive colloidal particles. The use of polymer particles gives many advantages in the design of new materials for tissue engineering, including the formation of larger pores,[186] independently tunable mechanical properties and microstructural morphology of the colloidal gels. For example, colloidal gel can be designed as a tissue scaffold using oppositely charged PLGA nanoparticles through electrostatic force.[187] Such colloidal gel can be easily molded to the desired shape. Colloidal gel often possesses shear-thinning behavior because the particle network can be disrupted with limited shear force, but upon removal of shear, the particle networks recovered quickly and returned to the gel state. This reversibility makes colloidal gels an excellent class of material for molding, extrusion, or injection of the tissue scaffold (Figure 2.28).

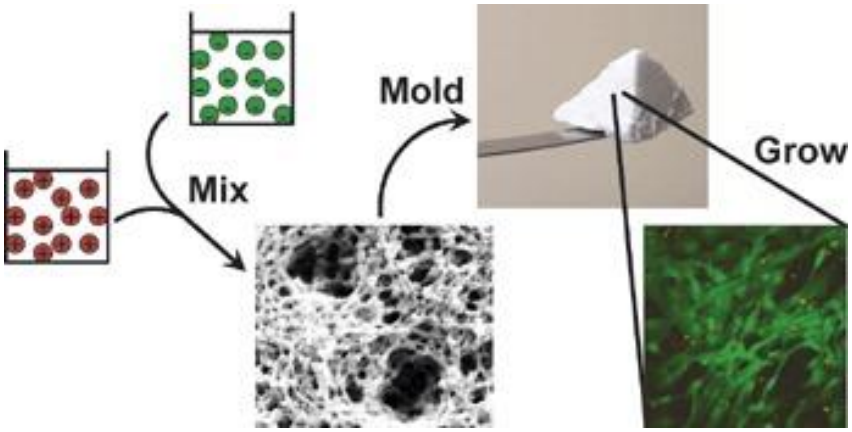

Figure 2.28. Schematic illustration of colloidal gel preparation using oppositely charged PLGA nanoparticles through electrostatic force. Adapted from ref. 187 Copyright 2008, Wiley-VCH.

Another approach in the design of colloidal material for tissue engineering consists in the use of smart and responsive material. This would mimic the composition and structural characteristics of natural organs using the principles of biomimetics, nano-assembly technology and additive manufacturing techniques. For example, temperature-responsive nanofibrillar hydrogels were prepared using rod-shaped cellulose nanocrystals functionalized with copolymers of *N*-isopropylacrylamide and *N*,*N*′-dimethylaminoethyl methacrylate.[188] Such nanofibrillar hydrogel were stable in cell culture medium at 37 ℃, but gel dissociation happened upon cooling to room temperature and cells can be grown in the hydrogel template and then released from the gel by decreasing temperature, and hence the release of cells following their culture in the hydrogels would enable to develop a potential substitute for damaged tissue (Figure 2.29).

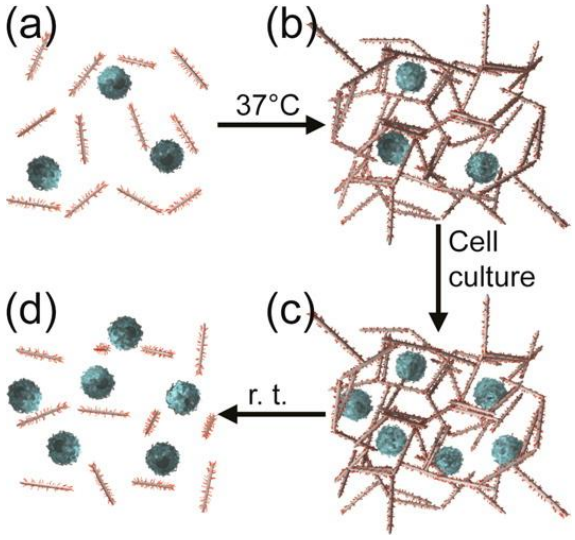

Figure 2.29. Schematics of the formation of thermoresponsive nanofibrillar cell-laden gel from copolymer-modified CNC building blocks. Adapted from ref. 188 Copyright 2016, American Chemical Society.

2.3.5 Sensors

In the past several decades, many small molecule-based sensors have been developed to detect various signals,[189] such as pH,[190] temperature,[191] and mechanical forces.[192] However, some obstacles hinder the application of small molecule sensors, such as water solubility, low structural stability, and difficulty in further functionalization.[193] Therefore, these small-molecule probes are integrated into polymer particles, which provide a versatile method to optimize the performance of the sensor.[194] Following this method, a variety of sensor devices, such as gas sensors, pH sensors, humidity sensors, and ion-selective sensors based

on polymer nanoparticle have been reported.[195]

One notable example are thermoresponsive energy transfer sensors (Figure 2.30).[196] The thermoresponsive PNIPAM chains were grafted on the surface of silica nanoparticles, where the thermoresponsive brushes were labeled with fluorescence resonance energy transfer donors, 4-(2-acryloyloxyethylamino)-7-nitro-2,1,3-benzoxadiazole, and photoswitchable acceptors, 1′-(2-methacryloxyethyl)-3′,3′-dimethyl-6-nitro-spiro(2*H*-1-benzo-pyran-2,2′-indo line) (SPMA). Under visible light, nonfluorescent spiropyran (SP) form transformed to the fluorescent merocyanine (MC) form, leading to the occurrence of a FRET process between the active residues. Upon heating, the FRET efficiency was tuned easily via the thermo-induced collapse of PNIPAM brush. The reason was that spatial distances between fluorescent donors and acceptors were controlled when decrease or increase the temperature.

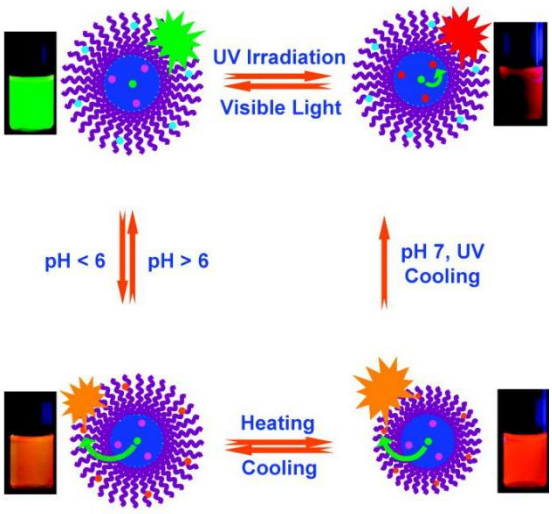

Figure 2.30. Schematic illustration for the construction of polymeric micelles-based reversible three-state switchable multicolor luminescent system. Adapted from ref. 196 Copyright 2009, Wiley-VCH.

A similar approach was used to prepare gas sensors. For example, CO_2 can be generated from many environments (Figure 2.31). For example, abnormal concentrations of CO_2 have been associated with metabolism-related diseases and the development of sensitive CO_2 sensors is essential. In such sensors, an initiator containing a gas-responsive moiety, 2,2′-azobis[2-(2-imidazolin-2-yl)propane], was used to prepared gas-stimuli responsive particles. The imidazoline groups were reacted with CO_2 dissolved in water, forming their bicarbonate salt, and their reverse reaction happened by introducing N_2 gas, hence the state of nanoparticle was controlled *via* the introduction of CO_2 and N_2, respectively. This method

shows dramatic improvement in the sensitivity and convenience of sample preparation compared with the previously reported gas sensor.

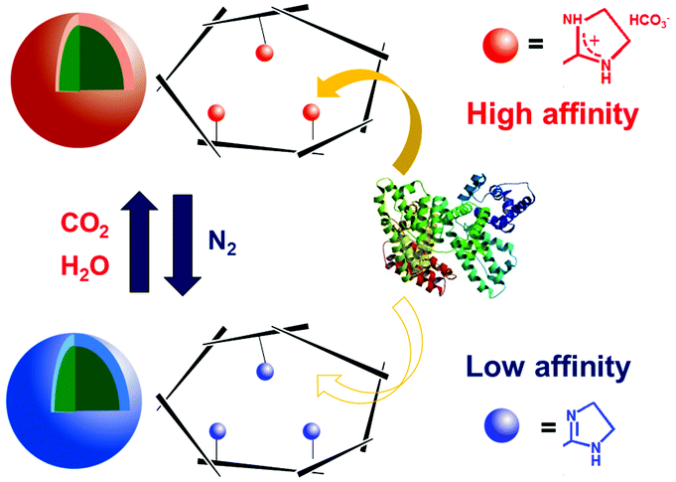

Figure 2.31. Gas-responsive core-shell MIP particles having a molecularly imprinted polymer shell layer. Adapted from ref. 197 Copyright 2018, The Royal Society of Chemistry

Chapter 3. Results and Discussion

The development and application of stimuli-responsive polymer materials are playing an essential role in the design of smart functional materials and have led to new and enhanced applications in many fields. One of the most commonly employed classes of smart polymers is thermo-responsive polymers, especially those who can reversibly undergo phase transition when the temperature is changed. Recently, stimuli-responsive polymers materials have been used to incorporate a stimuli-responsive "on-off" switch to other materials by the addition of responsive segments, and thus combining multiple properties in one system. Here, the "on-demand" control provided by thermoresponsive polymers was used to silence the intrinsic properties of the polymer material (section 3.1) or to endow nanoparticles with thermo-responsive colloidal stabilization (section 3.2). Moreover, those functionalized nanoparticles could find potential applications as delivery systems (section 3.3) where the release is controlled by the combined effect of temperature and oxydo-reductive stress.

First, the thermal on-demand control was used to regulate the activity of a light-responsive polymer. A dual temperature/light-responsive polymer was designed (section 3.1). A copolymer composed of N-isopropylacrylamide and a reversible spiropyrane-based photoacid was synthesized. The resulting

polyphotoacid was responsive to light irradiation at λ = 460 nm and released one proton for each spiropyrane unit but only when below the lower critical solution temperature (LCST). Increasing the temperature above the LCST induced the aggregation of the polymer and silenced the photoacid behavior. Hence, the temperature-induced phase transition of the polyphotoacid acted as a thermal on/off switch for the photoacid function.

Then, a library of nanoparticles stabilized with thermo-responsive polymer chains (Section 3.2). In this case, the thermal on-demand control was used to regulate the activity of a state of the nanoparticle suspension. Increasing the temperature above the LCST of the segments ensuring the colloidal stability led to the formation of well-controlled colloidal gels. The effect of the rigidity and the aspect ratio of the nanoparticles on the properties of the resulting fibrillar gels was also studied.

In addition, such nanoparticles and colloidal gels provide a new type of delivery system. Here the particles developed were used as a delivery system able to respond to temperature changes and oxydo-reductive stress in suspension (section 3.3).

3.1 A Reversible Light-Responsive Proton-Generator with on/off Thermoswitch*

The design of multi-responsive materials is a necessary step toward the design of smart materials. An interesting class of molecules is photoacid material. Such photoacids have great potential for biomedical applications because they can be used to control the pH locally and thus affect complex phenomena like cell growth and cell communication or even be used to trigger photocontrolled drug delivery. However, the introduction of the photoacid in a polymer can improve the solubility and compatibility of the photoacid in different media and can avoid leakage problems. Furthermore, it provides the opportunity to combine multiple functions in one polymer

In this section, a polymer-based photoacid that also has a thermal on/off switch around the physiological temperature was synthesized. The dual temperature/light response was realized by designing a copolymer composed of

N-isopropylacrylamide and a reversible spiropyrane-based photoacid (Figure 3.1.1). The polyphotoacid was responsive to light irradiation at λ = 460 nm and released one proton for each spiropyrane unit and was, therefore, able to acidify the solution. The opposite effect, the removal of protons and corresponding pH increase, was observed when either keeping the polyphotoacid in the dark for several minutes or more quickly by the irradiation of UV-light. Increasing the temperature above the lower critical solution temperature (LCST) silenced the photoacid behavior. Hence, the temperature-induced phase transition of the polyphotoacid acted as a thermal on/off switch for the photoacid function. This coupling of temperature- and light-responsive units in the polymer yielded a "thermophotoacid", a polymer that can adjust the pH value of the environment but only in a given temperature range.

3.1.1 Introduction

The pH-value is one of the most crucial parameters in nature, and it can regulate enzyme activity[198-202] and chemical reactivity.[203-207] Adjusting the pH value through light irradiation with photoacids enables control over the pH without any material transfer to/from the medium.[208-212] Thus, photoacids can be used for light-mediated spatiotemporal control of the pH-value. Recently, photoacid molecules have found applications in photodynamic therapy,[213] as modulators for enzymatic activity,[214] and regulators of chemical reactions.[215] However, the majority of the photoacid

molecules reported so far undergo irreversible proton dissociation. These photoacids can acidify the environment only once, which makes a reversible adjustment to the original pH not possible.

To reversibly adjust the pH value, switchable photoacids have been developed that can release and take-up protons in cycles.[216-218] In comparison to irreversible photoacid generators, these switchable photoacids can regulate the environmental pH value to higher or lower values upon ON/OFF switch of light or by changing the wavelength of irradiation. Reversible photoacids are compounds which have two photoisomeric states and for which the conversion from one state to the other can be reversibly triggered by light irradiation.

The spiropyran/merocyanide equilibrium represents one of the first long-lived reversible photoacids.[219] This family of molecules can be switched between a spiropyrane (neutral) and a merocyanine (charged/zwitterionic) form and can achieve a photo-induced pH-jump of several pH-units in an aqueous medium.[214] Based on this photo-reversible equilibrium between the spiropyrane and merocyanine forms, bond-breaking reactions,[209-223] molecular motors,[223-226] responsive hydrogels,[227] and inhibition of bacterial growth have been reported.[228]

Most of the works on photoacids presented so far are based on dissolved small-molecules photoacids in solution.[228-232] However, the challenging

immobilization of photoacid molecules into polymer supports, inorganic scaffolds, or biomolecules would open up novel possibilities. Firstly, the immobilization of the photoacid will allow for a light-mediated spatiotemporal control of the pH value since the photoacid would not diffuse as easily as a single small molecule. Additionally, the immobilization of photoacids can improve their compatibility with different media.[233] Moreover, the coupling of photoacids with other materials can create novel materials with switchable functions and properties. Of special interest would be the integration of photoacids into responsive polymer materials. The responsive polymer material can then alter and further control the photoacid functionality.

Here, a polymer-based photoacid has a thermal on/off switch around the physiological temperature. The dual temperature/light response was realized by designing a copolymer composed of N-isopropylacrylamide and a reversible spiropyrane-based photoacid (Figure 3.1.1). The polyphotoacid was responsive to light irradiation at λ = 460 nm and released one proton for each spiropyrane unit and was, therefore, able to acidify the solution. The opposite effect, the removal of protons and corresponding pH increase, was observed when either keeping the polyphotoacid in the dark for several minutes or more quickly by the irradiation of UV-light. Increasing the temperature above the lower critical solution temperature

(LCST) silenced the photoacid behavior and the irradiation of light at λ = 460 nm did not lead anymore to proton generation. Hence, the temperature-induced phase transition of the polyphotoacid acted as a thermal on/off switch for the photoacid function. This coupling of temperature- and light-responsive units in the polymer yielded a "thermophotoacid", a polymer that can adjust the pH value of the environment but only in a given temperature range.

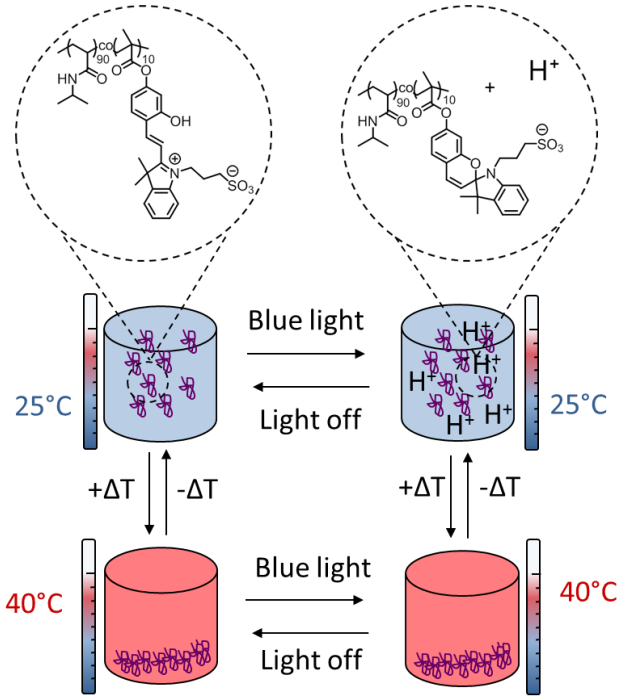

Figure 3. 1. 1. Temperature and light controlled proton generation in water mediated by a thermophotoacid. Irradiation at λ = 460 nm of a solution at 25 ℃ leads to the photoswitching of the photoacid and the subsequent acidification of the solution. When the irradiation is stopped, the pH value goes back to a neutral value.

Increasing the temperature above the LCST of the polymer deactivates the photoacid and no pH switch is observed. Hence, the temperature can be used as an on/off-switch for the photoacid.

3.1.2 Experimental part

Materials

N-Isopropylacrylamide (NIPAM, Sigma, 97%) was purified by recrystallization from toluene/hexane followed by drying under a vacuum and was stored at -20 ℃. 2,2′-Azobis(2-methylpropionitrile) (AIBN, Sigma, 98%) was recrystallized twice from methanol. Tetrahydrofuran (THF, Sigma, anhydrous, ≥99.9%), methacryloyl chloride (Sigma, 97%), 2,4-dihydroxybenzaldehyde (Sigma, 98%), 2,3,3-trimethylindolenine (Sigma, 98%), 1,3-propanesultone (Sigma, ≥99.9%), N,N-dimethylformamide (DMF, Sigma, anhydrous, 99.8%), triethylamine (TEA, Sigma, anhydrous, ≥99.9%) were used as received.

Instrumentation and Characterization

The number average molecular weight (Mn) and molecular weight distribution (dispersity index, Đ) of polymers were measured by size exclusion chromatography (SEC) in DMF (1 g L^{-1} LiBr added) at 60 ℃ and a flow rate of 1 mL min^{-1} with a PSS SECcurity as an integrated instrument, including a PSS

GRAM 100-1000 column and a refractive index (RI) detector. All NMR experiments were recorded on a Bruker AV300. The light scattering measurements were performed on an ALV spectrometer consisting of a goniometer and an ALV-5004 multiple-tau full-digital correlator (320 channels), which allows measurements over an angular range from 30 ° to 150. A He-Ne laser (wavelength of 632.8 nm) is used as a light source. For temperature-controlled measurements, the light scattering instrument was equipped with a thermostat from Julabo and the experiments were performed at a 90 ° angle and the temperature varied from 25 ℃ to 40 ℃. FT-IR spectra were carried out on a Varian 1000 FT-IR spectrometer. UV-Vis spectrophotometer studies were recorded on a Perkin Elmer Lambda 100 spectrophotometer at room temperature. The photo-isomerization reactions were performed on a blue LED with an emission wavelength of 460 nm. A METTLER TOLEDO S20 Seven Easy™ pH-meter was used.

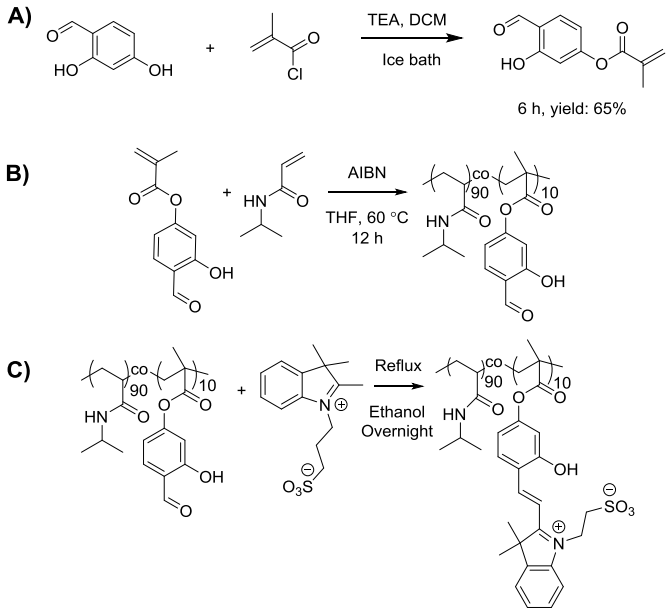

Figure 3.1.2. Synthesis of the thermoresponsive photoacid polymer. (A) Synthesis of the precursor aldehyde-monomer. (B) Free-radical copolymerization of NIPAM and aldehyde-monomer. (C) Postpolymerization functionalization of the aldehyde-units to form the thermo-responsive photoacid polymer.

3.1.3 Results and discussion

Synthesis hydroxyl methacryloyloxybenzaldehyde

The aldehyde monomer was prepared according to the previously reported procedure.[234] Briefly, methacryloyl chloride (5.0 g, 0.048 mol) in 10 mL of chloroform was added dropwise to a mixture of 2, 4-dihydroxybenzaldehyde (8.0 g, 0.058mol) and triethylamine (4.9 g, 0.048 mol) in 40 mL of chloroform over a 30 min-interval in an ice-water bath. After stirring for 1 h, the mixture was washed

with water and then concentrated under reduced pressure. The colorless solid obtained was purified by column chromatography over silica gel (gradient ethyl acetate: n-hexane from 1.2:1 to 1: 1 v/v), followed by recrystallization from ethanol to give the aldehyde monomer.

Synthesis of the thermoresponsive aldehyde-containing copolymer

The aldehyde copolymer was synthesized in dry THF by free-radical polymerization with AIBN as an initiator. NIPAM (2.24 g, 18.0 mmol), formyl-hydroxyphenyl methacrylate (400 mg, 2.0 mmol), and AIBN (32.8 mg, 0.2 mmol) were dissolved in dry THF (10 mL). After the mixture was degassed by three freeze-pump-thaw cycles, the solution was polymerized at 60 ℃ for 12 h. The polymer was precipitated in diethyl ether, collected by filtration and dried under a vacuum to yield a white powder.

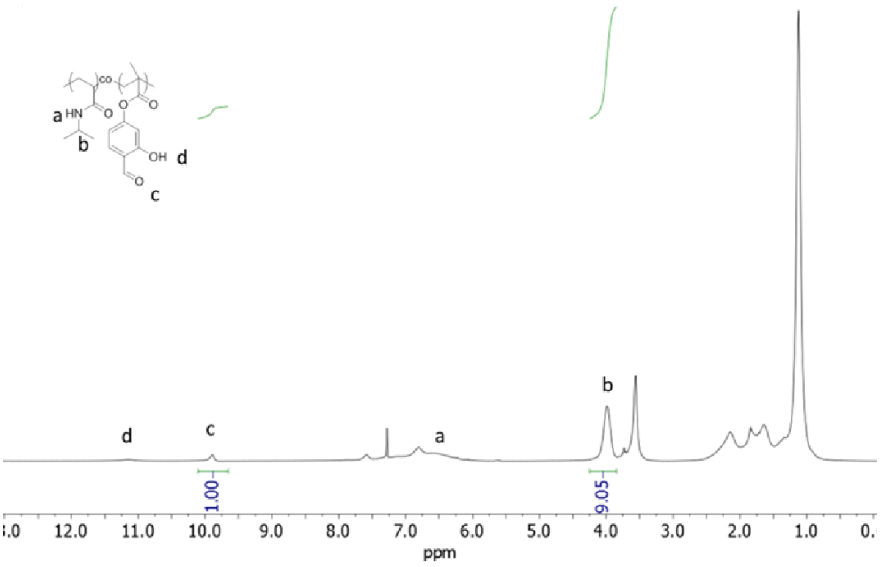

Figure 3.1.3. ^{1}H NMR spectra of aldehyde copolymer in $CDCl_3$,

Synthesis of the thermoresponsive polyphotoacid

The photoacid copolymer was prepared via two steps: First, 2, 3, 3-trimethyl-1-(3-sulfonatepropyl)-3H-indolium was synthesized according to literature.[235] Briefly, 2, 3, 3-trimethylindolenine (1.65 g, 0.01 mmol, Aldrich) was added to propane sulfone (1.26 g, 0.01 mmol, TCI). The mixture was stirred at 90 ℃ for 4 h under N_2. The purple solid was collected by filtration, washed with cold diethyl ether, and dried in vacuum.

Secondly, the 2, 3, 3-trimethyl-1-(3-sulfonatepropyl)-3H-indolium (560 mg, 2.0 mmol) was reacted with the aldehyde copolymer in anhydrous ethanol (20 mL). The mixture was refluxed overnight. The polymer was purified by dialysis in water

for 3 days to remove any residual byproducts. After freeze-drying, a dark-red solid was obtained.

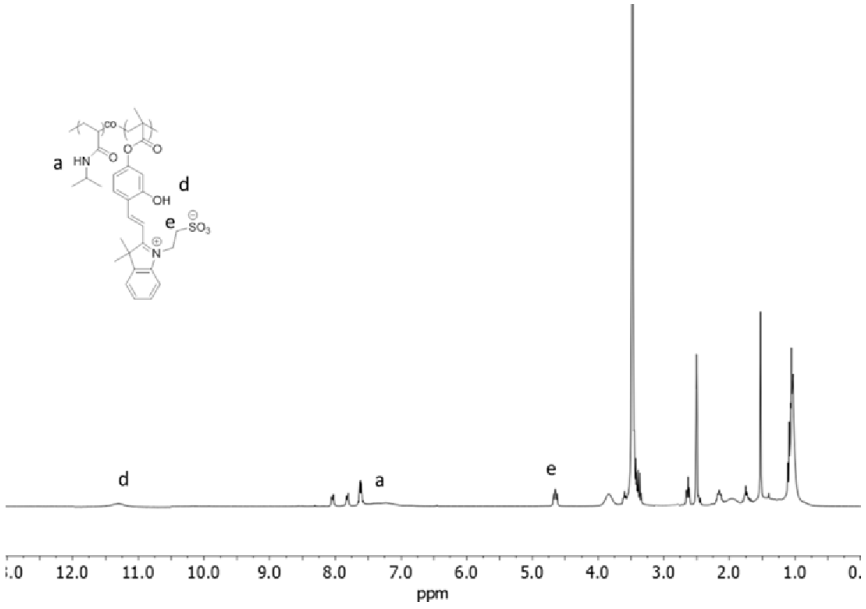

Figure 3.1.4. ^{1}H NMR spectra of Photoacid copolymer in DMSO.

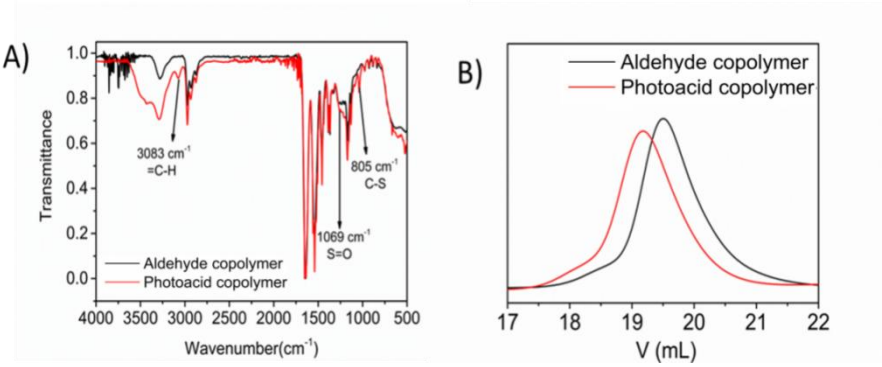

Figure 3.1.5. A) FT-IR spectra of aldehyde copolymer (black curve) and photoacid copolymer (red curve); B) Elugrams of the aldehyde copolymer (black curve) and of the photoacid copolymer (red curve) in DMF.

Table 3. 1. 1. Characterization of aldehyde copolymer and photoacid copolymer

Polymer	**NIPAM mol%**[a]	**M_n**[b]	**Đ**
Aldehyde copolymer	90	12200	1.45
Photoacid copolymer	90[c]	14700	1.55

[a] Calculated by ^{1}H NMR spectroscopy. [b] Measured by GPC using polystyrene standards in DMF.

The thermo-reversible photoacid polymer (TPA) was composed of two functional parts used as orthogonal switches for the control of the pH value in solution. The photoacid functionality was provided by the photoisomerization of the merocyanine side groups, which can adopt a spiropyran (SP) or the merocyanine (MC) form depending on the illumination conditions (Figure 3.1.1). When an aqueous solution of the copolymer was kept in the dark, the photochromic side groups were predominantly in the open-ring form, as indicated by the intense absorption signal at 460 nm in the UV-Vis spectrum (Figure 3.1.6. A, black trace). The close-ring, acidic SP isomer, was formed upon exposure of the TPA solution to blue light (460 nm, 0.16 W cm^{-2}), as indicated by the reduction of the MC signal intensity at 460 nm and the increase of absorbance of the SP peak at 310 nm.

To test the effect of the MC/SP photo-isomerization on the pH-value in solution, a 0.12 wt % photoacid polymer aqueous solution with a pH value of 5.0 was prepared. After irradiation with blue light (Figure 3.1.6. B), the pH value dropped

to 4.1, giving a difference in pH value (ΔpH) of 0.9 pH units. When the light was turned off, the pH value gradually returned to its original value and leveled off at a pH value of 5.0 in 3 min. Only a ΔpH of 0.9 units was observed, probably because the initial pH value of the polymer aqueous solution was acidic, which strongly prevented the ring-closing reaction. [236] When the initial pH value was adjusted to 7.2 by the addition of ca. 200 µL 0.5 mM sodium hydroxide solution, the ΔpH observed when the polymer solution was irradiated with blue light was 2.4 pH-units (Figure 3.1.6 C). The photo-induced proton transfer was repeated over multiple cycles by switching the light "ON" and "OFF" (Figure 3.1.6 D).

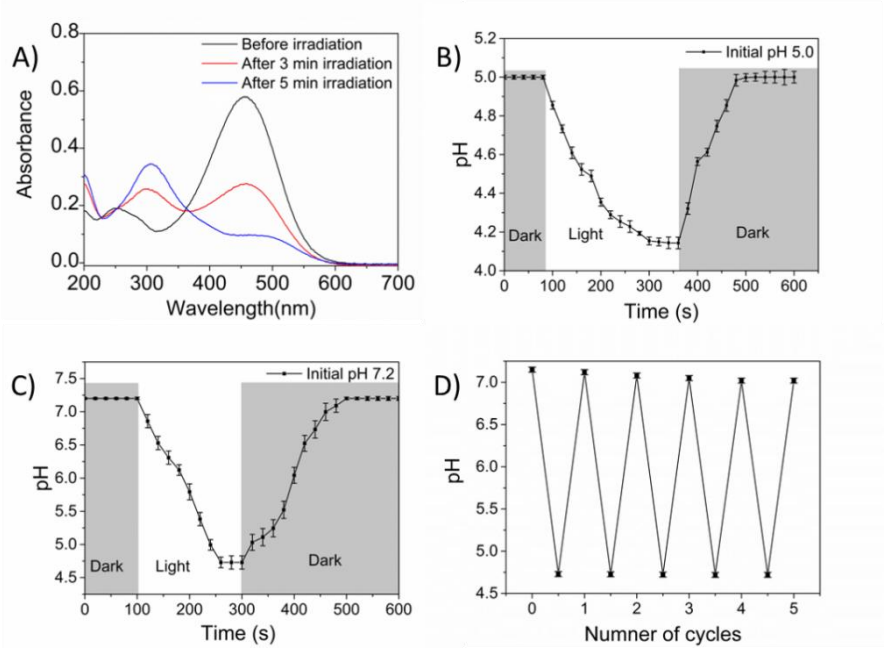

Figure 3. 1. 6. Influence of light irradiation on the properties of aqueous solutions of photoacid polymer. A) UV-Vis absorption spectra of photoacid polymer solution

in water. Photoacidity of an aqueous solution at room temperature and an initial pH value of 5.0 (B), and of 7.2 (C). D) Reversibility of the photoacid over multiple cycles under the same conditions as in C. All samples were measured at λ = 460 nm and 0.12 wt %.

To further understand the proton generation/capture of the poly(photoacid), the ΔpHs of the poly(photoacid) at different concentrations were measured. Figure 3.1. 7. A shows the ΔpH of different concentrations that were stored in the dark before they were irradiated with light at 460 nm. The experimental results displayed a gradual decrease in ΔpH as the concentration of photoacid polymer decreased. The experimental results suggested that the pKa of the poly(photoacid) was inferior to the pKa measured for small molecules analog in water (pKa = 4.3±0.3).[237] The dissociation constants of acidic or basic monomers decrease after polymerization.[221] The increased charge and the charge distribution within the polymer chains lead to a decrease of the dissociation constant of the monomer units with an increasing degree of ionization in the polymer.[239] Nonetheless, at every concentration, the photoacid units in the polymer contributed to a significant ΔpH after irradiation with blue light.

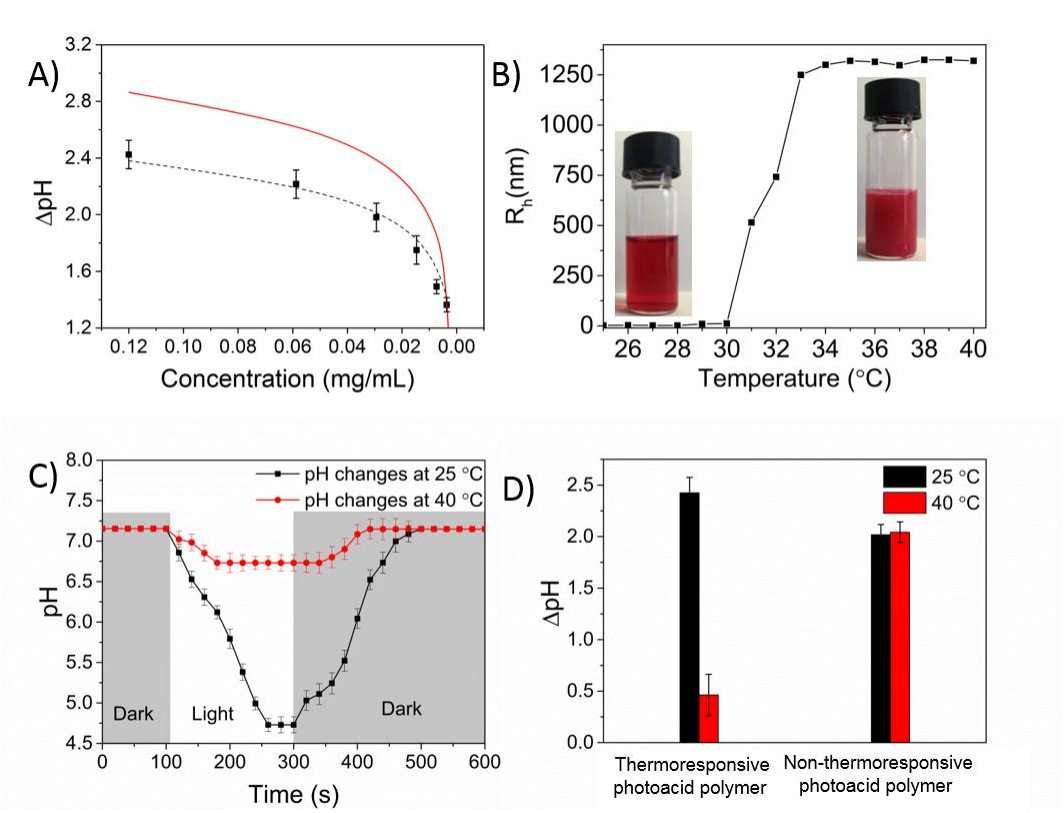

Figure 3.1.7. Concentration- and temperature-dependent photoacidity. A) Variation of pH value after irradiation. The red line represents the expected pH value variation created by the addition of a weak acid (pKa = 4.3) in a water solution with an initial pH value of 7.2. B) Temperature-dependent light scattering measurement of a photoacid polymer solution. Below 30 ℃ the poly(photoacid) is dissolved. An increase in the temperature leads to the desolvation of the polymer and yields micron-sized colloids. C) Photoacidity switch of a photoacid polymer solution at 25 ℃ and 40 ℃. D) Comparison of photoacidity of thermoresponsive and non-thermoresponsive photoacid polymers. Results were measured at

λ = 460 nm and 0.12 wt %.

Figure 3.1.7.B shows the thermal behavior of aqueous solutions of the poly(photoacid) prepared with NIPAM as a comonomer. The hydrodynamic radius of the polymer in solution was measured by dynamic light scattering (DLS) while systematically increasing the temperature between 25 to 40 ℃. Between 25 ℃ and 30 ℃, the sample was a clear aqueous solution. When the temperature was increased above 34 ℃, a coil-to-globule transition was observed, and large aggregates with a hydrodynamic radius of approximately 750 nm were observed. When the temperature was increased further, coagulation and precipitation of the globules were observed. The lower critical solution temperature (LCST), defined as the midpoint of the size transition monitor by DLS, was 31 ℃; similar to the LCST of PNIPAm homopolymers of 32 ℃. [240]

In order to gain a closer insight into the thermo-dependent proton generation and capture of the photoacid copolymer, the pH value was determined under light irradiation at room temperature and at 40 ℃ (Figure 3.1.7.C). When the temperature was below the LCST of the photoacid copolymer, the aqueous solution showed a strong photoacidity. However, when the temperature was increased above 40 °C, the photoacid copolymer showed a loss of the photoactivity, the ΔpH decreased from 2.4 units to 0.4 units. Turning off the irradiation of blue light

resulted in an increase of the pH value back to the initial value in both cases.

In order to verify that the thermal on/off switch stemmed from the coil-to-globule transition of the NIPAM-containing copolymer, a reference copolymer was synthesized. This polymer contained the photoacid functionality, however, the NIPAM comonomer was replaced with oligo(ethylene glycol) methyl ether methacrylate (OEGMA). The OEGMA-containing copolymer did not have an LCST between 25 and 40 °C and therefore the temperature should not influence the photoacidity of the copolymer. As expected, there was no influence of the temperature on the ΔpH when the OEGMA-containing photoacid copolymer solution was irradiated with blue light at either 25 or 40 °C (Figure 3.1.7.D).

3.1.4 Conclusions

In summary, a novel copolymer composed of thermo-responsive units and light-responsive photoacid units was reported. The photoacid copolymer was able to release reversibly protons to acidify its environment. The combination of the photoresponsive spiropyrane photoacid units, with thermoresponsive N-isopropylacrylamide monomers, led to the formation of a photoacid that can be switched on/off by changing the temperature above the LCST. Below the LCST the copolymer was water soluble and the photoacid was active. When the temperature was increased above the LCST, the photoacid was deactivated. Thus, using this

dual-responsive copolymer, the pH value of the environment can be modulated by both light and temperature. The results demonstrated that the combinations of photoacids with responsive polymers can extent pH value regulation not only with light, but also with other stimuli.

3.2 Colloidal Gels Made of Thermoresponsive Anisotropic Nanoparticles

In the previous section, heating the polymer solution above the LCST resulted in the collapse of the polymer chains and the desolation of the chain, efficiently preventing the formation of protons by the light-responsive moieties. This is the typical behavior of a polymer displaying a LCST. The coil-to-globule transition occurring above LCST led to the desolvation of the polymer chains and is usually concluded by the precipitation of the desolvated globules. However, the tethering of the LCST-polymer to an NP hinders and limits the globule formation, and instead of a precipitated solid, the formation of an arrested network of NPs can be obtained.

In this section, a library of colloidal polymer nanoparticles was functionalized with a thermoresponsive polymer. The core-shell NPs were prepared *via* polymerization induced self-assembly (PISA), sonication and core-crosslinking. In addition, and the aspect ratio and rigidity of colloidal nanoparticles were tuned by varying the reaction conditions. Colloidal gels were formed by the controlled aggregation of colloidal polymer nanoparticles in 3D into an interconnected network structure.

3.2.1 Introduction

Colloidal gels are formed when concentrated suspensions of colloidal particles organize through interparticle interactions to form a transient but arrested network.[241, 242] The transition between liquid-like colloidal suspension and the formation of colloidal gels depends on the volume fraction occupied by particles, the range and type of interaction between the particles, and the particle interaction potential.[243, 244] Colloidal gels are progressively gaining prominence in applications such as colloidal crystals,[245, 246] energy storage devices,[247] advanced ceramic materials,[248] and biomaterial,[249, 250] due to their unique structure, elasticity and mechanical stability. Harnessing the interplay between physico-chemical design of the nanocolloids and the properties of the resulting colloidal gels is consequently increasingly important.

The mechanisms leading to the formation of colloidal gels are complex. When the constituting building blocks are simple unfunctionalized rigid spherical particles, the gel formation is only driven by the volume fraction occupied by the particles and hard sphere interactions. However, when the colloids are functionalized with polymer chains, the situation is more complex because interdigitation and entanglement between the coronas of adjacent particles also need to be taken into account. [251] Furthermore, when the building blocks are anisotropic and flexible like

worm-like micelles, the entanglements between the colloids also plays a role in the final properties of the colloidal gels.[252]

Understanding and controlling the structure and the mechanical properties of the colloidal gels is crucial to develop materials for specific applications, e. g. photocatalysis,[253] sensors for chemical detection,[254, 255] tissue engineering.[256] This is mostly in the case of colloidal gels formed with anisotropic colloidal particles, which can be used to form fibrillar gels. Such gels are attracting interest since they have a fibrous structure reminiscent of the structure of the extracellular matrix, but also, the anisotropic colloids can be functionalizable and tunable in terms of composition, size, shape and rigidity.[257] Moreover, anisotropic colloids have a lower percolation threshold in comparison to their spherical counterpart, and hence fibrillar gels can be formed at low solid content or volume fraction.[258]

The mechanical behavior of colloidal suspensions and gels is influenced by multiple factors, such as size, shape, surface functionalization and softness of the nanoparticles. [259, 260] Soft colloids like microgels are known to interact with each other more strongly than hard colloids and lead to the formation of strong colloidal gels. [261] The colloid-colloid interaction is a critical parameter which is also influenced by the surface-functionalization of the colloids. For example, when the colloids are functionalized with end-tethered polymer chains, interpenetration and

interaction between the grafted polymer layer dictate the mechanical properties of the resulting colloidal gels. Moreover, colloids functionalized with limited chain grafting density and same chain length experience a more efficient interpenetration between the brush layer of adjacent colloids leading to stronger and more robust gels. [262, 263] In the case of anisotropic colloids, their mechanical properties are also influenced by their surface functionalization and the softness of the nanoparticles, but also affected by their aspect ratio and their orientation.[264] Therefore, in this work, we study how the physical properties of anisotropic nanoparticles with same surface chemistry and chemical composition but having different aspect ratio and rigidity influence the global properties of the colloidal gel so that develop the fibrillar gels for potential applications.

3.2.2 Experimental part

Materials

The monomers 2-(dimethylamino)ethylmethacrylate (99%, DMAEMA), benzyl methacrylate (98%, BzMA) and 2-(methacryloyloxy)ethyl acetoacetate (95%, AAEM) were purchased from Sigma-Aldrich and purified on an alumina oxide column. 4-Cyano-4-(2-phenylethanesulfanylthiocarbonyl) sulfanylpentanoic acid was synthesized as previously reported. [265] 4, 4'-Azobis(4-cyanovaleric acid) (ACVA)) or 2,2'-azobis(isobutyronitrile) (AIBN) were recrystallized twice before

use.

^{1}H NMR Spectroscopy

All NMR spectra were recorded on a Bruker Avance 300 MHz.

Dynamic Light Scattering (DLS)

Dynamic light scattering measurements were performed using a Malvern Zetasizer Nano S90 using a He-Ne laser (633 nm) and analysis angle of 90 °. The hydrodynamic diameter of the polymer structures was measured in water.

Transmission Electron Microscopy (TEM)

The nanostructures were analyzed using a JEOL-1400 transmission electron microscope at an accelerating voltage of 120 kV. Typically, TEM grid preparation was as follows: the samples were diluted with Milli-Q water to approximately 0.05 wt %. The TEM grid was dipped in the diluted solution, the excess solution was blotted with a filter paper, and the grid was then dried at room temperature. To stain the deposited nanoparticles, a 0.4% w/w aqueous solution of uranyl acetate was placed via micropipette on the grid for 20 s and then carefully blotted to remove excess stain.

Rheological Measurements

Rheological measurements were carried out on Bohlin Gemini rheometers

equipped either with coaxial cylinder geometry with a measuring bob radius of 25 mm, a measuring cup radius of 27.5 mm and 13.0 mL sample volume or a cone and plate geometry (1 ° cone angle and 40 mm diameter with a truncation gap of 500 μm). For the dynamical measurements, about 5 mL of gel was loaded onto the plate, and the cone was lowered to minimize the truncation gap, and the excess of gel was removed. Before experiments, samples were equilibrated within the geometry for 10 min. Oscillatory strain sweep measurements were run from 0.01 to 500% deformation at a fixed frequency of 1 rad/s. Oscillatory frequency sweep measurements were performed at different temperatures at a frequency of 1 rad/s, with a constant strain of 1%, which is within the linear viscoelastic regime of the hydrogels. Temperature for the frequency step was maintained from 25 to 45 ℃ for each frequency sweep.

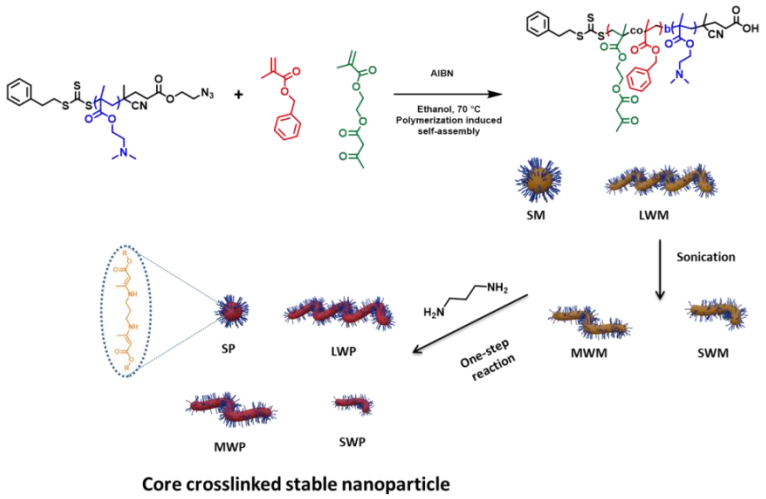

Figure 3.2.1. Synthesis of core cross-linked stable block copolymer nanoparticles.

Synthesis of Poly(2-(dimethylamino)ethyl methacrylate) PDMAEMA$_{31}$-CTAs

The chain transfer agent 4-cyano-4-(2-phenylethanesulfanylthiocarbonyl) sulfanylpentanoic acid (0.432 g, 1.27 mmol), the monomer DMAEMA (10.0 g, 63 mmol) were added to THF (10 g) with ACVA (36 mg, 0.127 mmol), the solution was degassed with argon in a ice bath for 0.5 h and then immersed into an oil bath at 70 ℃. After 6.5 h the polymerization was quenched using an ice bath. The monomer conversion was analyzed by ^{1}H NMR spectroscopy. PDMAEMA was purified by precipitation into cold hexane three times and dried under vacuum to yield a yellow product.

Synthesis of micelles (PDMAEMA$_{31}$-b-PBzMA$_x$) via Dispersion Polymerization in Ethanol

A typical RAFT dispersion polymerization was conducted at a concentration 15% w/w total solid fraction. First, PDMAEMA$_{31}$-CTA (144 mg, 0.028 mmol), BzMA (1.5 g, 8.4 mmol), and AIBN (0.90 mg, 0.006 mmol) were dissolved in ethanol (9.32 g), the reaction mixture was degassed with argon in an ice/water bath for 20 min, and then placed in a preheated oil bath at 70 ℃ for 24 h. According to ^{1}H NMR spectroscopy analysis, the final conversion of BzMA was above 99%. The

resulting polymers were analyzed by ^{1}H NMR spectroscopy and GPC.

During the following PDMA-PBzMA diblock copolymer syntheses, the degree of polymerization of the PBzMA block was systematically varied, which allowed to tune the morphology of the micelles.

Synthesis of Cross-linkable micelles ($PDMAEMA_{31}$-b-$PBxMA_{35}$-co-$AAEM_5$)

The synthesis of cross-linkable block copolymer was performed similarly to the synthesis of $PDMAEMA_{31}$-b-$PBzMA_x$ with a mixture $PDMAEMA_{31}$ (0.144 g, 0.028 mmol), BzMA (0.0184 g, 1.04 mmol), 2-(methacryloyloxy) ethyl acetoacetate (AAEM) (0.001 g, 4.67 umol) and AIBN (0.90 mg, 0.006 mmol) in EtOH (1.05 g). The reaction mixture was degassed with argon in an ice/water bath for 30 min, and then placed in a preheated oil bath at 70 ℃ for 24 h.

In order to control the density of cross-linking, the DP of AAEM of $PDMAEMA_{31}$-b-$PBxMA_x$-co-$AAEM_y$ was varied at 5 and 10, respectively.

Controlling the length of the micelles

A total of 1.0 g of the worm micelles was diluted to 3.25 wt% by the addition of ethanol. An ultrasound probe was then placed in the worm solution kept in an ice-bath and the worms were cut to smaller rods at different sonication time. The sonication was applied with pulses of 3 seconds on and 2 seconds off with a

Branson sonoprobe for certain time (90 s or 5 min) 35% amplitude (3 mm Tapered Micro Tip). After ultrasound cutting, the rod-like micelles were characterized by TEM.

Covalent crosslinking of the core of the polymer micelles

1,3-diaminopropane can react with the acetoacetate of the AAEM, located in the core of the micelles, via nucleophilic substitution to form an imine, resulting in the covalent stabilization of the micelles. The cross-linking reactions were conducted at 25 ℃ using 1,3-diaminopropane. The resulting cross-linked micelles were purified by dialysis against ethanol. The final suspensions were prepared by the redispersion of different concentration of worms and rod shape particle dispersions were prepared after removing ethanol and transferring particles in water.

3.2.3 Results and discussion

The first living soluble block PDMA macro-CTA was synthesized by solution polymerization in THF at 70 ℃ (Figure 3.2.1). After purification by precipitation into excess petroleum ether, The mean DP was determined to be 31 as judged by ^{1}H NMR spectroscopy (Figure 3.2.2), while THF GPC analysis indicated a final polydispersity of 1.22.

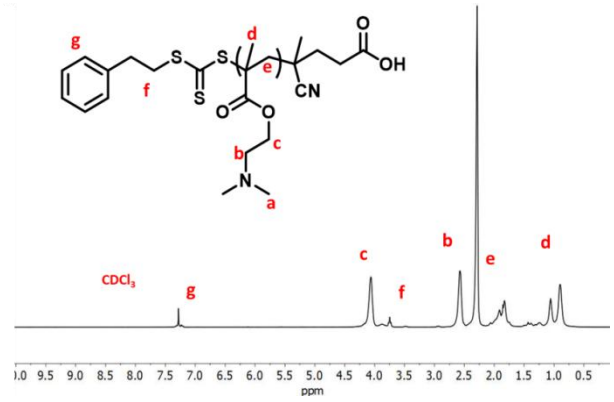

Figure 3.2.2. ^{1}H NMR spectra of Poly(2-(dimethylamino)ethyl methacrylate) in $CDCl_{3.}$

This $PDMA_{31}$ macro-CTA was then chain-extended with BzMA via RAFT dispersion polymerization in ethanol at 70 ℃ to produce a series of $PDMA_{31}$-PBzMA*x* diblock copolymers. Since the PBzMA chains are insoluble in ethanol, a range of copolymer morphologies can be generated via *in situ* self-assembly by varying the DP of the PBzMA chains. The control over the micellar structure was achieved by tuning the polymerization conditions for the synthesis of the second block and either spherical micelles (SM), long worm-like micelles (LWM) or vesicles were obtained.(Figure 3.2.3),

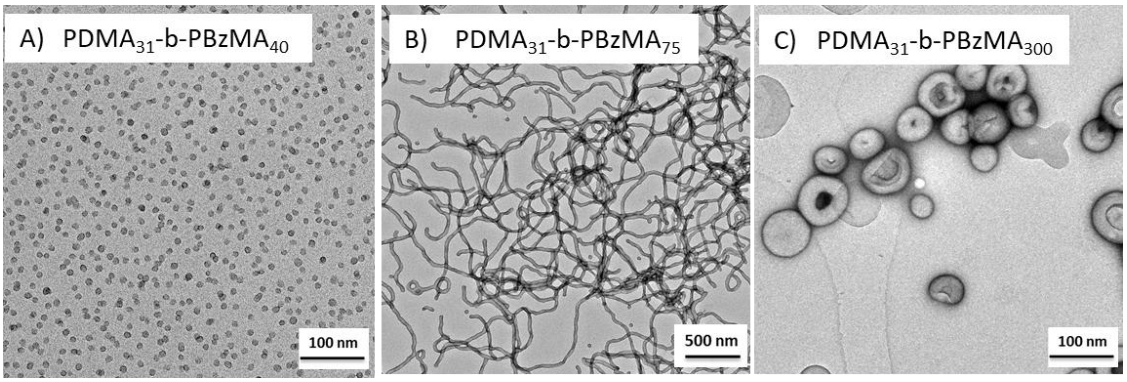

Figure 3.2.3. TEM images obtained for $PDMA_{31}$-*b*-$PBzMA_x$ diblock copolymer micelless synthesized at a total solids concentration of 15% via RAFT dispersion polymerization in ethanol. (a) Spheres (x = 40); (b) worms (x = 75) and (b) vesicles (x = 300)

To control the length of the worm-like micelle, the long worm micelle (LWM_0, $PDMA_{31}$-$PBzMA_{75}$) synthesized were subjected to ultrasound. The high local shear stress induced in the suspension during sonication can be used to efficiently cut the micelles as demonstrated with other block copolymer worm-like micelles. [266] The sonication of the long worm-like micelles resulted in a decrease of the average length of the micelles (Figure 3.2.4) while the diameter remained constant and the average aspect ratio of the micelles decreased from 65 to 24 and 9 after 90 s and 300 s of sonication, respectively (Table 3.2.1).

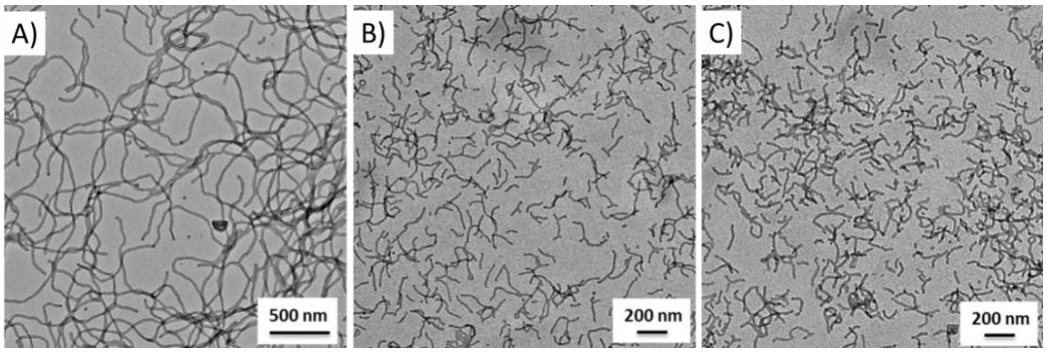

Figure 3.2.4. TEM images obtained for long worm micelles in ethanol. A) Before sonication, B) After 90s sonication, C) After 5min sonication.

In order to prepare the corresponding particles via the core-crosslinking of the micelles, a second monomer 2-(methacryloyloxy) ethyl acetoacetate, AAEM) was added to the hydrophobic block to allow for the post-polymerization crosslinking. AAEM can react with diamine to produce a crosslinked network and stabilized the micelles via the covalent cross-linking of the core. Hence the macro-RAFT agent, poly(2-(dimethylamino)ethyl methacrylate) (PDMA) with a fixed average degree of polymerization (N=31) was used to polymerized a monomer mixture composed of benzyl methacrylate (BzMA) and 2-(methacryloyloxy)ethyl acetoacetate (AAEM).

Table 3.2.1. Characterization of the nanoparticles prepared

NP_X	Composition	Length (nm) [a]	PDI [a]	Aspect ratio
SM_{NCC}	$PDMA_{31}$-$PBzMA_{40}$	25	0.03	1
SWM_{NCC}	$PDMA_{31}$-$PBzMA_{75}$	220	0.12	9
MWM_{NCC}		590	0.25	24
LWM_{NCC}		1700	0.06	69
SM_{LCC}	$PDMA_{31}$-$PBzMA_{35}$-co-$PAAEM_5$	22	0.03	1
SWM_{LCC}	$PDMA_{31}$-$PBzMA_{70}$-co-$PAAEM_5$	230	0.11	9
MWM_{LCC}		590	0.31	24
LWM_{LCC}		1670	0.07	68
SM_{HCC}	$PDMA_{31}$-$PBzMA_{30}$-co-$PAAEM_{10}$	26	0.22	1
SWM_{HCC}	$PDMA_{31}$-$PBzMA_{65}$-co-$PAAEM_{10}$	260	0.22	11
MWM_{HCC}		550	0.29	19
LWM_{HCC}		1700	0.11	70

X was the density of core of micelle, where 0 wt% at X= Non-core cross linking (NCC), 0.607 wt% at X= low core cross linking (LCC), 1.12 wt% at X= high core cross linking (HCC). [a] Calculated from the log-normal distribution of the size measured by TEM for N>75.

In order to tune the rigidity of micelle core, the concentration of AAEM in the feed during the synthesis of the micelle core was increased from 0 to 0.69 and 1.38 wt%. The acetoacetate groups of the AAEM can rapidly react with amine under mild conditions to form imines.[267] Therefore, using a diamine such as diaminopropane it was possible to cross-link the hydrophobic segments in the core of the micelles. The reaction in the core of micelles using diaminopropane yielded the corresponding nanoparticles in ethanol. The reaction between AAEM and diaminopropane was almost quantitative as followed by NMR spectroscopy and the resulting nanostructures were stabilized by the covalent cross-linking imine network at low core cross-linking (0.607 wt%, LCC) and high core cross-linking (1.12 wt%, HCC). These nanoparticles were transferred to water phase after core cross-linking; afterwards, the morphologies were measured using TEM as shown in Figure 3.2.5.

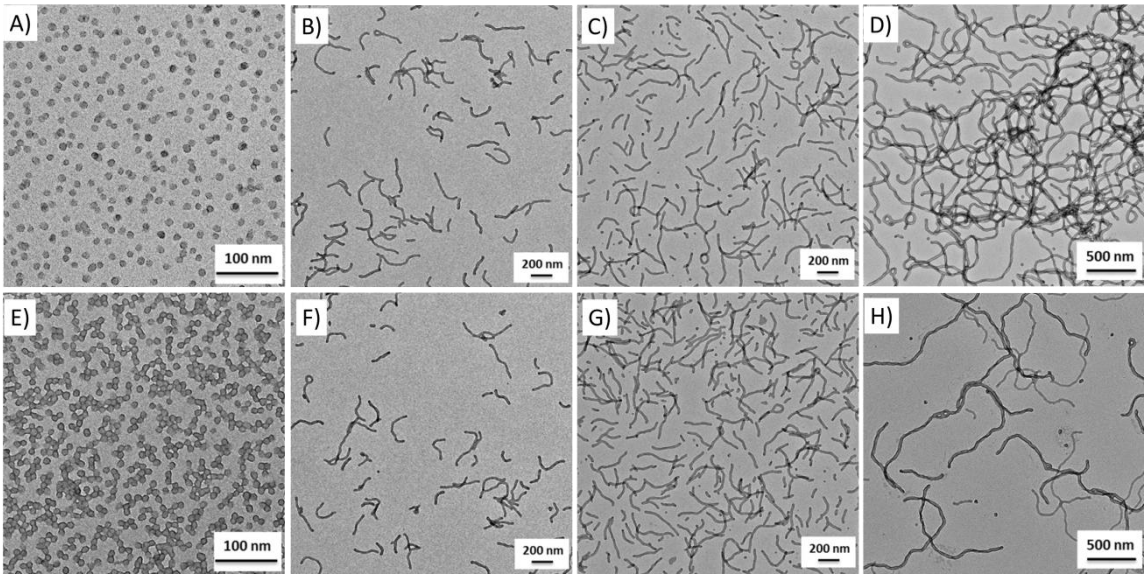

Figure 3.2.5. TEM images obtained for polymer nanoparticles after core cross linking in aqueous solution. A) $SP_{LCC,}$ B) $SWP_{LCC,}$ C) $MWP_{LCC,}$ D) $LWP_{LCC,}$ E) $SP_{HCC,}$ F) $SWP_{HCC,}$ G) $MWP_{HCC,}$ H) $LWP_{HCC,}$

The core crosslinking of the micelles was used to stabilize the colloids but also tune the stiffness of the particles. To evaluate the stiffness of the colloids, the persistence length (*P*) of MWM and LWM having a length between 300 and 1000 nm was calculated using the decay of the orientation correlation within the worm micelle: [268]

$$< \cos(\theta) >= e^{\frac{-l}{sP}} \qquad 1$$

Where θ is the angle between the tangent of two points of the micelle separated by a contour segment of length *l* as described in Figure 3.2.6 and *s* a structure

parameter set to 2 for object equilibrated on a 2D substrate. The persistence length increased from 128 ± 3 nm for uncrosslinked micelles to 253 ± 4 nm LWM_{LCC} crosslinked micelles and 331 ± 6 nm for the LWM_{HCC} micelles. Given that the persistence length is directly proportional to the bending stiffness, the result suggested that the moderately crosslinked worm-like micelles were twice as stiff as the uncrosslinked micelles and the heavily crosslinked micelles were 2.5 times more rigid than the uncrosslinked micelles respectively 0.5 nN nm^2 for uncrosslinked micelles, 1.0 nN nm^2 for moderately crosslinked micelles and 1.3 nN nm^2 for heavily crosslinked micelles.

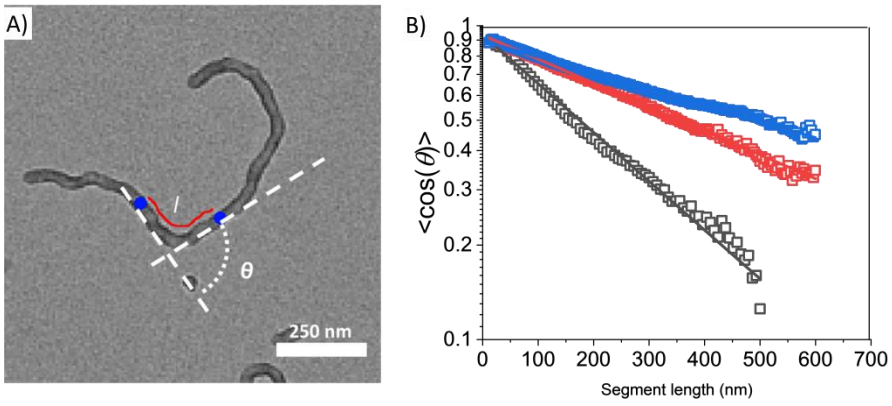

Figure 3.2.6. Persistence length of the micelles and crosslinked particles. A) Parameter for the determination of the persistence length. B) Decay of the tangent-tangent correlation for LWM_{NCC} (black), LWM_{LCC} (red), LWM_{HCC} (blue). The lines represent fits to equation 1.

The rheological properties of the LWM_{NCC} colloidal suspensions were studied at increasing solid content in water under steady shear conditions (Figure 3.2.7 A). The viscosity displayed two distinct regimes of shear-dependent behavior. At low concentration, the viscosity of the suspension increased moderately with the colloid concentration and displayed a Newtonian behavior, while at higher concentration the viscosity of the suspension increased more steeply with increasing concentration and the suspension displayed a shear-thinning behavior. This transition between the dilute and semi-dilute regime occurred at a critical concentration *C*' where the colloids started to interact with each other, whether through the interaction of the adjacent PDMA layer or colloid-colloid interaction. The critical concentration *C*' was defined as the inflection point in the plot of the variation of the zero-shear viscosity with the particle concentration.[269] However, *C*' was influenced by the aspect ratio and stiffness of the colloidal particles studied. For a given concentration, the viscosity of the suspension systematically decreased as the aspect ratio of the colloids decreased. Furthermore, the critical concentration *C*' required to observed the transition between the dilute and semi-dilute regime increased when the aspect ratio of the micelle decreased. This behavior can be attributed to the fact that anisotropic nanoparticles have a larger surface area volume in comparison to sphere, which favors colloid-colloid interaction.

Moreover, increasing the aspect ratio of the nanoparticle created the larger excluded volume resulting in a higher viscosity. [270] In addition, colloids with larger aspect ratio displayed a more pronounced shear thinning behavior, due to the alignment of the colloid in the direction of shear as the sample was subjected to shear.

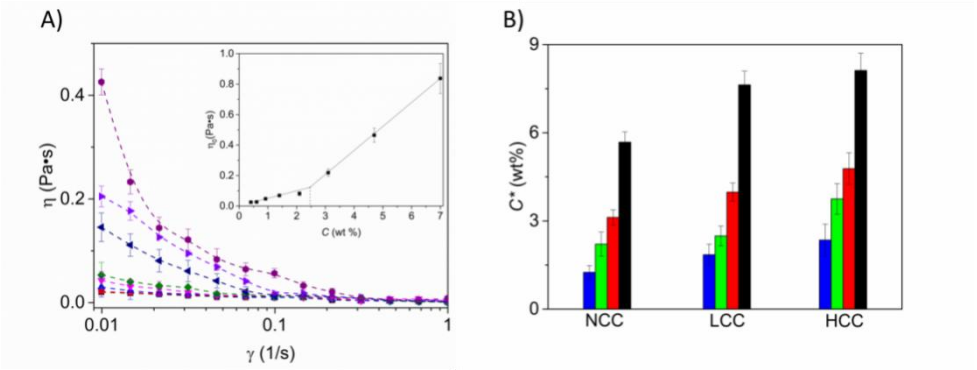

Figure 3.2.7. A) Dynamic viscosity of suspensions of LWM_{NCC} at different concentration. The inset represents the increase in the zero-shear viscosity of the suspensions with the concentration of the nanoparticles. B) Influence of architecture and rigidity on the transition between the dilute and semi-dilute regime. Sphere (black); Short worm (red); Medium worm (green); Long worm (blue)

In addition, the effects of the colloids rigidity on the viscosity of suspensions were investigated. As the stiffness of the colloid increased, the viscosity moderately decreased at a given concentration. In addition, as the stiffness of the colloid increased, the value of *C*' increased. Those results indicated that as the colloid

became stiffer, the colloid-colloid interactions decreased. (Figure 3.2.7 B)

The colloids in the suspensions effectively interacted, and likely interpenetrated and entangled at high concentrations (above *C*') and resulted in a transition from a liquid-like to gel-like behavior. The gel-like behavior of the concentrated suspension was analyzed by dynamic rheology (Figure 3.2.8). At the same concentration of polymer micelles in suspension, 10 wt%, the SWM_{NCC}, MWM_{NCC}, and LWM_{NCC} with different degree of crosslinking and rigidity formed gels, while the SM suspension displayed a liquid-like behavior (Figure 3.2.8 A).

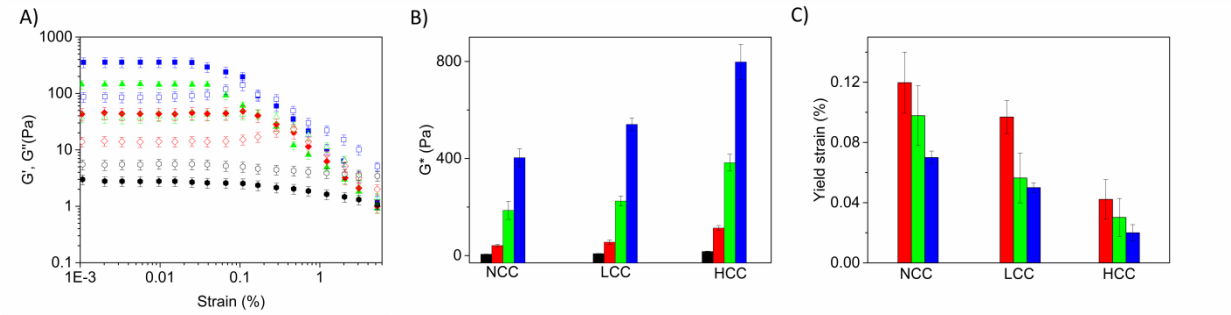

Figure 3.2.8. Viscoelastic behavior G' (filled symbols) and G" (open symbol) of 10 wt% suspensions of colloids in water. A)Effect of the aspect ratio of micelles, B) Effect of rigidity and aspect ratio for dynamic modulus (G*) of the colloids, and C) yield strain of the colloids. Sphere (Black); Short worm (red); Medium worm (green) and Long worm (blue).

However, the inverse was observed for all WM_{NCC} suspensions, which displayed a

linear-viscoelastic region with a higher elastic modulus than the viscous modulus at low deformation, the average complex modulus (G*) of the different gels increased as the aspect ratio of the colloidal building block increased. Given that the volume occupied by the different types of collloids was similar for all the colloids with different aspect ratios (at a given weight fraction), this increase in the colloid-colloid interactions cannot be directly ascribed to the interdigitation of the water-swelled PDMA canopy, rather the arrested gel-like behavior can only be ascribed to the geometry of the micellar core, and an increase in the aspect ratio of the micelles led to the formation of a more cohesive network, either because of the increased excluded volume of higher aspect ratio colloids or through colloid-colloid interaction.

However, when the colloidal gels were prepared with colloids having the same shape but different stiffness, an increase in the complex modulus (*G**) of the resulting gels was observed as the stiffness of the building block increased. Previous works also demonstrated that this is due to worm stiffening with the increase of core crosslinking density. [271-273] For example, the LWM_{NCC} led to an increase in *G** from 380 to 581 Pa at LWM_{LCC}, 813 Pa at LWM_{HCC} (Figure 3.2.8 B). These results represented the direct comparison of the stiffness of nanoparticle with different rigidity.

In addition, the fragility of the colloidal gels defined by the yield strain Υ_c. Figure 3.2.8 C shows that the yield strain of the gels was affected by the aspect ratio and rigidity of nanoparticle. The suspensions of sphere did not form gels in the concentration range studied. WM was stiffer (higher G^*) and more fragile (lower yield strain) with the increase of aspect ratio, moreover, for nanoparticle having different rigidity the formation of colloidal gels was observed for the three different core crosslinking density. The gels prepared with the higher crosslinking density was stiffest and the most fragile, the resulting colloidal gel showed the highest yield strain. Since the canopy of nanoparticle was always the same for all the nanoparticles, the nanoparticle with higher aspect ratio provided effective nanoparticles interactions because they were more flexible. When the the rigidity of the core of nanoparticle increased, the suspensions behaved in a more solid-like manner and these suspensions were tougher, with lower yield strain.

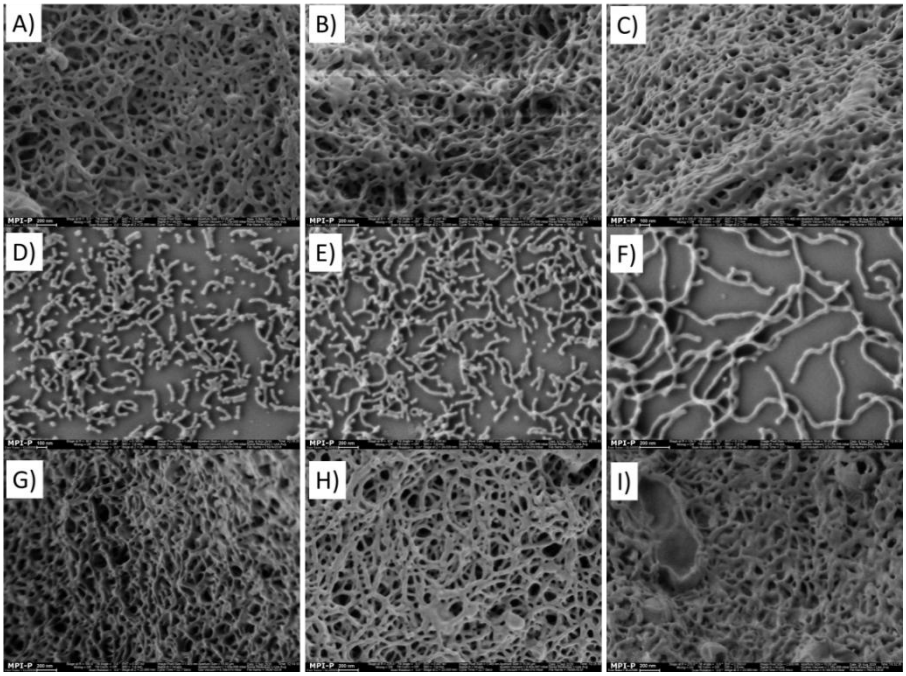

Figure 3.2.9. SEM images for gels made of SWM_{NCC} A), MWM_{NCC} B) and LWM_{NCC} C) at 10 wt%, RT; SWM_{NCC} D), MWM_{NCC} E) and LWM_{NCC} F) at 1.0 wt%, RT; and SWM_{NCC} D), MWM_{NCC} E) and LWM_{NCC} F) at 1.0 wt%, 45 ^{0} C. The scale bars are 100 nm.

Scanning electron microscopy was used to image the microstructure of the colloidal gels. Figure 3.2.9 A), B) and C) show representative images of the nanofibrillar structure of the colloidal gels. The mean fiber diameter in the hydrogels formed by SWM_{NCC}, MWM_{NCC}, and LWM_{NCC}, respectively.

The state of the swollen PDMA canopy also had a critical influence on the rheological properties of the colloidal gels. Free PDMA chains in aqueous solution

displayed a typical coil-to-globule transition above its lower critical solution temperature (LCST) around 35 ℃. Upon heating, the water-soluble hydrated chains of the PDMA collapse to form compact deswollen globules.[274, 275] When the PDMA chains were immobilized at the surface of the nanoparticles, upon heating, the colloidal system displayed a critical aggregation temperature (CAT) in lieu of a LSCT. Above the CAT where the PDMA chains were unswollen, the colloids lost the source of their colloidal stability resulting in the aggregation of the colloidal system, which was demonstrated by DLS. As the suspensions of SM was heated from 25 ℃ to 40 ℃ the hydrodynamic sized measured increased from 23 nm to 800 nm, and this thermal aggregation was reversible (Figure 3.2.10 A). For free PDMA chains, heating the solution above the LCST resulted in the precipitation of the polymer. However, in the case of the colloidal particles functionalized with the PDMA chains, heating the suspension above the CAT resulted in the formation of a gel even when using dilute suspension that only displayed a liquid-like behavior at room temperature. Furthermore, the aggregation was not accompanied by any gelation shrinkage and all the water present in the suspension was efficiently trapped in the colloidal gel.

The gelation through colloidal aggregation resulted in a variation of the mechanical properties of the suspension. The mechanical properties of thermally responsive

sphere suspensions were investigated by dynamical rheology. At 25 ℃, all the 1 wt% suspension of colloidal nanoparticles behaved like a liquid with a *G*" larger than the *G*'. As the temperature of the suspension increased, gelation of the suspension occurred as characterized by the *G*' being larger than the *G*", but their morphology did not change. The mechanical properties of the resulting colloidal gels were affected by the rigidity of the colloid and their aspect ratio. More rigid colloidal building block resulted in the formation of stiffer colloidal gels, and similarly the colloids with the highest aspect ratio also led to the formation of the stiffer colloidal gels (Figure 3.2.10 B). In addition, the transition between the liquid and the gel state was fully reversible (Figure 3.2.10 C). Moreover, the formation of all suspensions was summarized in Figure 3.2.10 D). Overall, during thermally induced gel formation gel, the nanocolloidal network became more persistent because of the stronger contacts between 'crowded' colloidal nanoparticles, hence providing an enhanced opportunity for inter-particle space jamming. Meanwhile, the interactions between PDMA and PDMA at the surface changed from repulsive to attractive above the LCST, which provided additional strength to the interparticle bonds. [276]

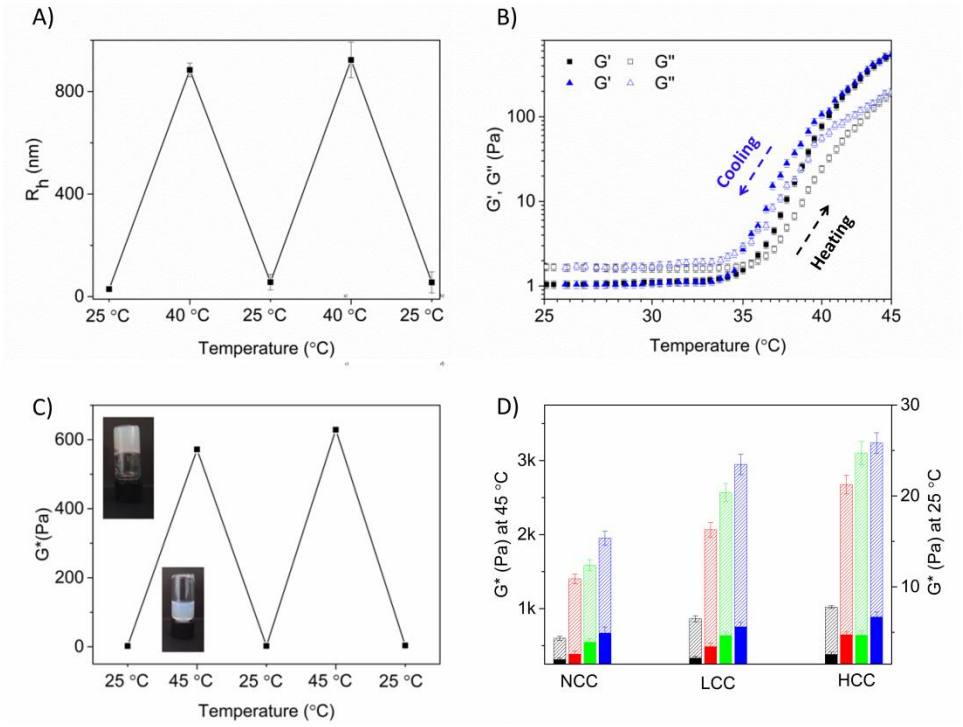

Figure 3.2.10. A) Hydrodynamic diameter variation exhibited by a 0.01 wt % SM aqueous suspension submitted to 25 ℃-45 ℃-25 ℃ temperature cycles, B) G' and G" plotted as a function of temperature for heating and cooling cycles for sphere suspension prepared using 1.0 wt %, heating C) Thermal cycling of SM 1.0 wt % using to demonstrate reversibility of the gelation process, D) Effect of the aspect ratio and rigidity of the colloids on the properties of the colloidal gels where G* at 25 ℃ (solid symbol); G* at 45 ℃ (open symbol), Sphere (Black); Short worm (red); Medium worm (green); Long worm (blue).

3.2.4 Conclusions

The study of colloidal suspensions containing building blocks with the same

composition and occupying similar volume fraction but with distinct rigidity and aspect ratio reveal new insights in the formation of colloidal gels. Suspensions of all particles displayed a non-Newtonian behavior. The viscoelastic behavior of all suspensions depended upon the concentration of the particles and the rigidity of the particle and aspect ratio. The critical concentration shifted to a higher concentration with increasing rigidity and aspect ratio. As the concentration increased, the colloidal particles formed fibrillar gel because of the entanglement of particles. One the one hand, the key effect on the sol-gel transition was the aspect ratio of particles; on the other hand, the stiffness of the resulting gels was influenced by the rigidity of particles. The formation of fibrillar gel more easily occurred with nanocolloids having a large aspect ratio because of more particle-particle interactions. Meanwhile, it was found that the mechanical properties of the gels were affected by both the aspect ratio and rigidity of particle. The longer and rigid colloids displayed a higher G' than the G'' at low strain, but they process smaller deformation. Finally, the suspensions of these particles exhibited a heating-induced transition from a flowing liquid to a self-supporting gel at low concentration 1.0 wt %. The present fibrillar gels could potentially find applications in strengthening and guiding regeneration of load-bearing soft.

3.3 Release From Thermo-responsive Anisotropic Nanocarriers

In the previous section, temperature-responsive polymer nanoparticles with different rigidity and aspect ratio were prepared, and the resulting colloidal gel studied. Such systems are also of high interest in the delivery of bioactive molecules. On the one hand, in suspensions, anisotropic NPs have unconventional interaction with cells, and the uptake and circulation time have been reported to differ from that of their spherical counterpart. Furthermore, the colloidal gels can also as a solid depot for the delivery of active principles.

To develop anisotopic multiresponsive delivery systems, the thermoresponsive NPs introduced in section 3.2 were modified in this section with redox-responsive moieties and use to study the release of model payload.

3.3.1 Introduction

Polymer nanoparticles have shown increasing success in drug delivery because of their properties, such as biocompatibility, permeability and retention effect, and targeting abilities against tumor tissue and cells. [277--281] More importantly, tuning the physico-chemical parameters of nanoparticles such as size, surface charge, surface functionalization, or stiffness can improve the delivery of active payloads.

Most carriers studied are spherical particles, and in such systems, the effects of size

and chemical composition are well documented.[282-286] However, recent data indicate that anisotropic particles display a distinct behavior in biological environments when compared to spherical analogs.[287] For example, different proteins are adsorbing on rod–shape particles in comparison to spherical one; the structure influence the internalization by cells;[288, 289] and anisotropic particles show longer circulation time. [290] Such a unique combination of properties is desirable for drug delivery. For example, intravenously-injected filamentous micelles displayed in circulation about ten times longer than spherical nanoacrriers,[291] and they undergo limited non-specific cell uptake making such particles interesting candidate for the sustained delivery of site-specific cargos. [287]

A lot of efforts have been devoted to understanding the effect of the nanocarrier shape on the cellular uptake, but there are conflicting reports on the effect of shape anisotropy on the particle/cell interactions. For example, reduced cell uptake of rod-like nanoparticles compared to sphere was found with gold nanoparticles and polymer nanoparticles,[292- 294] but enhanced cell uptake was frequently reported using rod-like micelles in comparison with spherical micelles.[295-299] This discrepancy might be the results of the hemodynamic forces exerted on particles during systemic circulation influenced by the aspect ratio and the stiffness of the particles, or the uptake rate and intracellular diffusion of the particles affected not

only by the size and aspect ratio but also by the surface chemistry. Additionally, the anisotropic nanocarriers can be functionalized with targeting ligands, which is another possible reason because the targeting ligands can direct bind between drugs and target sites, hence enhancing antitumor efficiency.[304]

The stiffness of the anisotropic nanocarriers significantly affects their behavior in biologic media. To date, many nanocarriers with controlled stiffness have been reported from soft carrier like liposomes[300] to solid nanoparticles.[301] However, the reason why stiffness is a critical factor remains elusive,[302] in part because it is challenging to quantify the rigidity of nanocarriers.[303]

Due to the impact of the shape of the nanocarriers, many different approaches have been developed to create carriers with anisotropic shape, ranging from self-assembly of copolymer to lithography.[305-307] The ideal carrier should possess features like easy preparation, tunable chemical composition and controlled dimension. While top-down methods like lithography or mechanical deformation are difficult to efficiently scale-up, bottom-up process like block copolymer self-assembly have other pitfalls. For example, block copolymers self-assemble into highly anisotropic polymer micelles with well-defined shape, but controlling the aspect ratio of the worm-like micelles has proven to be very challenging and can usually only be controlled in very dilute conditions. During the last few years,

many efforts have been devoted to forming the anisotropic micelle based on the PISA approach using RAFT polymerization,[308-310] the formation of anisotropic micelles using PISA can possess the feature as a conventional method has, but also directly produce self-assembled morphologies at very high solids contents and with reduced experimental effort.

Here, PISA was used to prepare worm-like micelle. Then using shearing forces,[311, 312] it was possible to tune the aspect ratio of the resulting particles. Finally, by the controlled crosslinking of the micelle core the stiffness of the particles was tuned. The resulting particles had different aspect ratios and rigidities, but the same diameter and surface chemistry. Additionally, give the presence of well-defined end groups generated by the combination of RAFT polymerization in the PISA process; it is possible to chemically functionalize the outer polymer layer.

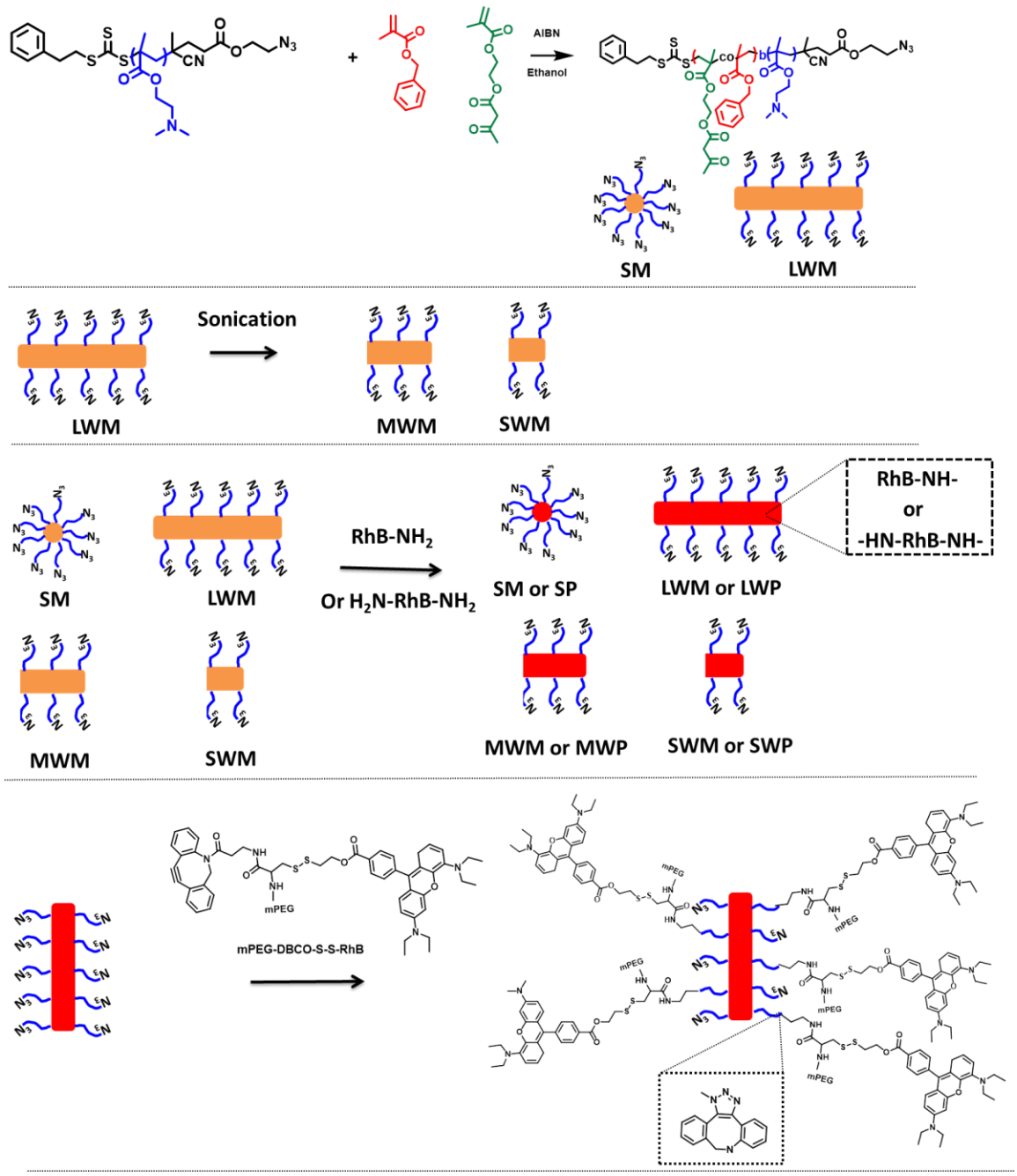

Figure 3.3.1. Design of multifunctionalized anisotropic nanoparticles for dye release study.

3.3.2 Experimental part

Materials

The monomers 2-(dimethylamino)ethylmethacrylate (99%, DMAEMA), benzyl methacrylate (98%, BzMA) and 2-(methacryloyloxy)ethyl acetoacetate (95%, AAEM) boc-L-cysteine (98.5%, Boc-Cys-OH), 2,2'-dithiodipyridine (98%), folic acid (97%, FA), poly(ethylene glycol) 2-aminoethyl ether acetic acid (NH_2-PEG-COOH, average Mn 5,000), methoxypolyethylene glycol 5,000 acetic acid N-succinimidyl ester (mPEG-NHS, average Mn 5,000), Rhodamine b (98.5%, RhB), were purchased from Sigma-Aldrich. Thiolated RhB was synthesized as previously reported.[313] RhB-NH_2 and H_2N-RhB-NH_2 were synthesized according to the literature.[314] Folic acid-PEG-NHS was synthesized according to literature.[315] 4, 4'-Azobis(4-cyanovaleric acid) (ACVA)) or 2,2'-azobis(isobutyronitrile) (AIBN) were recrystallized twice before use.

Synthesis of Azide-CTAs

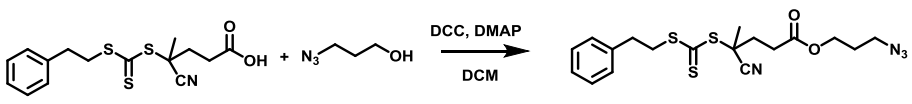

Figure 3.3.2 Synthetic route of CTA-azide.

4-Cyano-4-(2-phenylethanesulfanyl-thiocarbonyl)sulfanylpentanoic acid (CTA-COOH) (2.52 g, 0.01 mol), DCC (4.12 g, 0.02 mol) and DMAP (0.112 g, 9.18 x 10^{-4} mol) were dissolved in 50 mL of DCM, which was cooled to 0 ℃ with an ice bath and 3-azidopropanol (2.0 g, 0.011 mol) was added. The reaction mixture was warmed up to room temperature and then stirred for 24 h. DCM was removed by rotary evaporation. The residue was redispersed in diethyl ether and filtered. The filtrate was concentrated to a viscous residue and purified by silica column chromatography (1/4 petroleum ether/ethyl acetate) to give a yield of 80%.

Synthesis of Poly(2-(dimethylamino)ethyl methacrylate) $PDMAEMA_{31}$-CTAs

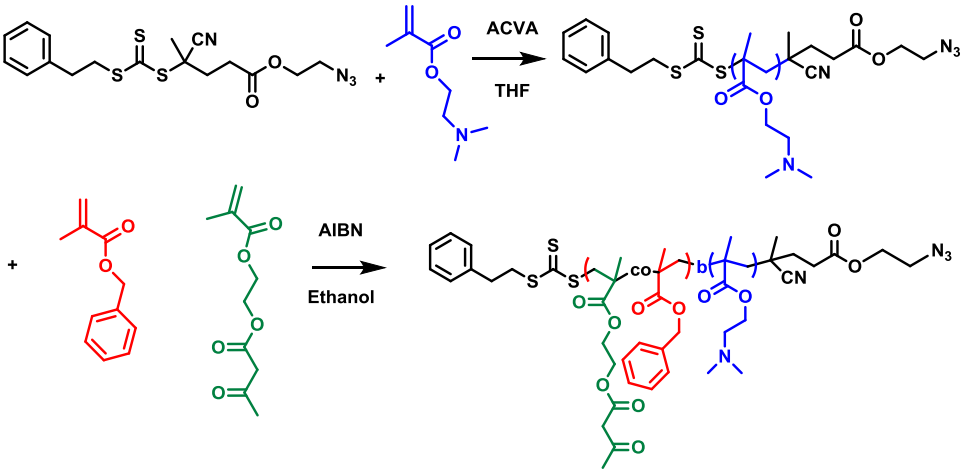

Figure 3.3.3 Synthesis of micelle by RAFT alcoholic dispersion polymerization at 70 ℃ *via* polymerization-induced self-assembly.

The synthetic route for the polymer micelles was the same as described in section

3.2 but substituting the CTA with the azide-functionalized CTA agent, synthesized through modification of the carboxylic acid group on the 4-cyano-4-(2-phenylethanesulfanyl-thiocarbonyl)sulfanylpentanoic acid.

Controlling the length of the micelles

The nanocarriers with different aspect ratio were prepared according to the section 3.2. After the ultrasound cutting, the rod-like micelles were characterized by TEM.

Labeling and crosslinking of the nanocarriers with dye

Amine groups can react with the acetoacetate of the AAEM, located in the core of the micelles, to form an imine via nucleophilic substitution. The micelles were labeled by the addition of RhB-NH_2 or H_2N-RhB-NH_2. The resulting strained nanocarriers were purified by dialysis against Milli-Q.

For the core staining reaction of spherical micelles with RhB-NH_2 7 mg spherical micelle was dispersed in 5.0 mL of ethanol. RhB-NH_2 (5 mg, 9.63 x 10^{-3} μmol) was added to the dispersion. The mixture was kept for 24 h and then dialysis against Milli-Q water for at least three days, afterwards, the dispersion of spherical micelle was used to quantify the efficiency of the functionalization reaction.

Synthesis of DBCO additive for nanocarrier functionalization

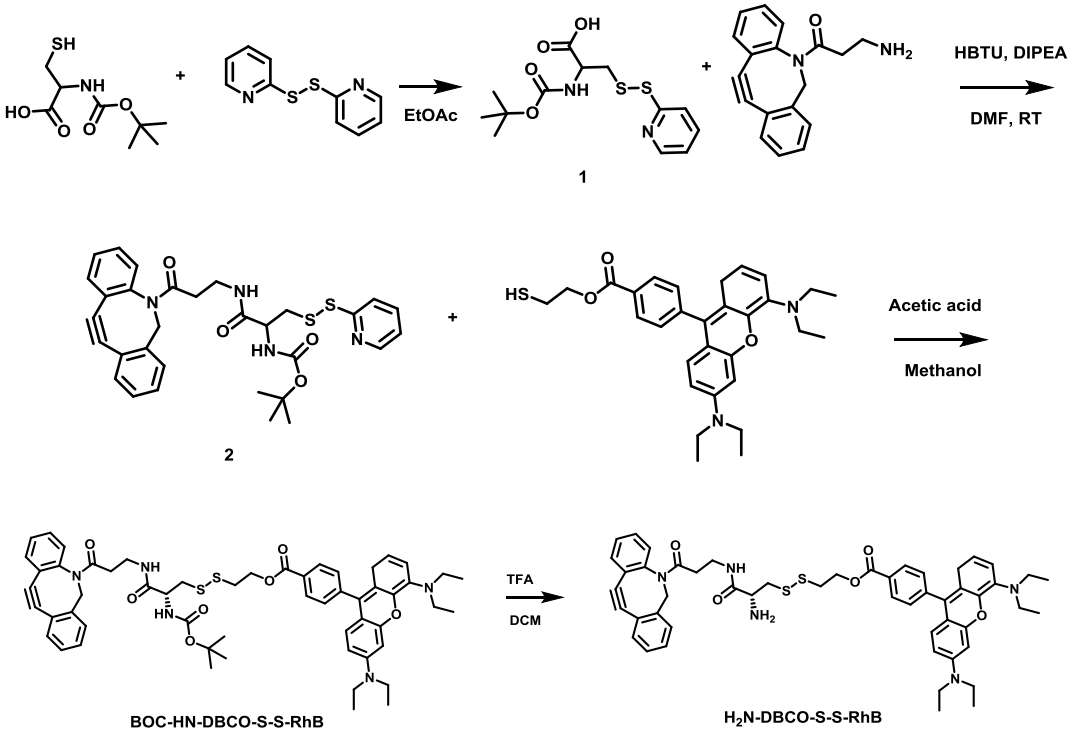

Figure 3.3.4 Synthesis of H_2N-BDCO-S-S-RhB.

The product 1 was synthesized according to the literature. [316] A solution of Boc-Cys-OH (0.221 g, 1 mmol) in EtOAc (10 mL) was added to 2, 2'-dipyridyldisulfide (0.55 g, 2.5 mmol) in EtOAc (10 mL) in one portion. After 15 min, 0.2 M $Cu(NO_3)_2$ (5 mL, 1 mmol) was added to the solution. The copper (Ⅱ) ion and 2-mercaptopyridine formed a blue precipitate, which was removed by filtration. After washing with water (once), the EtOAc solution was extracted with ice cold saturated Na_2CO_3 (15 mL, twice). The combined Na_2CO_3 solutions were extracted with ether (15 mL, once), and the ether solution was discarded. The aqueous solution was overlaid with EtOAc (15 mL) and acidified to pH 3.5 with

citric acid. The aqueous layer was extracted with EtOAc (twice), the combined EtOAc solutions were washed with water and brine and were then concentrated in vacuo to give a white solid. Recrystallization from EtOAc/ethyl ether (1:2) yielded a white powder (0.21 g, 0.65 mmol, 65%).

The product 2 was prepared using the product 1 (50 mg, 0.16 mmol), the DBCO-NH_2 (24 mg, 0.19 mmol), and DMF (1 mL) at 5 ℃ was added HBTU (86 mg, 0.19 mmol) followed by DIEA (0.23 mL, 0.65 mmol). The reaction mixture was stirred at RT for 16 h. The reaction mixture was then diluted with EtOAc (25 mL) and washed sequentially with 10% aq citric acid, sat aq $NaHCO_3$ (10 mL), and brine (10 mL). The combined organic phases were dried ($MgSO_4$) and concentrated in vacuo to give a gum. The resulting crude material was purified by column chromatography (30% DCM/EtOAc).

The product Boc-HN-DBCO-S-S-RhB was prepared using product 2 (0.25mmol, 122mg) dissolved in 5 mL methanol; afterwards, the thiolated RhB (0.3 mmol, 151 mg) was added to the solution with acetic acid (0.5mmol, 30mg), The mixture was stirred at room temperature for 24h. The concentrated product was chromatographed on a silica gel column with Methanol/CH_2Cl_2 (1:9 by volume) as eluent.

Boc-HN-DBCO-S-S-RhB (190 mg, 0.2 mmol) was dissolved in DCM (5 mL). TFA

(2.5 mL) was injected dropwise to this stirring solution and the reaction flask was wrapped with Al foil. The resultant solution was stirred at RT for 30 min. DCM and TFA were removed under high vacuum overnight to yield a red solid as the product in a quantitatively yield.

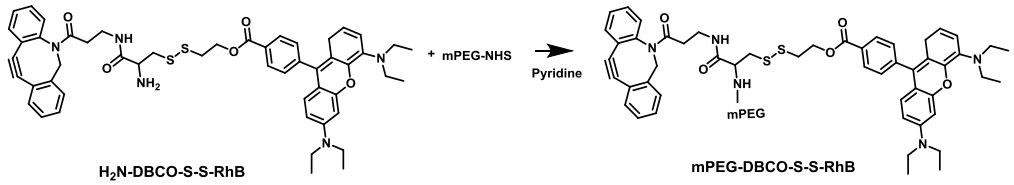

Figure 3.3.5 Synthesis of mPEG-DBCO-S-S-RhB.

36 mg of product H_2N-BDCO-S-S-RhB (0.04 mmol) in 10 ml of pyridine was reacted with of NHS-mPEG (200 mg, 0.04 mmol) under nitrogen atmosphere at room temperature for 24 h. The resultant solution was diluted with a dialysis bag (MWCO, 1k Da) against deionized water three times and freeze-dried.

Coupling of functionalized DCBO to the polymer micelles

The click conjugation followed the standard protocols. Polymer micelles (7.2 x 10^{-5} μmol) were dispersed in 5.0 mL of Milli-Q water. An excess of mPEG-DBCO-S-S-RhB (1.7 x 10^{-4} μmol) was added to the dispersion, then the reaction mixture was incubated the room temperature for 24 h. The reaction mixture was purified dialysis (MWCO, 14k Da) against deionized water for three days.

Dye loading and release experiment

All nanocarriers were used to explore the release behavior. Briefly, 1 mL of the nanocarriers solution was transferred to a dialysis bag (MWCO, 14k Da) and then was placed in 5 mL of PBS (pH 7.4) with or without 10 mM DTT. The drug-release process was conducted in a constant temperature oscillator that maintained a temperature of 37 ℃ and a constant shanking speed of 300 rpm. At predetermined time intervals, 1 mL of the medium was withdrawn, and then the same volume of a fresh medium was replenished. The amount of the dye released in the withdrawn solution was analyzed by measuring the fluorescence of dye using plate-reader.

3.3.3 Results and discussion

The azide functionalized chain transfer agent used during the RAFT polymerization was synthesized through modification of the carboxylic acid group on the trithiolcarbonate RAFT agent. This N_3-CTA was used to polymerized dimethylamino)ethylmethacrylate to form a macro-CTA. This $PDMA_{31}$-macro-CTA was then chain-extended with a mixture of BzMA and AAEM via RAFT dispersion polymerization in ethanol at 70 ℃ to produce a series of $PDMA_{31}$-PBzMA*x* diblock copolymers. The polymerization induced self-assembly (PISA) in alcoholic dispersion yielded spherical and worm-like

micelle, with the azide groups located at the end of the hydrophilic chains. The aspect ratio of the micelles was controlled by ultrasonication to break the long worm-like micelles following section 3.2. (Figure 3.3.6)

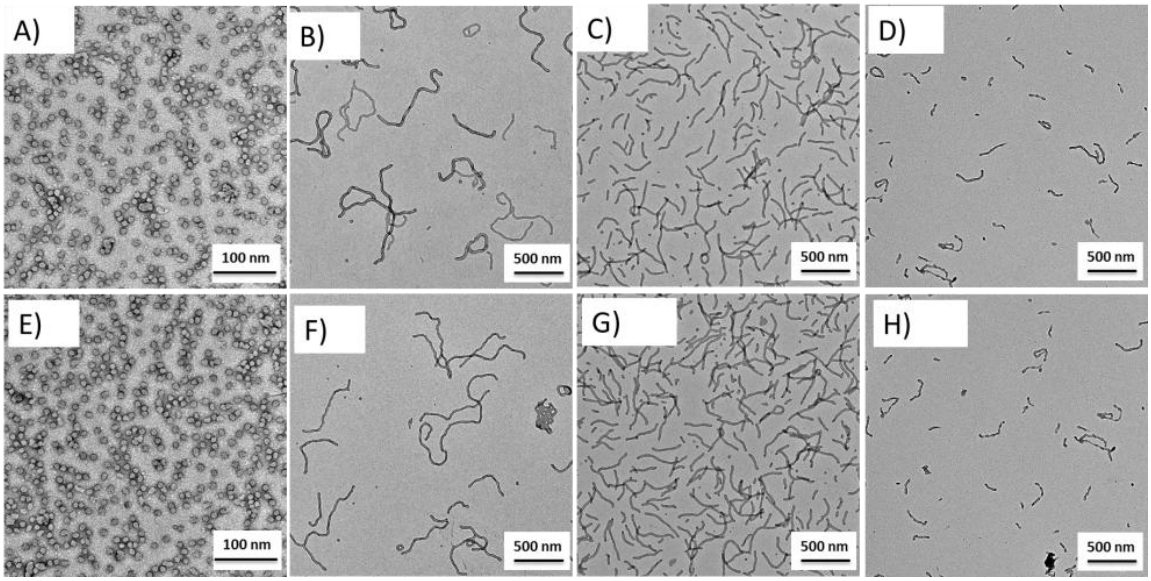

Figure 3.3.6 Representative TEM images of nanoparticles after core staining with dye; A), B), C) and D) repented RhB-NH_2 stained micelles; E), F), G) and H) repented H_2N-RhB-NH_2 stained particle.

Moreover, in order to label the core of the micelles, the AAEM units were reacted with either RhB-NH_2 or H_2N-RhB-NH_2. (Figure 3.3.6) The reaction between AAEM and H_2N-RhB-NH_2 simultaneously led to the labeling and the crosslinking of the micelles. The formation of the imine linkages was almost quantitative as quantified by fluorescence spectroscopy (Table 1). Based on the fluorescence of

free $RhB(NH_2)_2$ and composition and molecular weight of the block copolymers more than 90% of the AAEM groups have reacted with the RhB derivative.

Table 3.3.1. Functionalization of the nanoparticle core with $RhB(NH_2)_2$.

NP	C^a (umol/mL)	C^b (umol/mL)	Yield (%)
LWM	0.961	0.9425	98.1
MWM	1.012	0.9746	96.3
SWM	1.075	1.0621	98.8
SM	0.631	0.6064	96.1
LWP	0.961	0.4355	90.6
MWP	1.012	0.4594	90.8
SWP	1.075	0.5138	95.6
SP	0.631	0.0588	93.4

[a] Calculated from the solid content and composition of micelle, [b] Calculated from the calibration curves for the Rhodamine-based fluorescence detection.

The resulting crosslinked nanoparticles were covered with a layer of hydrophilic poly(dimethyl amioethyl methacrylate) terminated with azide groups that can be functionalized using copper-free click chemistry based on the reaction of a cyclooctyne (DBCO) moiety with an azide-labeled nanoparticles, known as

strain-promoted alkyne azide cycloaddition (SPAAC). Cyclooctynes are thermostable with very narrow and specific reactivity toward azides, resulting in almost quantitative yields of stable triazoles. [317] Thus, to functionalize the hydrophilic layer tethered to the nanoparticles a multifunctional DBCO derivative was prepared. At the center of this difunctional DBCO derivative was a cysteine unit, the carboxylic acid of the cysteine was attached to DBCO-NH_2, the amine of the cysteine was use to irreversibly attached a molecules here PEG-COOH was used, but alternatively targeting moieties like Folic acid could be inserted and finally, the thiol group of the cysteine was used to create a redox-responsive disulfide bridge that could be used for the controlled delivery of a payload. Here, as a model payload, rhodamine-SH was attached to the cysteine. The resulting DBCO-PEG-S-S-RhB was then tethered to the nanoparticles. The fluorescence of the Rhodamine was used to quantify the yield of the DBCO/azide conjugation. Based on a calibration realized with rhodamine-SH, the efficiency of the functionalization of the azides groups with the multifunctional DBCO was between 73-75% (Table 2). Performing the chemistry on the nanoparticles did not influence the structure. The morphology of the particles remained the same after the reaction as before (Figure 3.3.7).

Table 3.3. 2. Click efficiency and dye loading on the surface of nanoparticle.

NP	C^a (umol/mL)	C^c (umol/mL)	*E* (%)
LWM	12.8×10^{-3}	9.34×10^{-3}	73
MWM	13.4×10^{-3}	10.1×10^{-3}	75
SWM	14.4×10^{-3}	10.6×10^{-3}	74
SM	8.4×10^{-3}	6.22×10^{-3}	74

[a] Calculated from the solid content and composition of nanoparticles, [c] Calculated from the calibration curves for the Rhodamine-based fluorescence detection.

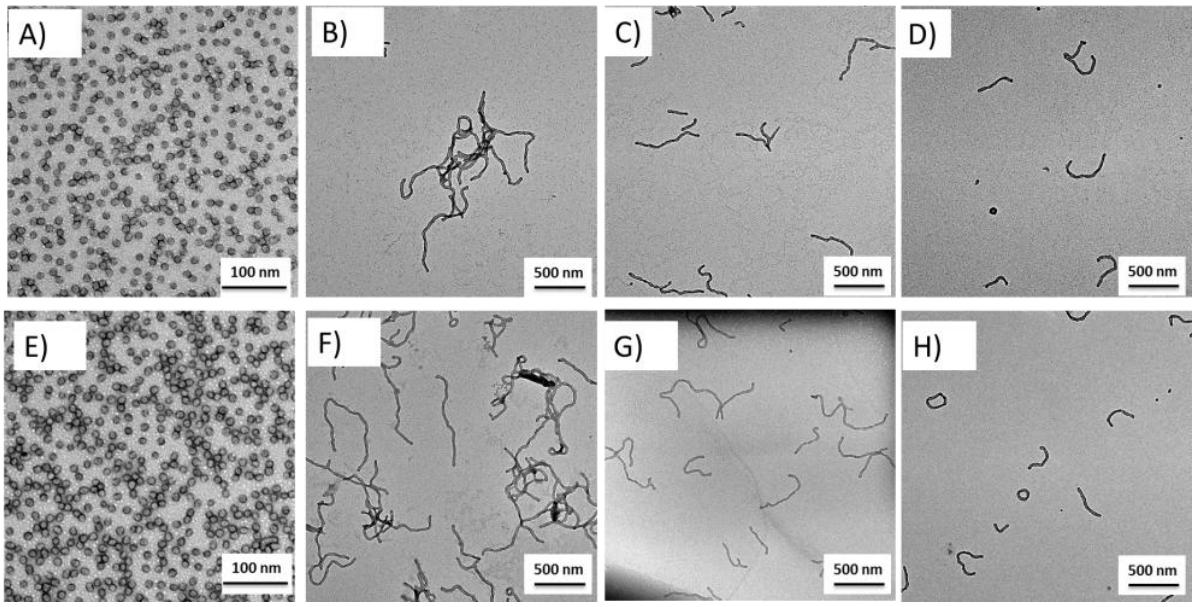

Figure 3.3.7 Representative TEM images of nanoparticles after surface functionalization with mPEG-DBCO-S-S-RhB; A), B), C) and D) repented

RhB-NH_2 stained micelles; E), F), G) and H) repented H_2N-RhB-NH_2 stained particle.

Table 3.3.3. Characterization of the nanoparticle.

NP	Length (nm) [a]	Aspect ratio	ZP (mV)
LWM	1700	69	14.0 ±3.65
MWM	590	24	12.9 ±3.44
SWM	220	9	13.1 ±3.17
SM	25	1	10.9 ±4.23
LWP	1670	68	13.0 ±4.12
MWP	230	24	14.1 ±2.22
SWP	590	9	12.3 ±4.32
SP	1670	1	9.9 ±3.21

[a] Calculated from the log-normal distribution of the size measured by TEM for N>75.

The nanocarriers functionalized with multifunctional DBCO derivative were used to explore the redox release of the payload. The release study was performed in PBS with or without 10 mM DTT using the dialysis method. PBS solution with 10 mM DTT has been widely use to simulate the high GSH level in the tumor

microenvironment.[318] Under such conditions, both the crosslinked and the un-crosslinked particles of different aspect ratio displayed the same release behaviors which suggested that the aspect ratio and crosslinking did not alter the conformation of the PDMAEMA chains and the accessibility of the payload. Within the first 24 h, 80% of the payload was rapidly released into the medium, and the final cumulative release at 72 h reached 94%. However, even in the absence of DTT some release of the payload (7%) was also observed, which probably due to the presence of remaining untethered payload or due to the partial light sensitivity of the disulfide bond. [319] (Figure 3.3.8 A) and B))

Furthermore, when the concentration of nanoparticles in suspension is increased to 1 wt%, colloidal gels can be obtained when the temperature of the suspension is increased. When the colloidal gel formed with the spherical micelle were immersed in a GSH solution, a sharp release of dye was observed within the first 12 h and was followed by a gradual release of dye at 72 h. However, the nanofibrillar gels showed lower dye release 60% after 72 h (Figure 3.3.8 C). Moreover, the Figure 3.3.8 D) shows that with the increase of concentration of nanocarriers, the cumulative release decreased. The reason was that higher concentration led to a stronger colloidal network resulting in a lower dye release.

The diffusion and transport phenomenon in the solid depots for by the gelation of the colloids are likely the reason for the slower release observed.

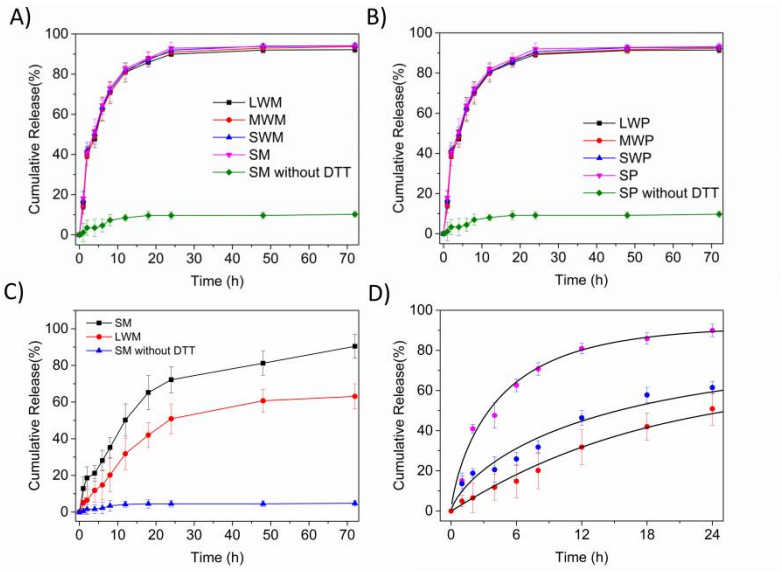

Figure 3.3.8 Dye-release profiles of A) Micelle, B) Particle at 0.5 wt% and RT, C) SM gel and LWM gel at 1.0 wt% and 45 ℃, with or without 10 mM DTT and D) LWM at 0.5 wt % (Magenta, RT) , 1.0 wt% (Blue, 45 ℃) and 1.0 wt% (Red, 45 ℃)

3.3.4 Conclusion

In summary, we have demonstrated a technique to directly prepare nanoparticles with different aspect ratio and rigidity with a functional surface. A redox-responsive polymer nanoplatform was successfully developed. The payload release was evaluated by standard methods, which demonstrated the release

behaviors were not influenced by the aspect ratio and rigidity of nanoparticle. This methodology of producing multifunctional anisotropic nanoparticles will have utility in bio-applications in order to further study how the physical parameters influence the behavior of drug delivery.

Chapter 4. Summary and outlook

The need for the development of new smart and responsive polymer systems led to the synthesis of multi-stimulus-responsive polymer with unique and controllable properties; novel anisotropic polymer nanoparticles used for the formation of colloidal gels and their use as nanocarriers.

First, moities responding to light and temperature were combined in one single system. The dual temperature/light responsive was realized by designing a copolymer composed of N-isopropylacrylamide and a reversible spiropyrane-based photoacid. The polyphotoacid was responsive to light irradiation at λ = 460 nm and released one proton for each spiropyrane unit and was, therefore, able to acidify the solution. The opposite effect, the removal of protons and corresponding pH increase, was observed when either keeping the polyphotoacid in the dark for several minutes or more quickly by the irradiation of UV-light. Increasing the temperature above the lower critical solution temperature (LCST) silenced the photoacid behavior because of the formation of deswolen polymer nanostructures and the irradiation of light at λ = 460 nm did not lead anymore to proton generation. Hence, the temperature-induced phase transition of the polyphotoacid acted as a thermal on/off switch for the photoacid function.

Then, the microstructure and mechanical properties of colloidal gels were tune by changes in temperature but also by tuning the aspect ratio and the rigidity of the polymer nanoparticles. A library of nanoparticles with different aspect ratio and rigidity were prepared using polymerization induced self-assembly to prepare the micelles. The resulting micelles were composed of a reactive core and a temperature-responsive shell. The aspect ratio of the worm-like micelles formed was tuned with shear forces generated by ultrasonication, while the rigidity of the particles was tune by the controlled crossliking of the reactive core. Finally, to address the effect of the colloid properties on the properties of the resulting colloidal gels, we study how the macroscopic behavior of colloidal gels composed of nanoparticles with same surface chemistry and chemical composition but having different aspect ratio and rigidity, and the influence of the colloid design on the formation of fibrillar gels.

Then the thermos-responsive nanoparticles were functionalized with oxydo-reduction-responsive functionality and used as nanocarriers. Azide-functionalized anisotropic nanoparticles were formed using PISA. Those particles had a controlled composition, aspect ratio and rigidity. At a temperature below the critical aggregation of the nanoparticles, the reduction-triggered release of a payload was the same for the nanocarriers which ever their aspect ratio or

rigidity. However, an increase in temperature can be used to slow down the release of all nanoparticles. More interestingly, when the nanoparticles formed strong colloidal gels, the temperature increased led to an aspect ratio- and rigidity-dependent release.

This thesis showed the promising perspectives and possibilities of smart materials to provide materials with precisely tunable functions. It explores the possibility of using such attractive functional materials in many applications such as coatings, smart switch, rheology modifier, and drug delivery. The materials presented here can be developed for targeted applications.

Specifically, photoacid polymer (Chapter 3.1) can be developed further to broaden the scope of potential applications. The mechanisms of many enzymes are dramatically influenced by the cellular pH value, resulting in many diseases. Hence photoacids have great potential for biomedical applications by controlling the local pH so that the activities of enzyme. This may be achieved by linking photoacids to biomaterials or functionalizing them to target biomolecules, membranes, or organelles. Moreover, photocontrolled drug delivery is another possible application.

In Chapter 3.2, in comparison with the hydrogels formed by molecules, nanofibrillar hydrogel possesses more advantages, including larger pore size,

higher stiffness, and interesting rheological properties. Therefore, nanofibrillar hydrogels are very promising materials for a broad range of applications requiring specific mechanical or transport properties. Nanofibrillar hydrogels can be used as injectable gels and as an artificial extracellular matrix for three-dimensional culture, which can create more complex biological structures.

In Chapter 3.3, nanoparticles are widely investigated as therapeutic and contrast agent carriers because of their fundamental advantages over traditional methods. It is noticeable that most early nanocarriers studies focus on the spherical particles, but there has been increasing interest in non-spherical nanoparticles for nanomedicine as they were found to have superior properties, including circulation times, cell uptake, biodistribution and cellular internalization. To understand this, the wormlike nanoparticles with different aspect ratio and rigidity can be used to study how those parameters influence the behavior of delivery, which may lead to a better understanding of therapeutic.

Chapter 5. Acknowledgements

Long Yang (杨龙)

Mainz, 19th September 2020

Chapter 6. Publications

Chapter 7. Literature

1. Staudinger, H. From organic chemistry to macromolecules. *Wiley, New York,* **1970**.
2. Mülhaupt, R. Hermann Staudinger and the origin of macromolecular chemistry. *Angew. Chem., Int. Ed.*, **2004,** *43*, 1054-1063.
3. Theato, P. Synthesis of well-defined polymeric activated esters. *J. Polym. Sci., Part A: Polym. Chem.*, **2008**, *46*, 6677-6687.
4. Hoffman, A. S. "Intelligent" polymers in medicine and biotechnology. *Macromol. Symp*., **1995**, *98*, 645-664.
5. Galaev, I.; Mattiasson, B. Smart polymers: applications in biotechnology and biomedicine, *CRC Press, Taylor & Francis Group, Boca Raton, USA*, **2007**.
6. Dai, S.; Ravi, P.; Tam, K. C. pH-Responsive polymers: synthesis, properties and applications. *Soft Matter*, **2008**, *4*, 435-449.
7. Heskins, M.; Guillet, J. E.; Solution properties of poly (N-isopropylacrylamide). *J. Macromol. Sci., Chem.*, **1968**, *2*, 1441-1455.
8. Davis, D. A.; Hamilton, A.; Yang, J.; Cremar, L. D.; Gough, D. Van.; Potisek, S. L.; Ong, M. T.; Braun, P. V.; Mart ńez, T. J.; White, S. R. Force-induced activation of covalent bonds in mechanoresponsive polymeric materials. *Nature*, **2009**, *459*, 68-72.
9. Chi, X.; Ji, X.; Xia, D.; Huang, F. A dual-responsive supra-amphiphilic polypseudorotaxane constructed from a water-soluble pillar [7] arene and an azobenzene-containing random copolymer. *J. Am. Chem. Soc*., **2015**, *137*, 1440-1443.
10. Parasuraman, D.; Serpe, M. J. Poly (N-Isopropylacrylamide) Microgels for Organic Dye Removal from Water. *ACS Appl. Mater. Interfaces*, **2011**, *3*, 2732-2737.
11. Ma, M.; Guo, L.; Anderson, D. G.; Langer, R. Bio-inspired polymer composite actuator and generator driven by water gradients. *Science*, **2013**, *339*, 186-189.
12. Zhao, Q.; Dunlop, J. W.; Qiu, X.; Huang, F.; Zhang, Z.; Heyda, J.; Dzubiella, J.; Antonietti, M.; Yuan, J. An instant multi-responsive porous polymer actuator driven by solvent molecule sorption. *Nat. Commun*., **2014**, *5*, 4293.
13. Hu, Z.; Zhang, X.; Li, Y. Synthesis and application of modulated polymer gels. *Science*, **1995**, *269*, 525
14. Koerner, H.; Price, G.; Pearce, N. A.; Alexander, M.; Vaia, R. A. Remotely actuated polymer nanocomposites-stress-recovery of carbon-nanotube-filled thermoplastic elastomers. *Nat. Mater*., **2004**, *3*, 115-120.
15. Wang, F.; Lai, Y. H.; Han, M. Y. Stimuli-Responsive Conjugated Copolymers Having Electro-Active Azulene and Bithiophene Units in the Polymer Skeleton: Effect of Protonation and p-Doping on Conducting Properties. *Macromolecules*, **2004**, *37*, 3222-3230.

16. Seker, F.; Malenfant, P. R.; Larsen, M.; Alizadeh, A.; Conway, K.; Kulkarni, A. M.; Goddard, G.; Garaas, R. On-Demand Control of Optoelectronic Coupling in Gold Nanoparticle Arrays. *Adv. Mater*., **2005**, *17*, 1941-1945.
17. Bao, J.; Chen, W.; Liu, T.; Zhu, Y.; Jin, P.; Wang, L.; Liu, J.; Wei, Y.; Li, Y., Bifunctional Au-Fe3o4 Nanoparticles for Protein Separation. *ACS Nano*. **2007**, *1*, 293-298.
18. Gao, J.; Gu, H.; Xu, B., Multifunctional Magnetic Nanoparticles: Design, Synthesis, and Biomedical Applications. *Acc. Chem. Res*. **2009**, *42*, 1097-1107.
19. Abu‐Reziq, R.; Wang, D.; Post, M.; Alper, H., Platinum Nanoparticles Supported on Ionic Liquid‐Modified Magnetic Nanoparticles: Selective Hydrogenation Catalysts. *Adv. Synth. Catal*. **2007**, *349*, 2145-2150.
20. Dai, S.; Ravi. P.; Tam, K. C. pH-Responsive polymers: synthesis, properties and applications. *Soft Matter*, **2008,** *4*, 435-449.
21. Heskins, M.; Guillet, J. E. Solution properties of poly (N-isopropylacrylamide). *J. Macromol. Sci., Chem.*, **1968,** *2*, 1441-1455.
22. Davis, D. A.; Hamilton, A.; Yang, J.; Cremar, L. D.; Gough, D. Van.; Potisek, S. L.; Ong, M. T.; Braun, P. V.; Mart ńezand, T. J.; White, S. R. Force-induced activation of covalent bonds in mechanoresponsive polymeric materials. *Nature*, **2009,** *459*, 68-72.
23. Roy, D.; Brooks, W. A.; Sumerlin, B. S. New directions in thermoresponsive polymers. *Chem. Soc. Rev.*, **2013,** *42*, 7214-7243.
24. Ward, M. A.; Georgiou, T. K. Thermoresponsive polymers for biomedical applications. *Polymers*, **2011,** *3*, 1215-1242.
25. Bordat, A.; Boissenot, T.; Nicolas, J.; Tsapis, N. Thermoresponsive polymer nanocarriers for biomedical applications. *Adv. Drug Delivery Rev.*, **2019**, *138*, 167-192.
26. Bertrand, O.; Gohy, J. F. Photo-responsive polymers: synthesis and applications. *Polym. Chem.*, **2017,** *8*, 52-73.
27. Wang, T.; Farajollahi, M.; Choi, Y.; Lin, I. T.; Marshall, J. N.; Thompson, M.; Kar-Narayan, S.; Madden, J.; Smoukov, S. Adaptation of sensor morphology: an integrative view of perception from biologically inspired robotics perspective. *Interface Focus*, **2016,** *6*, 1-19.
28. Hu, J.; Liu, S. Responsive polymers for detection and sensing applications: current status and future developments. *Macromolecules*, **2010,** *43*, 8315-8330.
29. Bajpai, A.; Shukla, S. K.; Bhanu, S.; Kankane, S. Responsive polymers in controlled drug delivery. *Prog. Polym. Sci.*, **2008**, *33*, 1088-1118.
30. Parasuraman, D.; Serpe, M. Poly (N-Isopropylacrylamide) Microgels for Organic Dye Removal from Water. *ACS Appl. Mater. Interfaces*, **2011,** *3*, 2732-2737.
31. Ma, M.; Guo, L.; Anderson, D. G.; Langer, R. Bio-inspired polymer composite actuator and generator driven by water gradients. *Science*, **2013,** *339*, 186-189.

32. Zhao, Q.; Dunlop, J. W.; Qiu, X.; Huang, F.; Zhang, Z.; Heyda, J.; Dzubiella, J.; Antonietti, M.; Yuan, J. An instant multi-responsive porous polymer actuator driven by solvent molecule sorption. *Nat. Commun.*, **2014,** *5*, 4293.

33. Hu, Z.; Zhang, X.; Li, Y. Synthesis and application of modulated polymer gels. *Science*, **1995,** *269*, 525.

34. Koerner, H.; Price, G.; Pearce, N. A.; Alexander, M.; Vaia, R. A. Remotely actuated polymer nanocomposites-stress-recovery of carbon-nanotube-filled thermoplastic elastomers. *Nat. Mater.*, **2004,** *3*, 115-120.

35. Wang, F.; Lai, Y. H.; Han, M. Y. Stimuli-Responsive Conjugated Copolymers Having Electro-Active Azulene and Bithiophene Units in the Polymer Skeleton: Effect of Protonation and p-Doping on Conducting Properties. *Macromolecules*, **2004,** *37*, 3222-3230.

36. Seker, F.; Malenfant, P. R.; Larsen, M.; Alizadeh, A.; Conway, K.; Kulkarni, A. M.; Goddard, G.; Garaas, R. On-Demand Control of Optoelectronic Coupling in Gold Nanoparticle Arrays. *Adv. Mater.*, **2005,** *17*, 1941-1945.

37. Min, S. H.; Kwak, S. K.; Kim, B. Su. Atomistic simulation for coil-to-globule transition of poly(2-dimethylaminoethyl methacrylate). *Soft Matter*, **2015,** *11*, 2423-2433.

38. Vasile, C.; Kulshreshtha, A. K. Handbook of Polymer Blends and Composites; *Shawbury, UK*, **2003.**

39. Phillips, D. J.; Gibson, M. I. Towards being genuinely smart: 'isothermally-responsive' polymers as versatile, programmable scaffolds for biologically-adaptable materials. *Polym. Chem.*, **2015,** *6*, 1033-1043.

40. Song, Z.; Wang, K.; Gao, C.; Wang, S.; Zhang, W. A New Thermo-, pH-, and CO2-Responsive Homopolymer of Poly[N-[2-(diethylamino)ethyl]acrylamide]: Is the Diethylamino Group Underestimated? *Macromolecules*, **2016,** *49*, 162 -171.

41. Karjalainen, E.; Aseyev, V.; Tenhu, H.Influence of hydrophobic anion on solution properties of PDMAEMA. *Macromolecules*, **2014,** *47*, 2103-2111.

42. Plamper, F. A.; Schmalz, A.; Ballauff, M.; Müller, A. H. Tuning the Thermoresponsiveness of Weak Polyelectrolytes by pH and Light: Lower and Upper Critical-Solution Temperature of Poly(N,N-dimethylaminoethyl methacrylate). *J. Am. Chem. Soc.*, **2007,** *129*, 14538-14539.

43. Thavanesan, T.; Herbert, C.; Plamper, F. A. Insight in the Phase Separation Peculiarities of Poly(dialkylaminoethyl methacrylate)s. *Langmuir*, **2014,** *30*, 5609-5619.

44. Bütün, V.; Armes, S.; Billingham, N. Synthesis and aqueous solution properties of near-monodisperse tertiary amine methacrylate homopolymers and diblock copolymers. *Polymer*, **2001,** *42*, 5993-6008.

45. Shamim, N.; Hong, L.; Hidajat, K.; Uddin, M. S. Thermosensitive-polymer-coated magnetic nanoparticles: adsorption and desorption of bovine serum albumin. *J. Coll. and Interf. Sci.*, **2006,** *304*, 1-8.

46. Abulateefeh, S. R.; Spain, S. G.; Thurecht, K. J.; Aylott, J. W.; Chan, W. C.; Garnett, M. C.; Alexander, C. Enhanced uptake of nanoparticle drug carriers via a thermoresponsive shell enhances cytotoxicity in a cancer cell line. *Biomater. Sci.,* **2013,** *1*, 434-442.

47. Felber, A. E.; Dufresne, M. H.; Leroux, J. C. pH-sensitive vesicles, polymeric micelles, and nanospheres prepared with polycarboxylates. *Adv. Drug Delivery Rev.,* **2012,** *64*, 979-992.

48. Bingöl, B.; Strandberg, C.; Szabo, A.; Wegner, G. Copolymers and hydrogels based on vinylphosphonic acid. *Macromolecules,* **2008,** *41*, 2785-2790.

49. Jiang, F. J.; Chen, S.; Cao, Z. Q.; Wang, G. J. A photo, temperature, and pH responsive spiropyran-functionalized polymer: Synthesis, self-assembly and controlled release. *Polymer,* **2016,** *83*, 85-91.

50. Taktak, F.; Butun, V. Synthesis and physical gels of pH- and thermo-responsive tertiary amine methacrylate based ABA triblock copolymers and drug release studies. *Polymer,* **2010,** *51*, 3618-3626.

51. Hoffman, A. S. Hydrogels for biomedical applications. *Adv. Drug Delivery Rev.,* **2012,** *64*, 18-23.

52. Lorenzo, C. A.; Fernandez, B. B.; Puga, A. M.; Concheiro, A. Crosslinked ionic polysaccharides for stimuli-sensitive drug delivery. *Adv. Drug Delivery Rev.,* **2013,** *65*, 1148-1171.

53. Jiang, T. Y.; Wang, Z. Y.; Tang, L. X.; Mo, F. K.; Chen, C. Polymer micellar aggregates of novel amphiphilic biodegradable graft copolymer composed of poly(aspartic acid) derivatives: Preparation, characterization, and effect of pH on aggregation. *J. Appl. Polym. Sci.,* **2006,** *99*, 2702-2709.

54. Weissman, J. M.; Sunkara, H. B.; Tse, A. S.; Asher, S. A. Thermally Switchable Periodicities and Diffraction from Novel Mesoscopically Ordered Materials, *Science,* **1996,** *274*, 956-960.

55. Chiappelli, M. C.; Hayward, R. C. Photonic Multilayer Sensors from Photo‐Crosslinkable Polymer Films. *Adv. Mater.,* **2012,** *24*, 6100-6104.

56. Johnson, K. C.; Mendez, F.; Serpe, M. J. Detecting solution pH changes using poly (N-isopropylacrylamide)-co-acrylic acid microgel-based etalon modified quartz crystal microbalances. *Anal. Chim. Acta*, **2012,** *739*, 83-88.

57. Zhang, Q. M.; Li, X.; Islam, M. R.; Wei, M.; Serpe, M. J. Light switchable optical materials from azobenzene crosslinked poly (N-isopropylacrylamide)-based microgels. *J. Mater. Chem. C*, **2014,** *2*, 6961-6965.

58. Seo, J.; Song, M.; Jeong, J.; Nam, S.; Heo, I.; Park, S. Y.; Kang, I. K.; Lee, J. H.; Kim, H.; Kim, Y. Broadband pH-Sensing Organic Transistors with Polymeric Sensing Layers Featuring Liquid Crystal Microdomains Encapsulated by Di-Block Copolymer Chains. *ACS Appl. Mater. Interfaces*, **2016,** *8*, 23862-23867.

59. Ulbrich, K.; Subr, V. Polymeric anticancer drugs with pH-controlled activation. *Adv. Drug Delivery Rev.,* **2004,** *56*, 1023-1050.

60. Kratz, F.; Mueller, I. A.; Ryppa, C.; Warnecke, A. Prodrug strategies in anticancer chemotherapy. *ChemMedChem,* **2008,** *3*, 20-53.

61. Gillies, E. R.; Fréchet, M. J. A new approach towards acid sensitive copolymer micelles for drug delivery. *Chem. Commun.,* **2003,** 1640-1641.

62. Zheng, L.; Zhang, X.; Wang, Y.; Liu, F.; Peng, J.; Zhao, X.; Yang, H.; Ma, L.; Wang, B.; Chang, C.; Wei, H. Fabrication of acidic pH-cleavable polymer for anticancer drug delivery using a dual functional monomer. *Biomacromolecules,* **2018,** *19*, 3874-3882.

63. Hu, L.; Zhang, Q.; Liu, X.; Serpe, M. J. Stimuli-responsive polymers for sensing and actuation. *Mater. Horiz.,* **2019,** *6*, 1774-1793.

64. Wei, M.; Gao, Y.; Li, X.; Serpe, M. J. Stimuli-responsive polymers and their applications. *Polym. Chem.,* **2017,** *8*, 127-143.

65. Zhao, Y. Light-responsive block copolymer micelles. *Macromolecules,* **2012,** *45*, 3647-3657.

66. Wang, D.; Wang, X. Amphiphilic azo polymers: Molecular engineering, self-assembly and photoresponsive properties. *Prog. Polym. Sci.,* **2013,** *38*, 271-301.

67. Yu, H.; Kobayashi, T. Photoresponsive block copolymers containing azobenzenes and other chromophores. *Molecules,* **2010,** *15*, 570-603.

68. Yager, K. G.; Barrett, C. J. Novel photo-switching using azobenzene functional materials. *J. Photochem. Photobiol., A,* **2006,** *182*, 250-261.

69. Lee, H. I.; Wu, W.; Oh, J. K.; Mueller, L.; Sherwood, G.; Peteanu, L.; Kowalewski, T.; Matyjaszewski, K. Light‐induced reversible formation of polymeric micelles. *Angew. Chem., Int. Ed.,* **2007,** *46*, 2453-2457.

70. Menon, S.; Ongungal, R. M.; Das, S. Photocleavable glycopolymer aggregates. *Polym. Chem.,* **2013,** *4*, 623-628.

71. Xing, Q.; Li, N.; Jiao, Y.; Chen, D.; Xu, J.; Xu, Q.; Lu, J. Near-infrared light-controlled drug release and cancer therapy with polymer-caged upconversion nanoparticles. *RSC Adv.,* **2015,** *5*, 5269-5276.

72. Zhou, Y. N.; Zhang, Q.; Luo, Z. H. A Light and pH Dual-Stimuli-Responsive Block Copolymer Synthesized by Copper(0)-Mediated Living Radical Polymerization: Solvatochromic, Isomerization, and "Schizophrenic" Behaviors. *Langmuir,* **2014,** *30*, 1489-1499.

73. Kumar, K.; Knie, C.; Bléger, D.; Peletier, M. A.; Friedrich, H.; Hecht, S.; Broer, D. J.; Debije, M. G.; J. Schenning, A. P. H. A chaotic self-oscillating sunlight-driven polymer actuator. *Nat Commun.,* **2016,** *7*, 11975.

74. Cabane, E.; Malinova, V.; Menon, S.; Palivana, C. G.; Meier, W. Photoresponsive polymersomes as smart, triggerable nanocarriers. *Soft Matter*, **2011**, *7*, 9167-9176.

75. Florea, L.; Wagner, K.; Wagner, P.; Wallace, G. G.; Benito-Lopez, F.; Officer, D. L.; Diamond, D. Photo-Chemopropulsion-Light-Stimulated Movement of Microdroplets. *Adv. Mater.,* **2014**, *26*, 7339-7345.

76. Yu, Q.; Su, X.; Zhang, T.; Zhang, Y. M.; Li, M.; Liu, Y.; Zhan, S. X. A. Non-invasive fluorescence switch in polymer films based on spiropyran-photoacid modified TPE. *J. Mater. Chem. C*, **2018**, *6*, 2113-2122.

77. Maity, C.; Hendriksen, W. E.; van Esch, J. H.; Eelkem, R. Spatial structuring of a supramolecular hydrogel by using a visible-light triggered catalyst. *Angew. Chem., Int. Ed.*, **2015**, *54*, 998-1001.

78. Shi, Z.; Peng, P.; Strohecker, D.; Liao, Y. Long-lived photoacid based upon a photochromic reaction. *J. Am. Chem. Soc*. **2011**, *133*, 14699-14703.

79. Liao, Y. Design and applications of metastable-state photoacids. *Acc. Chem. Res*. **2017**, *50*, 1956-1964.

80. Xiao, H.; Song, H.; Yang, Q.; Cai, H.; Qi, R.; Yan, L.; Liu, S.; Zheng, Y.; Huang, Y.; Liu, T.; Jing, X. A prodrug strategy to deliver cisplatin (IV) and paclitaxel in nanomicelles to improve efficacy and tolerance. *Biomaterials,* **2012,** *33*, 6507-6519.

81. Sun, H.; Guo, B.; Li, X.; Cheng, R.; Meng, F.; Liu, H.; Zhong, Z. Shell-sheddable micelles based on dextran-SS-poly (ε-caprolactone) diblock copolymer for efficient intracellular release of doxorubicin. *Biomacromolecules,* **2010,** *11*, 4, 848-854.

82. Ma, N.; Li, Y.; Xu, H.; Wang, Z.; Zhang, X. Dual redox responsive assemblies formed from diselenide block copolymers. *J. Am. Chem. Soc.* **2010,** *132*, 442-443.

83. Li, W.; Stover, H. D. H. Porous monodisperse poly(divinylbenzene) microspheres by precipitation polymerization. *J. Polym. Sci., Polym. Chem. Ed.,* **1998,** *36*, 1543-1551.

84. Bai, F.; Huang, B.; Yang, X. L.; Huang, W. Q. Synthesis of monodisperse porous poly (divinylbenzene) microspheres by distillation-precipitation polymerization. *Polymer*, **2007**, *48*, 3641-3649.

85. Delcea, M.; Mohwald, H.; Skirtach, A. G. Stimuli-responsive LbL capsules and nanoshells for drug delivery. *Adv. Drug Delivery Rev*., **2011**, *63*, 730-747.

86. Bantchev, G.; Lu, Z. H.; Lvov, Y. Layer-by-layer nanoshell assembly on colloids through simplified washless process. *J. Nanosci. Nanotechnol.,* **2009,** *9*, 396-403.

87. Patra, D.; Sanyal, A.; Rotello, V. M. Colloidal Microcapsules: Self-Assembly of Nanoparticles at the Liquid-Liquid Interface. *Chem.-Asian J.,* **2010,** *5*, 2442-2453.

88. Shim, S. E.; Yang, S. H.; Choi, H. H.; Choe, S. Fully crosslinked poly(styrene-co-divinylbenzene) microspheres by precipitation polymerization and their superior thermal properties. *J. Polym. Sci., Polym. Chem. Ed.,* **2004,** *42*, 835-845.

89. Downey, J. S.; McIsaac, G.; Frank, R. S.; Stover, H. D. H. Poly (divinylbenzene) microspheres as an intermediate morphology between microgel, macrogel, and coagulum in cross-linking precipitation polymerization. *Macromolecules,* **2001,** *34*, 4534-4541.

90. Cameron, N. S.; Corbierre, M. K.; Eisenberg, A. 1998 EWR Steacie Award Lecture Asymmetric amphiphilic block copolymers in solution: a morphological wonderland. *Can. J. Chem.*, **1999,** *77*, 1311-1326.

91. Rao, J. P.; Geckeler, K. E. Polymer nanoparticles: preparation techniques and size-control parameters. *Progress in Polymer Science.* **2011,** *36*, 887-913.

92. Karan, S.; Jiang, Z. W.; Livingston, A. G. Sub-10 nm polyamide nanofilms with ultrafast solvent transport for molecular separation. *Science*, **2015,** *348*, 1347-1351.

93. Smith, W. V.; Ewart, R. H. Kinetics of emulsion polymerization. *J. Chem. Phys.*, **1948,** *16*, 592.

94. Bonham, J. A.; Faers, M. A.; Duijneveldt, J. S. Non-aqueous microgel particles: synthesis, properties and applications. *Soft Matter*, **2014,** *10*, 9384-9398.

95. Chern, CS. Emulsion polymerization mechanisms and kinetics. *Progress in Polymer Science.* **2006,** *31*, 443-486.

96. Thickett, S. C.; Gilbert, R. G. Emulsion polymerization: State of the art in kinetics and mechanisms. *Polymer.* **2007,** *48*, 6965-6991.

97. Rao, J. P.; Geckeler, K. E. Polymer nanoparticles: Preparation techniques and size-control parameters. *Progress in Polymer Science.* **2011,** *36*, 887-913.

98. Kobitskaya, E.; Ekinci, D.; Manzke, A.; Plettl, A.; Wiedwald, U.; Ziemann, P.; Biskupek, J.; Kaiser, U.; Ziener, U.; Landfester, K., Narrowly Size Distributed Zinc-Containing Poly (Acrylamide) Latexes Via Inverse Miniemulsion Polymerization. *Macromolecules,* **2010,** *43*, 3294-3305.

99. Lorenz, S.; Hauser, C. P.; Autenrieth, B.; Weiss, C. K.; Landfester, K.; Mailänder, V., The Softer and More Hydrophobic the Better: Influence of the Side Chain of Polymethacrylate Nanoparticles for Cellular Uptake. *Macromol. Biosci.* **2010,** *10*, 1034-1042.

100. Landfester, K., Synthesis of Colloidal Particles in Miniemulsions. *Annu. Rev. Mater. Res.* **2006,** *36*, 231-279.

101. Kriwet, B.; Walter, E.; Kissel, T., Synthesis of Bioadhesive Poly (Acrylic Acid) Nano-and Microparticles Using an Inverse Emulsion Polymerization Method for the Entrapment of Hydrophilic Drug Candidates. *J. Control. Release,* **1998,** *56*, 149-158.

102. Schork, F. J.; Luo, Y.; Smulders, W.; Russum, J. P.; Butté, A.; Fontenot, K., Miniemulsion Polymerization. *Polymer particles,* **2005,** 129-255.

103. Landfester, K., Miniemulsion Polymerization and the Structure of Polymer and Hybrid Nanoparticles. *Angew. Chem. Int. Ed.* **2009,** *48*, 4488-4507.

104. Landfester, K.; Schork, F. J.; Kusuma, V. A. *Comptes Rendus Chimie*, **2003,** *6*, 1337-1342

105. Crucho, C. I. C. Barros, M. T. *Materials Science and Engineering: C*, **2017,** *80*, 771-784.

106. Landfester, K., Polyreactions in Miniemulsions. *Macromol. Rapid Commun.* **2001,** *22*, 896-936.

107. Antonietti, M.; Landfester, K., Polyreactions in Miniemulsions. *Prog. Polym. Sci.* **2002,** *27*, 689-757.

108. Asua, J. M., Miniemulsion Polymerization. *Prog. Polym. Sci.* **2002,** *27*, 1283-1346.

109. Landfester, K. Miniemulsion Polymerization and the Structure of Polymer and Hybrid Nanoparticles. *Angew. Chem. Int. Ed.* 2009, 48, 4488-4507

110. Weiss, C. K.; Ziener, U.; Landfester, K. A Route to Nonfunctionalized and Functionalized Poly(n-butylcyanoacrylate) Nanoparticles: Preparation in Miniemulsion. Macromolecules, 2007, 40, 928-938.

111. Piradashvili, K.; Fichter, M.; Mohr, K.; Gehring, S.; Wurm, F. R.; Landfester. K. Biodegradable Protein Nanocontainers. Biomacromolecules, **2015,** *16*, 815-821.

112. Soula, R.; Saillard, B.; Spitz, R.; Claverie, J.; Llaurro, M. F.; Monnet, C. Catalytic Copolymerization of Ethylene and Polar and Nonpolar α-Olefins in Emulsion. *Macromolecules,* **2002,** *35*, 1513-1523.

113. Pecher, J.; Mecking, S. Nanoparticles from Step-Growth Coordination Polymerization. *Macromolecules,* **2007,** *40*, 7733-7735.

114. Piradashvili, K.; Fichter, M.; Mohr, K.; Gehring, S.; Wurm, F. R.; Landfester, K., Biodegradable Protein Nanocontainers. *Biomacromolecules,* **2015,** 16, 815-821.

115. Hamley, I.W. The Physics of Block Copolymers; Oxford University Press: New York, NY, USA, **1998**; Volume 19.

116. Khandpur, A. K.; Foerster, S.; Bates, F. S.; Hamley, I. W.; Ryan, A. J.; Bras, W.; Almdal, K.; Mortensen, K. Polyisoprene-polystyrene diblock copolymer phase diagram near the order-disorder transition. *Macromolecules,* **1995,** *28*, 8796-8806.

117. Bates, F. S.; Fredrickson, G. H. Block copolymers-designer soft materials. *Phys Today,* **1999,** *52*, 32-38.

118. Bates, F. S.; Fredrickson, G. H. Block copolymer thermodynamics: Theory and experiment. *Annu Rev Phys Chem,* **1990,** *41*, 525-557.

119. Feng, H.; Changez, M.; Hong, K.; Mays, J. W.; Kang, N. G. 2-Isopropenyl-2-oxazoline: Well-Defined Homopolymers and Block Copolymers via Living Anionic Polymerization. *Macromolecules,* **2017,** *50*, 54-62.

120. Hamley, I. W. Nanostructure fabrication using block copolymers. *Nanotechnology*, **2003,** *14*, R39-R54.

121. Alexandridis, P.; Lindman, B., Elsevier: Amsterdam, The Netherlands, 2000.

122. Mai, Y.; Eisenberg, A. Self-assembly of block copolymers. *Chem. Soc. Rev.*, **2012,** *41*, 5969-5985.

123. Kabanov, A. V.; Batrakova, E. V.; Alakhov, V. Y. Pluronic Block Copolymers as Novel Polymer Therapeutics for Drug and Gene Delivery. *J. Controlled Release,* **2002,** *82*, 189-212.

124. Harada, A.; Kataoka, K. Supramolecular assemblies of block copolymers in aqueous media as nanocontainers relevant to biological applications. *Prog. Polym. Sci.*, **2006,** *31*, 949-982.

125. Israelachvili, J. ‘‘Intermolecular & Surface Forces’’, 2nded.,Academic Press, London 19915

126. Doncom, K. E. B.; Blackman, L. D.; Wright, D. B.; Gibson, M. I.; O'Reilly, R. K. Dispersity effects in polymer self-assemblies: a matter of hierarchical control. *Chem. Soc. Rev.,* **2017,** *46*, 4119-4134.

127. Dionzou, M.; Morere, A.; Roux, C.; Lonetti, B.; Marty, J. D.; Mingotaud, C.; Joseph, P.; Goudouneche, D.; Payre, B.; Leonetti, M.; Mingotaud, A. F. Comparison of methods for the fabrication and the characterization of polymer self-assemblies: what are the important parameters? *Soft Matter,* **2016,** *12*, 2166-2176.

128. Gabaston, L. I.; Jackson, R. A.; Armes, S. P. Living Free-Radical Dispersion Polymerization of Styrene. *Macromolecules,* **1998,** *31*, 2883-2888.

129. Min, K.; Matyjaszewski, K. Atom Transfer Radical Dispersion Polymerization of Styrene in Ethanol, *Macromolecules,* **2007,** *40*, 7217-7222,

130. Song, J.S.; Winnik, M. A. Monodisperse, Micron-Sized Reactive Low Molar Mass Polymer Microspheres by Two-Stage Living Radical Dispersion Polymerization of Styrene. *Macromolecules,* **2006,** *39*, 8318-8325.

131. Tan, J.; Rao, X.; Wu, X.; Deng, H.; Yang, J.; Zeng, Z. Photoinitiated RAFT Dispersion Polymerization: A Straightforward Approach toward Highly Monodisperse Functional Microspheres. *Macromolecules,* **2012,** *45*, 8790-8795.

132. Zheng, G.; Pan, C. Reversible Addition-Fragmentation Transfer Polymerization in Nanosized Micelles Formed in Situ. *Macromolecules,* **2006,** *39*, 95-102.

133. Min, K.; Matyjaszewski, Krzysztof. Atom Transfer Radical Dispersion Polymerization of Styrene in Ethanol. *Macromolecules,* **2007,** *40*, 7217-7222.

134. Kim, K. H.; Kim, J.; Jo, W. H. Preparation of hydrogel nanoparticles by atom transfer radical polymerization of N-isopropylacrylamide in aqueous media using PEG macro-initiator. *Polymer,* **2005,** *46*, 2836-2840.

135. Tang, W.; Matyjaszewski, K. Effects of Initiator Structure on Activation Rate Constants in ATRP. *Macromolecules,* **2007,** *40*, 1858-1863.

136. Tang, W.; Matyjaszewski, K. Kinetic Modeling of Normal ATRP, Normal ATRP with $[Cu^{II}]_0$, Reverse ATRP and SR&NI ATRP. *Macromol. Theory Simul.* **2008,** *17*, 359-375.

137. Patten, T. E.; Matyjaszewski, K. Atom transfer radical polymerization and the synthesis of polymeric materials. *Adv. Mater.,* **1998,** *10*, 901-915.

138. Fischer, H. The persistent radical effect in controlled radical polymerizations. *J. Polym. Sci., Part A: Polym. Chem*. **1999,** *37*, 1885-1901.

139. Patten, T. E; Matyjaszewski, K. Atom Transfer Radical Polymerization and the Synthesis of Polymeric Materials. *Adv. Mater,*. **1998,** *10*, 901-915.

140. Lowe, A. B. RAFT alcoholic dispersion polymerization with polymerization-induced self-assembly. *Polymer*, **2016,** *106*, 161-181.

141. Sugihara, S.; Armes, S. P.; Blanazs, A.; Lewis, A. L. Non-spherical morphologies from cross-linked biomimetic diblock copolymers using RAFT aqueous dispersion polymerization. *Soft Matter,* 2011, 7, 10787-10793.

142. Chambon, P.; Blanazs, A.; Battaglia, G.; Armes, S. P. Facile synthesis of methacrylic ABC triblock copolymer vesicles by RAFT aqueous dispersion polymerization. *Macromolecules,* **2012,** *45*, 5081-5090.

143. Zhang, W. J.; Hong, C. Y.; Pan, C. Y. Fabrication of Spaced Concentric Vesicles and Polymerizations in RAFT Dispersion Polymerization. Macromolecules, **2014,** *47*, 1664-1671.

144. Kang, Y.; Pitto-Barry, A.; Willcock, H.; Quan, W. D.; Kirby, N.; Sanchez, A. M.; O'Reilly, R. K. Exploiting nucleobase-containing materials – from monomers to complex morphologies using RAFT dispersion polymerization. *Polym. Chem.*, 2015, 6, 106-107.

145. Z, Daniel.; R, Liam P. D.; Armes, S. P. Synthesis of Diblock Copolymer Nanoparticles via RAFT Alcoholic Dispersion Polymerization: Effect of Block Copolymer Composition, Molecular Weight, Copolymer Concentration, and Solvent Type on the Final Particle Morphology. *Macromolecules,* **2013,** *46*, 128-139.

146. Figg, C. A.; Simula, A.; Gebre, K. A.; Tucker, B. S.; Haddleton, D. M.; Sumerlin, B. S. Polymerization-induced thermal self-assembly (PITSA). *Chem. Sci.*, **2015,** *6*, 1230-1236.

147. Liu, F.; Urban, M. W. Recent advances and challenges in designing stimuli-responsive polymers. *Prog. Polym. Sci.* **2010**, *35*, 3-23.

148. Li, M.; Wu, Q.; Song, K.; Qing, Y.; Wu, Y. Cellulose Nanoparticles as Modifiers for Rheology and Fluid Loss in Bentonite Water-based Fluids. *ACS Appl. Mater. Interfaces* **2015**, *7*, 5006-5016

149. Jhaveri, S. J.; Hynd, M. R.; Dowell-Mesfin, N.; Turner, J. N.; Shain, W.; Ober, C. K. Release of nerve growth factor from HEMA hydrogel-coated substrates and its effect on the differentiation of neural cells. *Biomacromolecules,* **2009**, *10*, 174-183.

150. Hoffman, A. S. The origins and evolution of "controlled" drug delivery systems. *J. Control. Release*, **2008**, *132*, 153-163.

151. Bayer, C. L.; Peppas, N. A. Advances in recognitive, conductive and responsive delivery systems. *J. Control. Release,* **2008**, *132*, 216-221.

152. Mendes, P. M. Stimuli-responsive surfaces for bio-applications. *Chem. Soc. Rev.* **37**, 2512-2529 (2008).

153. Luzinov, I.; Minko, S.; Tsukruk, V. V. Responsive brush layers: from tailored gradients to reversibly assembled nanoparticles. *Soft Matter,* **2008**, *4*, 714-725.

154. Motornov, M.; Minko, S.; Eichhorn, K. J.; Nitschke, M.; Simon, F.; Stamm. M. Reversible tuning of wetting behavior of polymer surface with responsive polymer brushes. *Langmuir,* **2003**, 19, 8077-8085.

155. Liu, Z.; Calvert, P. Multilayer hydrogels as muscle-like actuators. *Adv. Mater.* **2000**, *12*, 288-291.

156. Cohen-Stuart, M. A.; Huck, W. T. S.; Genzer, J.; Müller, M.; Ober, C.; Stamm, M.; Sukhorukov, G. B.; Szleifer, I.; Tsukruk, V. V.; Urban, M.; Winnik, F.; Zauscher, S.; Luzinov, I.; Minko, S. Emerging applications of stimuli-responsive polymer materials. *Nat. Mater.*, **2010**, *9*, 101-113.

157. Maji, S.; Cesur, B.; Zhang, Z.; De Geest, B. G.; Hoogenboom, R. Poly (N-isopropylacrylamide) coated gold nanoparticles as colourimetric temperature and salt sensors. *Polym. Chem.*, **2016**, *7*, 1705-1710.

158. Paek, K.; Yang, H.; Lee, J.; Park, J.; Kim, B. J. Efficient colorimetric pH sensor based on responsive polymer-quantum dot integrated graphene oxide. *ACS Nano*, **2014**, *8*, 2848-2856.

159. Menezes, R. R.; Marques, L. N.; Campos, L. A.; Ferreira, H. S.; Santana, L. N. L.; Neves, G.A.Use of statistical design to study the influence of CMC on the rheological properties of bentonite dispersions for water-based drilling fluids. *Appl. Clay Sci*. **2010**, *49*, 13-20.

160. Mahto, V.; Sharma, V. P. Rheological study of a water based oil well drilling fluid. *J. Pet. Sci. Eng.* **2004**, *45*, 123-12.

161. Yan, L.; Wang, C.; Xu, B.; Sun, J.; Yue, W.; Yang, Z. Preparation of a novel amphiphilic comb-like terpolymer as viscosifying additive in low-solid drilling fluid. *Mater. Lett*. **2013**, *105*, 232-235.

162. Wang, Z.; Volinsky, A. A.; Gallant, N. D. Crosslinking effect on polydimethylsiloxane elastic modulus measured by custom-built compression instrument. J. *Appl. Polym. Sci.* **2014**, *131*, 41050.

163. Li, M.; Wu, Q.; Song, K.; Qing, Y.; Wu, Y. Cellulose Nanoparticles as Modifiers for Rheology and Fluid Loss in Bentonite Water-based Fluids. *ACS Appl. Mater. Interfaces*, **2015**, *7*, 5006-5016.

164. Cai, J.; Chenevert, M. E.; Sharma, M. M.; Friedheim, J. E. Decreasing water invasion into Atoka shale using nonmodified silica nanoparticles. *SPE Drill. Completion*, **2012**, *27*, 103-112.

165. Lu, P. J.; Weitz, D. A. Colloidal particles: crystals, glasses, and gels. *Annu. Rev. Condens. Matter Phys.*, **2013**, *4*, 217-233.

166. Peter, J. Lu.; Jacinta, C. C.; Hans, M. W.; Andrew, B. S.; David, A. W. Fluids of clusters in attractive colloids. *Phys. Rev. Lett.*, **2006**, *96*, 028306.

167. Trappe, V.; Prasad, V.; Cipelletti, L.; Segre, P. N.; Weitz, D. A. Jamming phase diagram for attractive particles. *Nature*, **2001**, *411*, 772-775.

168. Scheer, P.; Laar, T.; Gucht, J.; Vlassopoulos, D.; Sprakel, J. Fragility and strength in nanoparticle glasses. *ACS Nano*, **2017**, *11*, 6755-6763.

169. Shchukin, D. G.; Zheludkevich, M.; Yasakau, K.; Lamaka, S.; Ferreira, M. G. S.; Möhwald, H. Layer-by-Layer assembled nanocontainers for self-healing corrosion protection. *Adv. Mater.*, **2006**, *18*, 1672-1678.

170. Zheludkevich, M. L.; Tedim, J.; Ferreira, M.G.S."Smart" coatings for active corrosion protection based on multi-functional micro and nanocontainers. *Electrochim. Acta*, **2012**, *82*, 314-323.

171. Shchukin, D. G.; Moehwald, H. Self-repairing coatings containing active nanoreservoirs. *Small*, **2007**, *3*, 926-943.

172. Lamaka, S. V.; Shchukin, D. G.; Andreeva, D. V.; Zheludkevich, M. L.; Möhwald, H.; Ferreira, M. G. S. Sol-gel/polyelectrolyte active corrosion protection system. *Adv. Funct. Mater.*, **2008**, *18*, 3137-3147.

173. Glinel, K.; Déjugnat, C.; Prevot, M.; Schöler, B., Schönhoff, M.; Klitzing, R. Responsive polyelectrolyte multilayers. *Colloids Surf. A Physicochem. Eng. Aspects*, **2007**, *303*, 3-13.

174. Huang, M.; Zhang, H.; Yang, J. Synthesis of organic silane microcapsules for self-healing corrosion resistant polymer coatings. *Corros. Sci.*, **2012**, *65*, 561-566.

175. Szabó, T.; Telegdi, J.; Nyikos, L. Linseed oil-filled microcapsules containing drier and corrosion inhibitor-their effects on self-healing capability of paints. P*rog. Org. Coat.*, **2015**, *84*, 136-142.

176. Leal, D. A.; Riegel-Vidotti, I. C.; Ferreirac, M. G. S.; Bruno, C. E. M. Smart coating based on double stimuli-responsive microcapsules containing linseed oil and benzotriazole for active corrosion protection. *Corros. Sci.*, **2018**, *130*, 56-63.

177. Yang, H.; Fung, S.; Pritzker, M.; Chen, P. Surface-Assisted Assembly of an Ionic-Complementary Peptide: Controllable Growth of Nanofibers. *J. Am. Chem. Soc.* **2007,** *129*, 12200-12210.

178. Keyes-Baig, C.; Duhamel, J.; Fung, S.; Bezaire, J.; Chen, P. Self-assembling peptide as a potential carrier of hydrophobic compounds. *J. Am. Chem. Soc.* **2004,** *126*, 7522-7532.

179. Fung, S.; Yang, H.; Bhola, P. T.; Sadatmousavi, P.; Muzar, E.; Liu, M.; Chen, P. Bright Blue Photo‐ and Electroluminescence from Eu2+‐Doped GaN/SiO2 Nanocomposites. *Adv. Funct. Mater.* **2008,** *18*, 1-10.

180. Qiao, W.; Wang, B.; Wang, Y.; Yang, L.; Zhang, Y.; Shao, P. *Journal of Nanomater,* **2010,** 1-10.

181. Wang, C.; Ye, Y.; Hochu, G. M.; Sadeghifar, H.; Gu, Zhen. Enhanced Cancer Immunotherapy by Microneedle Patch-Assisted Delivery of Anti-PD1 Antibody. *Nano Lett.* **2016,** *16*, 2334-2340.

182. Wang, X.; Hu, J.; Liu, G.; Tian, J.; Wang, H.; Gong, M.; Liu, S. Reversibly Switching Bilayer Permeability and Release Modules of Photochromic Polymersomes Stabilized by Cooperative Noncovalent Interactions. *J. Am. Chem. Soc.* **2015,** *137*, 15262-15275.

183. Baier, G.; Fichter, M.; Kreyes, A.; Klein, K.; Mailänder, Volker,; Gehring, S.; Landfester, K. Glutathione Responsive Hyaluronic Acid Nanocapsules Obtained by Bioorthogonal Interfacial "Click" Reaction. *Biomacromolecules*, **2016,** *17*, 148-153.

184. Langer, R.; Vacanti, J. P. *Tissue engineering. Science*. **1993,** *260*, 920-926.

185. Van Blitterswijk, C. *Tissue Engineering, 1st ed. London: Elsevier*; **2008.**

186. Ruhe, P. Q.; Hedberg, D.; E. L.; Padron, N. T.; Spauwen, P. H. M.; Jansen, J. A.; Mikos, A. G. Porous poly(D,L-lactic-co-glycolic acid)/calcium phosphate cement composite for reconstruction of bone defects. Tissue Eng. 2006; 12: 789-800.

187. Wang, Q.; Wang. L.; Detamore. M. S., Berkland, C. Biodegradable Colloidal Gels as Moldable Tissue Engineering Scaffolds. *Adv. Mater.* **2008,** *20*, 236-239.

188. Baier, G.; Fichter, M.; Kreyes, A.; Klein, K.; Mailänder, V,; Gehring, S.; Landfester, K. Glutathione Responsive Hyaluronic Acid Nanocapsules Obtained by Bioorthogonal Interfacial "Click" Reaction. *Biomacromolecules,* **2016,** *17*, 148-153.

189. deSilva, A. P.; Gunaratne, H. Q. N.; Gunnlaugsson, T.; Huxley, A. J. M.; McCoy, C. P.; Rademacher, J. T.; Rice, T. E. Signaling Recognition Events with Fluorescent Sensors and Switches. *Chem. Rev.* **1997,** *97*, 1515-1566.

190. Han, J.; Burgess, K. Fluorescent Indicators for Intracellular pH. *Chem. Rev.* **2010,** *110*, 2709-2728.

191. Zelent, B.; Kusba, J.; Gryczynski, I.; Johnson, M. L.; Lakowicz, J. R. Time-resolved and steady-state fluorescence quenching of N-acetyl-l-tryptophanamide by acrylamide and iodide. *Biophys. Chem.* **1998,** *73*, 53-75.

192. Sagara, Y.; Kato, T. Mechanically induced luminescence changes in molecular assemblies. *Nat. Chem.* **2009,** *1*, 605-610.

193. Hu, J.; Liu, S. Responsive Polymers for Detection and Sensing Applications: Current Status and Future Developments. *Macromolecules,* **2010,** *43*, 8315-8330.

194. Yildiz, I.; Deniz, E.; Raymo, F. M. Fluorescence modulation with photochromic switches in nanostructured constructs. *Chem. Soc. Rev.* **2009,** *38*, 1859-1867.

195. Adhikari, B.; Majumdar, S. Polymers in sensor applications. *Prog. Polym. Sci.* **2004,** *29*, 699-766.

196. Wu, T.; Zou, G.; Hu, J. M.; Liu, S. Y. Fabrication of Photoswitchable and Thermotunable Multicolor Fluorescent Hybrid Silica Nanoparticles Coated with Dye-Labeled Poly(N-isopropylacrylamide) Brushes. *Chem. Mater.* **2009,** *21*, 3788-3798.

197. Kitayama, Y.; Isomura, M. Gas-stimuli-responsive molecularly imprinted polymer particles with switchable affinity for target protein. *Chem. Commun*., **2018**, *54*, 2538-2541.

198. Chadwick, L. E.; Lovell, J. B.; Egner, V. E. The relationship between pH and the activity of cholinesterase from flies. *Biol. Bull*. **1954**, *106*, 139-148.

199. Intlekofer, A. M.; Wang, B.; Liu, H.; Shah, H.; Fontaine, C. C.; Rustenburg, A. S.; Salah, S.; Gunner, M. R.; Chodera, J. D.; Cross, J. R.; Thompson, C. B. L-2-Hydroxyglutarate production arises from noncanonical enzyme function at acidic pH. *Nat. Chem. Biol*. **2017**, *13*, 494-500.

200. Gan, S. W.; Ng, L.; Lin, X.; Gong, X.; Torres, J. Structure and ion channel activity of the human respiratory syncytial virus (hRSV) small hydrophobic protein transmembrane domain. *Protein Sci.* **2008**, *17*, 813-820.

201. Mitchell, P. Coupling of phosphorylation to electron and hydrogen transfer by a chemi-osmotic type of mechanism. *Nature*, **1961**, *191*, 144.

202. de Silva, S. A.; Loo, K. C.; Amorelli, B.; Pathirana, S. L.; Nyakirang'ani, M.; Dharmasena, M.; Demarais, S.; Dorcley, B.; Pullay, P.; Salih, Y.A fluorescent "off-on-off" proton switch derived from natural products and further studies of first-generation fluorescent photoinduced electron transfer (PET) systems. *J. Mater. Chem.* **2005**, *15*, 2791-2795.

203. Koo, C. K.; Lam, B.; Leung, S. K.; Lam, M. H.; Wong, W. Y. A "Molecular Pivot-Hinge'' Based on the pH-Regulated Intramolecular Switching of Pt-Pt and π-π Interactions. *J. Am. Chem. Soc*. **2006**, *128*, 16434.

204. Mashaghi, S.; van Oijen, A. M. External control of pH in micro droplets. *Sci. Rep*. **2015**, *129*, 11837.

205. de Silva, A. P.; McClenaghan, N. D. Molecular-Scale Logic Gates. *Chem. Eur. J.* **2004**, *10*, 574-586.

206. Silvi, S.; Constable, E. C.; Housecroft, C. E.; Beves, J. E.; Dunphy, E. L.; Tomasulo, M.; Raymo, F. M.; Credi, A. All-Optical Integrated Logic Operations Based on Chemical Communication between Molecular Switches. *Chem. Eur. J.* **2009**, *15*, 178-185.

207. Ros, O. Design and synthesis of photoacid generating systems. *J. Photopolym. Sci. Technol.* **2008**, *21*, 493-497.

208. Crivello, J. V. Design of photoacid generating systems. *J. Photopolym. Sci. Technol*. **2009**, *22*, 575-582.

209. Shizuka, H. Excited-state proton-transfer reactions and proton-induced quenching of aromatic compounds. *Acc. Chem. Res*. 1985, *18*, 141-147.

210. Tolbert, L. M.; Solntsev, K. M. Excited-State Proton Transfer: From Constrained Systems to "Super" Photoacids to Superfast Proton Transfer. *Acc. Chem. Res*. 2002, *35*, 19-27.

211. Nunes, R. M. D.; Pineiro, M.; Arnaut, L. G. Photoacid for Extremely Long-Lived and Reversible pH-Jumps. *J. Am. Chem. Soc.* **2009**, *131*, 9456-9462.

212. Yue, X.; Yanez, C. O.; Yao, S.; Belfield, K. D. Selective cell death by photochemically induced pH imbalance in cancer cells. *J. Am. Chem. Soc.* **2013**, *135*, 2112-2115.

213. Kohse, S.; Neubauer, A.; Pazidis, A.; Lochbrunner, S.; Kragl, U. Photoswitching of enzyme activity by laser-induced pH-jump. *J. Am. Chem. Soc.* **2013**, *135*, 9407-9411.

214. Nakashima, T.; Tsuchie, K.; Kanazawa, R.; Li, R.; Iijima, S.; Galangau, O.; Nakagawa, H.; Mutoh, K.; Kobayashi, Y.; Abe, J.; Kawai, T. Self-Contained Photoacid Generator Triggered by Photocyclization of Triangle Terarylene Backbone. *J. Am. Chem. Soc.* **2015**, *137*, 7023-7026.

215. Haberfield, P. Phototropic molecules. 1. Phase transfer as a method for detecting transient species. *J. Am. Chem. Soc.* **1987**, *109*, 6177-6187.

216. Emond, M.; Saux, T. L.; Maurin, S.; Baudin, J. B.; Plasson, R.; Jullien, L. 2-Hydroxyazobenzenes to Tailor pH Pulses and Oscillations with Light. *Chem. Eur. J.* **2010**, *16*, 8822-8831.

217. Johns, V. K.; Peng, P.; DeJesus, J.; Wang, Z.; Liao, Y. Visible-Light-Responsive Reversible Photoacid Based on a Metastable Carbanion. *Chem. Eur. J.* **2014**, *20*, 689-692.

218. Shi, Z.; Peng, P.; Strohecker, D.; Liao, Y. Long-Lived Photoacid Based upon a Photochromic Reaction. *J. Am. Chem. Soc.* **2011**, *133*, 14699-14703.

219. Wang, Z.; Johns, V. K.; Liao, Y. Controlled release of fragrant molecules with visible light. *Chem. Eur. J.* **2014**, *20*, 14637-14640.

220. Maity, C.; Hendriksen, W. E.; van Esch, J. H.; Eelkema, R.Spatial structuring of a supramolecular hydrogel by using a visible-light triggered catalyst. *Angew. Chem., Int. Ed.* **2015**, *54*, 998-1001.

221. Fu, C.; Xu, J.; Boyer, C. Photoacid-mediated ring opening polymerization driven by visible light. *Chem. Commun.* **2016**, *52*, 7126-7129.

222. Silvi, S.; Arduini, A.; Pochini, A.; Secchi, A.; Tomasulo, M.; Raymo, F. M.; Baroncini, M.; Credi, A. A simple molecular machine operated by photoinduced proton transfer. *J. Am. Chem. Soc.* **2007**, *129*, 13378-13379.

223. Shi, Q.; Chen, C. F. Switchable Complexation between (O-Methyl)6-2,6-helic[6]arene and Protonated Pyridinium Salts Controlled by Acid/Base and Photoacid. *Org. Lett*, **2017**, *19*, 3175-3178.

224. Yang, L. P.; Jia, F.; Cui, J. S.; Lu, S. B.; Jiang, W. Light-controlled switching of a non-photoresponsive molecular shuttle. *Org. Lett.* 2017, *19*, 2945.

225. Shi, Z.; Peng, P.; Johns, V. K.; Liao, Y. Novel photo-switchable conducting materials based on a reversible photoacid and polyaniline. *Polym. Prepr.* 2012, *53*, 125-126.

226. Luo, Y.; Wang, C.; Peng, P.; Hossain, M.; Jiang, T.; Fu, W.; Liao, Y.; Su, M. Visible light mediated killing of multidrug-resistant bacteria using photoacids. *J. Mater. Chem. B.* 2013, *1*, 997-1001.

227. Samanta, D.; Klajn, R. Aqueous light-controlled self-assembly of nanoparticles. *Adv. Opt. Mater.* **2016**, *4*, 1373-1377.

228. Kundu, P. K.; Samanta, D.; Leizrowice, R.; Margulis, B.; Zhao, H.; Börner, M.; Udayabhaskararao, T.; Manna. D.; Klajn. R. Light-controlled self-assembly of non-photoresponsive nanoparticles. *Nat. Chem.* **2015**, *7*, 646-652.

229. Tatum, L. A.; Foy, J. T.; Aprahamian, I. Waste management of chemically activated switches: using a photoacid to eliminate accumulation of side products. *J. Am. Chem. Soc.* **2014**, *136*, 17438-17441.

230. Han, B.; Li, F.; Lei, L.; Yang, B.; Li, Z. ON/OFF states of a microbial fuel cell controlled by an optical switching system. *RSC Adv*. **2014**, *4*, 27277-27280.

231. Wang, Z.; Liao, Y. Reversible dissolution/formation of polymer nanoparticles controlled by visible light. *Nanoscale*. **2016**, *8*, 14070-14073.

232. Johns, K. V.; Patel, P. K.; Hassett, S.; Calvo-Marzal, P.; Qin, Y.; Chumbimuni-Torres, K. Y. Visible light activated ion sensing using a photoacid polymer for calcium detection. *Anal. Chem.* **2014**, *86*, 6184-6187.

233. Sumaru, K.; Takagi, T.; Satoh, T.; Kanamori, T. Photo-and Thermoresponsive Dehydration of Spiropyran-Functionalized Polymer Regulated by Molecular Recognition. *Macromol. Rapid Commun*. **2018**, *39*, 1700234

234. Anthonysamy, A.; Balasubramanian, S.; Usha, G.; Velmurugan, D. Synthesis, spectroscopic, structural and electrochemical studies of nickel(II) and copper(II) complexes derived from 2-hydroxy-4-methacryloyloxybenzaldehyde. *Transition Met Chem*. **2008**, *33*, 681-690.

235. Mason, S. J.; Hake, J. L.; Nairne, J.; Cummins, W. J.; Balasubramanian, S. Solid-phase methods for the synthesis of cyanine dyes. *J. Org. Chem.* **2005**, *70*, 2939-2949.

236. Sumaru, K.; Takagi, T.; Satoh, T.; Kanamori, T. Photo-induced reversible proton dissociation of spirobenzopyran in aqueous systems. *J. Photochem. Photobiol. A.* **2013**, *261*, 46-52.

237. Vallet, J.; Micheau, J. C.; Coudret, C.Switching a pH indicator by a reversible photoacid: a quantitative analysis of a new two-component photochromic system. *Dyes Pigm.,* **2016**, *125*, 179-184.

238. Bodnarchuk, M.S.; Doncom, K. E. B.; Wright, D. B.; Heyes, D. M.; Dini, D.; O'Reilly, R. K. Polyelectrolyte pKa from experiment and molecular dynamics simulation. *RSC Adv.* **2017**, *7*, 20007-20014.

239. Colombani, O.; Lejeune, E.; Charbonneau, C.; Chassenieux, C.; Nicolai, T. Ionization of amphiphilic acidic block copolymers. *J. Phys. Chem. B*, **2012**, *116*, 7560-7565.

240. Halperin, A.; Kröger, M.; Winnik, F. M. Poly(N-isopropylacrylamide) Phase Diagrams: Fifty Years of Research. *Angew. Chem. Int. Ed*. **2015**, *54*, 15342-15367.

241. Lu, P. J.; Weitz, D. A. Colloidal Particles: Crystals, Glasses, and Gels. *Annu. Rev. Condens. Matter Phys.*, **2013**, *4*, 217-233.

242. Joshi, Y. M. Dynamics of Colloidal Glasses and Gels. *Annu. Rev. Chem. Biomol. Eng.*, **2014**, 5, 181-202.

243. Lu, P. J.; Zaccarelli, E.; Ciulla, F.; Schofield, A. B.; Sciortino, F.; Weitz, D. A. Gelation of Particles with Short-Range Attraction. *Nature* **2008**, *453*, 499-503.

244. Tadros, T. Interparticle Interactions in Concentrated Suspensions and their Bulk (Rheological) Properties. *Adv. Colloid Interface Sci.,* **2011**, *168*, 263-277.

245. Meng, Z. J.; Zhang, J.; Deng, X.; Liu, J.; Yu, Z.; Abell, C. Bioinspired hydrogel microfibres colour-encoded with colloidal crystals. *Mater. Horiz.*, **2019**, *6*, 1938-1943,

246. Chen, J.; Xu, L.; Yang, M.; Chen, X.; Chen, X.; Hong, W. Highly Stretchable Photonic Crystal Hydrogels for a Sensitive Mechanochromic Sensor and Direct Ink Writing. *Chem. Mater.*, **2019**, *31*, 8918-8926.

247. Xiong, Z.; Yun, X.; Qiu, L.; Sun, Y.; Tang, B.; He, Z.; Xiao, J.; Chung, D.; Ng, T. W.; Yan, H.; Zhang, R.; Wang, X.; Li, D. A Dynamic Graphene Oxide Network Enables Spray Printing of Colloidal Gels for High-Performance Micro-Supercapacitors. *Adv. Mater*., **2019**, *31*, 1804434.

248. Wang, H.; Hansen, M. B.; Lowik, D. W.; van Hest, J.; Li, Y.; Jansen, J. A.; Leeuwenburgh, S. C. Oppositely charged gelatin nanospheres as building blocks for injectable and biodegradable gels. *Adv. Mater.*, **2011**, *23*, H119.

249. Cabeen, M. T.; Jacobs-Wagner, C. Bacterial cell shape. *Nat. Rev. Microbiol.*, **2005**, *3*, 601-610.

250. Hoffman, A. S. Hydrogels for Biomedical Applications. *Adv. Drug Delivery Rev*., **2002**, *54*, 3-12.

251. Wichaita, W.; Kim, Y. G.; Tangboriboonrat, P.; Thérien-Aubin, H. Polymer-functionalized polymer nanoparticles and their behaviour in suspensions. *Polym. Chem*., **2020**, *11*, 2119-2128.

252. Zou, W.; Tan, G.; Jiang, H.; Vogtt, K.; Weaver, M.; Koenig, P.; Beaucage, G.; Larson, R. G. From well-entangled to partially-entangled wormlike micelles. *Soft Matter*, **2019**, *15*, 642-655.

253. Rechberger, F.; Niederberger, M. Translucent nanoparticle-based aerogel monoliths as 3-dimensional photocatalysts for the selective photoreduction of CO_2 to methanol in a continuous flow reactor. *Mater. Horiz*., **2017**, *4*, 1115-1121.

254. Riley, B. J.; Chun, J.; Um, W.; Lepry, W. C.; Matyas, J.; Olszta, M. J.; Li, X.; Polychronopoulou, K.; Kanatzidis, M. G. Chalcogen-based aerogels as sorbents for radionuclide remediation. *Environ. Sci. Technol*., **2013**, *47*, 7540-7547.

255. Yao, Q.; Brock, S. L. Optical sensing of triethylamine using CdSe aerogels. *Nanotechnology*, **2010**, *21*, 115502.

256. Discher, D. E.; Mooney, D. J.; Zandstra, P. W. Growth factors, matrices, and forces combine and control stem cells. *Science* **2009**, *324*, 1673-1677.

257. Prince, E., Kumacheva, E. Design and applications of man-made biomimetic fibrillar hydrogels. *Nat Rev Mater*, **2019**, *4*, 99-115.

258. Schilling, T.; Jungblut, S.; Miller, M. A. Depletion-induced percolation in networks of nanorods. *Phys. Rev. Lett*., **2007**, *98*, 108303.

259. Lu, P. J.; Conrad, J. C.; Wyss, H. M.; Schofield, A. B.; Weitz, D. A. Fluids of Clusters in Attractive Colloids. *Phys. Rev. Lett*., **2006**, *96*, 028306.

260. Trappe, V.; Prasad, V.; Cipelletti, L.; Segre, P. N.; Weitz, D. A. Jamming phase diagram for attractive particles. *Nature* **2001**, *411*, 772-775.

261. van der Scheer, P.; van de Laar, T.; van der Gucht, J.; Vlassopoulos, D.; Sprakel, J. Fragility and Strength in Nanoparticle Glasses. *ACS Nano*, **2017**, *11*, 6755-6763.

262. Ethier, J. G.; Hall, L. M. Structure and Entanglement Network of Model Polymer-Grafted Nanoparticle Monolayers. *Macromolecules*, **2018**, *51*, 9878-9889.

263. Mohraz, A.; Solomon, M. J. Gelation and internal dynamics of colloidal rod aggregates. *J. Colloid Interface Sci*., **2006**, *300*, 155-162.

264. Lang, C.; Hendricks, J.; Zhang, Z.; Reddy, N. K.; Rothstein, J. P.; Lettinga, M. P.; Vermant, J.; Clasen, C. Effects of particle stiffness on the extensional rheology of model rod-like nanoparticle suspensions. *Soft Matter*, **2019**, *15*, 833-841.

265. Jones, E. R.; Semsarilar, M.; Blanazs, A.; Armes, S. P. Efficient Synthesis of Amine-Functional Diblock Copolymer Nanoparticles via RAFT Dispersion Polymerization of Benzyl Methacrylate in Alcoholic Media. *Macromolecules*, **2012**, *45*, 12, 5091-5098.

266. Guérin, G.; Wang, H.; Manners, I.; Winnik, M. A. Fragmentation of Fiberlike Structures: Sonication Studies of Cylindrical Block Copolymer Micelles and Behavioral Comparisons to Biological Fibrils. *J. Am. Chem. Soc.*, **2008**, *130*, 14763-14771.

267. Vollick, B.; Kuo, P. Y.; Therien-Aubin, H.; Yan, N.; Kumacheva, E. Composite cholesteric nanocellulose films with enhanced mechanical properties. *Chem. Mater*., 2017, 29, 2, 789-795.

268. Baschnagel, J.; Meyer, H.; Wittmer, J.; Kulić, I.; Mohrbach, H.; Ziebert, F.; Nam, G. M.; Lee, N. K.; Johner, A. Semiflexible Chains at Surfaces: Worm-Like Chains and beyond. *Polymers*, **2016**, *8*, 286.

269. Voudouris, P.; Choi, J.; Dong, H.; Bockstaller, M. R.; Matyjaszewski, K.; Fytas, G. Effect of shell architecture on the static and dynamic properties of polymer-coated particles in solution. *Macromolecules*, **2009**, *42*, 2721-2728.

270. Petukhov, A. V.; Tuinier, R.; Vroege, G. J. Entropic patchiness: Effects of colloid shape and depletion. *Curr. Opin. Colloid Interface Sci*., **2017**, *30*, 54-61.

271. Wang, X. ; Guerin, G.; Wang, H.; Wang, Y.; Manners, I. ; Winnik, M. A. Cylindrical block copolymer micelles and co-micelles of controlled length and architecture. *Science* **2007**, *317*, 644-647.

272. Cates, M. E. Reptation of living polymers: dynamics of entangled polymers in the presence of reversible chain-scission reactions. *Macromolecules*, **1987**, *20*, 2289-2296.

273. Lovett, J. R. ; Ratcliffe, L. P. D. ; Warren, N. J. ; Armes, S. P. A Robust Cross-Linking Strategy for Block Copolymer Worms Prepared via Polymerization-Induced Self-Assembly. *Macromolecules*, **2016**, *49*, 2928-2941.

274. Niskanen, J.; Wu, C.; Ostrowski, M.; Fuller, G. G.; Hietala, S.; Tenhu, H. Thermoresponsiveness of PDMAEMA. Electrostatic and Stereochemical Effects. *Macromolecules*, **2013**, *46*, 2331-2340.

275. Chen, S. C.; Kuo, S. W.; Liao, C. S.; Chang, F. C. Syntheses, Specific Interactions, and pH-Sensitive Micellization Behavior of Poly[vinylphenol-b-2-(dimethylamino)ethyl methacrylate] Diblock Copolymers, *Macromolecules*, **2008**, *41*, 8865-8876.

276. Braim, S. A.; Shakesheff, K. M.; Saunders, B. R.; Alexander, C. Thermoresponsive magnetic colloidal gels via surface-initiated polymerisation from functional microparticles, *J. Mater. Chem. B*, **2016**, *4*, 962-972.

277. Huang, X., El-Sayed, I. H., Qian, W.; El-Sayed, M. A. Cancer cell imaging and photothermal therapy in the near-infrared region by using gold nanorods. *J. Am. Chem. Soc*., **2006**, *128*, 2115-2120.

278. Kim, B., Rutka, J. T.; Chan, W. C. Nanomedicine. *N. Engl. J. Med*. **2010**, 2434-2443.

279. Leung, S. L.; Zha, Z.; Teng, W.; Cohn, C.; Dai, Z.; Wu, X. Organic-inorganic nanovesicles for doxorubicin storage and release. *Soft Matter* **2012**, *8*, 5756-5764.

280. Liong, M.; Lu, J.; Kovochich, M.; Xia, T.; G. Ruehm, S.; E. Nel, A.; Tamanoi, F.; Zink, J. I. Multifunctional inorganic nanoparticles for imaging, targeting, and drug delivery. *ACS Nano* **2008**, *2*, 889-896.

281. Slowing, I. I., Trewyn, B. G., Giri, S. & Lin, V. Y. Mesoporous silica nanoparticles for drug delivery and biosensing applications. Adv. Funct. Mater. 17, 1225-1236 (2007)

282. Sun, X. K.; Rossin, R.; Turner, J. L.; Becker, M. L.; Joralemon, M. J.; Welch, M. J.; Wooley, K. L. An assessment of the effects of shell cross-linked nanoparticle size, core composition, and surface PEGylation on in vivo biodistribution. *Biomacromolecules*, **2005**, *6*, 2541-2554.

283. Cortez, C.; Tomaskovic-Crook, E.; Johnston, A. P.; Scott, A. M.; Nice, E. C.; Heath, J. K.; Caruso, F. Influence of size, surface, cell line, and kinetic properties on the specific binding of A33 antigen-targeted multilayered particles and capsules to colorectal cancer cells. *ACS Nano*, **2007**, *1*, 93-102.

284. Goodman, T. T.; Olive, P. L.; Pun, S. H. Increased nanoparticle penetration in collagenase-treated multicellular spheroids. *Int. J. Nanomed*., **2007**, *2*, 265-274.

285. Rejman, J.; Oberle, V.; Zuhorn, I. S.; Hoekstra, D. Size-dependent internalization of particles via the pathways of clathrin-and caveolae-mediated endocytosis. *Biochem. J*., **2004**, *377*, 159-169.

286. Zauner, W.; Farrow, N. A.; Haines, A. M. R. In vitro uptake of polystyrene microspheres: effect of particle size, cell line and cell density. *J. Controlled Release*, **2001**, *71*, 39-51.

287. Meyer, R. A.; Green, J. J. Shaping the future of nanomedicine: Anisotropy in polymeric nanoparticle design. *Wiley Interdiscip. Rev*., **2016**, *8*, 191-207.

288. Qiu, L.; Xu, C. R.; Zhong, F.; Hong, C. Y.; Pan, C. Y. Fabrication of Functional Nano-objects through RAFT Dispersion Polymerization and Influences of Morphology on Drug Delivery. *ACS Appl. Mater. Interfaces*, **2016**, *8*, 18347-18359.

289. Visalakshan, R. M.; García, L. E. G.; Benzigar, M.R.; Ghazaryan, A.; Simon, J.; Mierczynska-Vasilev, A.; Michl, T.D.; Vinu, A.; Mailänder, V.; Morsbach, S. The influence

of nanoparticle shape on protein corona formation. *Small*, **2020**, *16*, 2000285.

290. Khine, Y. Y.; Stenzel, M. H. Surface modified cellulose nanomaterials: a source of non-spherical nanoparticles for drug delivery. *Mater. Horiz.*, **2020**, *7*, 1727-1758.

291. Geng, Y.; Dalhaimer, P.; Cai, S.; Tsai, R.; Tewari, M.; Minko, T.; Discher, D. E. Shape effects of filaments versus spherical particles in flow and drug delivery. *Nat. Nanotechnol.*, **2007**, *2*, 249-255.

292. Chithrani, B. D.; Ghazani, A. A.; Chan, W. C. W. Determining the size and shape dependence of gold nanoparticle uptake into mammalian cells. *Nano Lett.*, **2006**, *6*, 662-668.

293. Chithrani, B. D.; Chan, W. C. W. Elucidating the mechanism of cellular uptake and removal of protein-coated gold nanoparticles of different sizes and shapes. *Nano Lett.*, **2007**, *7*, 1542-1550.

294. Florez, L.; Herrmann, C.; Cramer, J. M.; Hauser, C. P.; Koynov, K.; Landfester, K.; Crespy, D.; Mailänder, V. How Shape Influences Uptake: Interactions of Anisotropic Polymer Nanoparticles and Human Mesenchymal Stem Cells. *Small*, **2012**, *8*, 2222-2230.

295. Park, J. H.; von Maltzahn, G.; Zhang, L.; Schwartz, M. P.; Ruoslahti, E.; Bhatia, S. N.; Sailor, M. J. Magnetic iron oxide nanoworms for tumor targeting and imaging. *Adv. Mater.*, **2008**, *20*, 1630-1635.

296. Park, J. H.; von Maltzahn, G.; Zhang, L.; Derfus, A. M.; Simberg, D.; Harris, T. J.; Ruoslahti, E.; Bhatia, S. N.; Sailor, M. J. Systematic surface engineering of magnetic nanoworms for in vivo tumor targeting. *Small*, **2009**, *5*, 694-700.

297. Barua, S.; Yoo, J. W.; Kolhar, P.; Wakankar, A.; Gokarn, Y. R.; Mitragotri, S. Particle shape enhances specificity of antibody-displaying nanoparticles. *Proc. Natl. Acad. Sci. U. S. A.*, **2013**, *110*, 3270-3275.

298. Karagoz, B.; Esser, L.; Duong, H. T.; Basuki, J. S.; Boyer, C.; Davis, T. P. Polymerization-Induced Self-Assembly (PISA)-control over the morphology of nanoparticles for drug delivery applications. *Polym. Chem.*, **2014**, *5*, 350-355.

299. Qiu, L.; Xu, C. R.; Zhong, F.; Hong, C. Y.; Pan, C. Y. Fabrication of Functional Nano-objects through RAFT Dispersion Polymerization and Influences of Morphology on Drug Delivery. *ACS Appl. Mater. Interfaces*, **2016**, *8*, 18347-18359.

300. Et-Thakafy, O.; Delorme, N.; Gaillard, C.; Mériadec, C.; Artzner, F.; Lopez, C.; Guyomarch, F. Mechanical Properties of Membranes Composed of Gel-Phase or Fluid-Phase Phospholipids Probed on Liposomes by Atomic Force Spectroscopy. *Langmuir*, **2017**, *33*, 5117-5126.

301. Stern, T.; Kaner, I.; Laser Zer, N.; Shoval, H.; Dror, D.; Manevitch, Z.; Chai, L.; Brill-Karniely, Y.; Benny, O. Rigidity of Polymer Micelles Affects Interactions with Tumor Cells. *J. Controlled Release*, **2017**, *257*, 40-50.

302. Anselmo, A. C.; Mitragotri, S. Impact of Particle Elasticity on Particle-Based Drug Delivery Systems. *Adv. Drug Delivery Rev.* **2017**, *108*, 51-67.

303. Wang, Z.; Wu, Z.; Liu, J. Zhang, W. Particle morphology: an important factor affecting drug

delivery by nanocarriers into solid tumors. *Expert Opinion on Drug Delivery*, **2018**, *15*, 379-395.

304. Stern, T.; Kaner, I.; Laser Zer, N.; Shoval, H.; Dror, D.; Manevitch, Z.; Chai, L.; Brill-Karniely, Y.; Benny, O. Rigidity of Polymer Micelles Affects Interactions with Tumor Cells. *J. Controlled Release*, **2017**, *257*, 40-50.

305. Pires, D.; Hedrick, J. L.; De Silva, A.; Frommer, J.; Gotsmann, B.; Wolf, H.; Despont, M.; Duerig, U.; Knoll, A.W. Nanoscale three-dimensional patterning of molecular resists by scanning probes, *Science* **2010**, *328*, 732-735.

306. Venkataraman, S.; Hedrick, J. L.; Ong, Z. Y.; Yang, C.; Rachel Ee, P. L.; Hammond, P. T.; Yang, Y. Y. The effects of polymeric nanostructure shape on drug delivery. *Adv. Drug Delivery Rev*, **2011**, *63*, 1228-1246.

307. Jang, S. G.; Audus, D. J.; Klinger, D.; Krogstad, D. V.; Kim, B. J.; Cameron, A.; Kim, S. W.; Delaney, K. T.; Hur, S. M.; Killops, K. L. Striped, ellipsoidal particles by controlled assembly of diblock copolymers. *J. Am. Chem. Soc*., **2013**, *135*, 6649-6657.

308. Liu, G.; Qiu, Q.; Shen, W.; An, Z. Aqueous dispersion polymerization of 2-methoxyethyl acrylate for the synthesis of biocompatible nanoparticles using a hydrophilic RAFT polymer and a redox initiator. *Macromolecules*, **2011**, *44*, 5237-5245.

309. Blanazs, A.; Madsen, J.; Battaglia, G.; Ryan, A. J.; Armes, S. P. Mechanistic insights for block copolymer morphologies: how do worms form vesicles? *J. Am. Chem. Soc*., 2011, 133, 16581-16587

310. Li, Y.; Armes, S. P. RAFT synthesis of sterically stabilized methacrylic nanolatexes and vesicles by aqueous dispersion polymerization. *Angew. Chem., Int. Ed*., **2010**, *49*, 4042-4046.

311. Jones, E. R.; Semsarilar, M.; Blanazs, A.; Armes, S. P. Efficient synthesis of amine-functional diblock copolymer nanoparticles via RAFT dispersion polymerization of benzyl methacrylate in alcoholic media. *Macromolecules*, **2012**, *45*, 5091-5098.

312. Guérin, G.; Wang, H.; Manners, I.; Winnik, M. A. Fragmentation of Fiberlike Structures: Sonication Studies of Cylindrical Block Copolymer Micelles and Behavioral Comparisons to Biological Fibrils. *J. Am. Chem. Soc*., **2008**, *130*, 14763-14771.

313. J Song,.; Duan, B; Wang, C.; Zhou, J.; Pu, L.; Fang, Z.; Wang, P.; Thye Lim, T.; Duan, H. SERS-Encoded Nanogapped Plasmonic Nanoparticles: Growth of Metallic Nanoshell by Templating Redox-Active Polymer Brushes. *J. Am. Chem. Soc*., **2014**, *136*, 6838-6841.

314. Chen, X.; Wu, Q.; Henschke, L.; Weber, G.; Weil, T. An efficient and versatile approach for the preparation of a rhodamine B ester bioprobe library. *Dyes and Pigments*, **2012**, *94*, 296-303.

315. Yoo, H. S.; Park, T. G. Folate-receptor-targeted delivery of doxorubicin nano-aggregates stabilized by doxorubicin-PEG-folate conjugate. *J Control Release*, **2004**, *100*, 247-56.

316. Huang, H.; Carey, R. I. Preparations of Boc-Cys(S-Pyr)-OH and Z-Cys(S-Pyr)-OH and their applications in orthogonal coupling of unprotected peptide segments. *J. Peptide Res*. **1988**,

51, 290-296.

317. Jewett, J. C.; Sletten, E. M.; Bertozzi, C. R. Rapid Cu-Free Click Chemistry with Readily Synthesized Biarylazacyclooctynones. *J. Am. Chem. Soc*. **2010**, *132*, 3688-3690.

318. Kaur, S.; Prasad, C.; Balakrishnan, B.; Banerjee, R. Trigger responsive polymeric nanocarriers for cancer therapy. *Biomater. Sci*., **2015**, *3*, 955-987.

319. Agarwal, A.; Diedrich, J. K.; Julian, R. R. Direct Elucidation of Disulfide Bond Partners Using Ultraviolet Photodissociation Mass Spectrometry. *Anal. Chem*. 2011, *83*, 6455-6458.